ADDIS ABABA UNIVERSITY

SCHOOL OF MECHANICAL & INDUSTRIAL ENGINEERING

Delamination of Composite material using Virtual Crack Closure Technique and Cohesive zone Method for Automotive structure and semi-structure

A Thesis submitted to the school of Mechanical & Industrial Engineering of Addis Ababa University in partial fulfillment of the Degree of Masters of Science

In

Mechanical Engineering (Mechanical Design Stream)

By: Nebiyu Abebe

Advisor: Dr. Daniel Tilahun

Co. Advisor: Ato. Mulugeta H/Mariam

Nov, 2017

ADDIS ABABA UNIVERSITY

ADDIS ABABA INSTITUTE OF TECHNOLOGY

SCHOOL OF MECHANICAL AND INDUSTRIAL ENGINEERING

Delamination of Composite material using Virtual Crack Closure Technique and Cohesive zone Method for Automotive structure and semi-structure

By: Nebiyu Abebe

Approved by board of examiners

Ato. Getasew Taddese	_____	_____
Head of the school	Signature	Date
Dr. Daniel Tilahun	_____	_____
Advisor	Signature	Date
Ato. Mulugeta H/Mariam	_____	_____
Co. Advisor	Signature	Date
Ato. Tolosa. D	_____	_____
Internal Examiner	Signature	Date
Ato Behailu M	_____	_____
External Examiner	Signature	Date

Declaration

I the undersigned, declare that this thesis entitled `` **Delamination of Composite material using Virtual Crack Closure Technique and Cohesive zone Method for Automotive structure and semi-structure**'' is the result of my own research carried out under the supervision of Dr. Daniel Tilahun and Ato Mulugeta. It has not been presented in any from in any other university and all sources of material used for this thesis are accordingly sited and acknowledged.

Nebiyu Abebe Achamyeleh	Date

This is to certify that the above declaration made by the candidate is correct to the best of my knowledge.

Dr. Daniel Tilahun	Date
Ato. Mulugeta H/Mariam	Date

Acknowledgment

In 1st of October, my thesis finished after about one and five mounts every day work. This period was one of the difficult period in my life; I have experienced lots of up and downs, lots of hopeful and disappointing moments, finally I could finish it with GOD help. My thesis is always associated with some names that I will never ever forget them and if these people were not in my life this could never be happened.

First of all I would like to thank my great and knowledgeable university adviser**, Dr. Daniel Tilahun** and co-adviser **Ato Mulugeta H/Maram** they spent lots of energy, attention in the beginning and along my thesis way, I am always thankful of them.

Also I would like to say special thank you to my family for their full support to the end. A lots of thank to **Ato Behailu Mamo** my teacher, who supported me in every aspect and I will never forget what he has done for me, and of course I cannot forget the dear name **Telile Homa** who always has done her best for me, So thank you very much dear **Telile.**

Very specifically and sincerely I would like to say my best of thanks to **Bruck Alemu** and his wife **Rediet Assegid**, **Maereg Ambelu and Alemayehu Worku** your advice and support mean a lot for me for those difficult moments. **Temesgen Terefe** and **Etalem Abera** who were helping me in every editorial work.

The last but not the least I would like to everyone who spent their time and energy on my thesis even more than me. Thank you all.

Abstract

This paper studied Mode I delamination of Composite material using Virtual Crack Closure Technique and Cohesive Zone methods for Automobile Application. Quasi-Isotropic glass fiber/epoxy composite material is developed using Autodesk composite simulation design software. Mode I isotropic delamination propagation of quasi-isotropic composite material modeled on ABAQUS@10.14 for both Virtual Crack Closure Technique and Cohesive Zone methods. Virtual Crack Closure Technique with different mesh density as well different viscosity to overcome convergence difficulty are investigated. In Cohesive Zone method interface is assumed as damageable homogenous zero thickness layer of cohesive element between two composite layers. Load-Displacement curve is investigated by varying interfacial strength, penalty stiffness and viscosity to improve convergence by lowering either both or one, but excessively lowering is done taking care of over-softening. Design of quasi-isotropic composite with stacking sequence of $[(-45^0,45^0,90_2^0\ ,\ 0_2^0\ )_2\ ]_s$ has Elastic modulus of 30900MPa, Shear modulus of 10300MPa and Poisson's ratio of 0.293, using this material property critical delamination load and displacement are obtained from the analytical method , Virtual Crack Closure Technique and Cohesive Zone methods simulation are 32N,5.9mm and 32.35 N,4.9mm and 30.82N, 5.58mm respectively.

Key words: Delamination; Quasi-isotropic; Virtual Crack Closure Techniques; Cohesive Zone methods;

List of Figures

Chapter One

Chapter Two

Chapter Three

Chapter Four

List of Tables

Chapter Two

Chapter Four

Nomenclature

DCB	Double-cantilever beam
FPZ	Fracture process zone
CZM	Cohesive-zone model
FEA	Finite-element analysis
CTOD	Crack Tip Opening Displacement
CFRP	Carbon fiber-reinforced polymer
ENF	End-notch flexure
DCZM	Discrete cohesive zone model
CCZM	Continuum cohesive zone model
DOF	Degrees of freedom
MVCCT	Modified virtual crack closure technique
TSEM	Two Stop Extension Model
4ENF	Four-point bend end notched flexural
ELS	End loaded split
EPEM	Elasto-Plastic Fracture Mechanic
MMB	Mixed-mode bending
CDM	Continuum damage mechanics
VCCT	Virtual crack closure technique
ONF	Over notched flex

Chapter One

1. Introduction

1.1. Background

A composite material is made by combining two or more dissimilar materials. They are combined in such a way that the resulting composite material or composite possesses superior properties which are not obtainable with a single constitute material. So in technical technique terms, we can define a composite as a multiphase material from a combination of materials, differing in composition or form, which remain bonded together, but retain their identities and properties, without going into any chemical reaction. Composite are one of the most advanced and adaptable engineering material known in many progresses in the field of material science and technology.

Glass fiber reinforced is strong and lighter. Which contain carbon fibers and can be expensive to produce but are commonly used wherever high strength to weight ratio and rigidity are required, such as aerospace and automotive industry. However, fiber reinforced composite are weak in there through thickness direction. This weakness can result in part falling of delamination or crack initiation and propagation either external load or impact event.

Delamination of composite material is necessary in order to minimize loss of automotive structure. Delamination is one of most common failure mode of composite material. For automotive application composite may Cause accident if it is not well managed, monitor and maintained [1].

Application of glass fiber or carbon fiber reinforced composite offer numerous new design possibility for structural component of automobile, this advanced material are not only light in weight but also stiff, strong, durable and it can be used to build different parts of automobiles body and structure like car seat, wheel, side beam, front beam, suspension, bottom plat and others [1].

Now a day number of vehicle on the road is growing at a rapidly throughout the world. In addition, the desire of personalization of each car will lead to a smaller number of vehicle in each production run, as a result more flexible and more cost effective production method will be required, but production of composite is relatively, ask longer processing time and relatively raw material are expensive and it can be difficult to achieve high quality and production [2].

In the world of composites, *Laminated Composites* are the most widely used composites because of the familiar manufacturing and performance characteristics. The main feature of laminated composites is the stacking of *laminas* to ensure a global characteristic. Laminated composites are customized for planar structures to attain high strength allowable. However, the resin rich layer between the laminas has no reinforcement in through-the-thickness direction that sometimes yields separation of the laminas, causing a crack called *delamination crack* or simply *delamination*. Form of delamination damage is particularly insidious, since the delamination crack may propagate undetected under the action of static or dynamic loads, leading to the ultimate failure of the component in addition to inducing reductions in stiffness and compressive load-carrying capacity of the laminate. Unlikely encountered in in-plane failures, the delamination would result in incapability of the structure only in compressive strength. Therefore, it could not be revealed until a compressive loading is applied at critical load or with special detection techniques. Consequently, the delamination analysis literally attracts researchers in composite technology due to its insidious characteristic [3].

Application of new progressive materials is getting today into different industry areas, car producers are trying to reduce the car weight and increase the car toughness against the impact for better safety. That´s the space for the composite materials, like carbon, aramid or fiberglass base, implementation. Through the use of these materials, it´s possible to decrease the original components weight in preservation of functional, toughness and application possibilities, properties for which are today's components made from fiber composites used not only for sport and luxury cars, but also already for serial produced cars. Price availability of this kind of components is by using of progressive technologies for their production continually lower, what is positive tendency in view of their larger utilization. The production of composite structures for car industry is the most advanced new market and their utilization in the car components production has a big potential also in the future view.

Applications of new materials as plastics or composites are allowing the constructors to design variously shapes of components. Modern car design is affecting the security, performance, aerodynamics, fuel consumption, production costs and many other important factors. Composite materials are also used for better look of exterior and interior parts such as seats, dashboards,

bumpers, diffusor and so on. Nowadays there are many different studies and prototypes of full carbon and glass fiber car bodies

Fig 1. 1 Powertrain and chassis of a typical composite vehicle

Moreover, the delamination damage is frequently encountered in composite structures. A recent survey on problems concerning composite parts for deferent application shows that delamination, caused by impact, presents 60% of all damage observed in composite structures [3].

1.1.1. Approaches for delamination

When it comes to failure, cracks are the most common defects in joints and composite laminates. They cause fracture, delamination and debonding. The emphasis in this literature research is put on crack failure in and around an adhesively bonded joint. Research on cracks have been extensive and have resulted in many models and failure criteria. Finite element methods have become the preferred method for analysis on composite delamination.

There are four well-known approaches to failure analysis that are based on finite element method: continuum mechanics, fracture mechanics, extended finite element method and damage mechanics from those continuum mechanics, fracture mechanics and damage mechanics are mostly used.

1.1.2. Continuum mechanics

The most common and well-known approach for material failure analysis is via continuum mechanics. Approaches based on continuum mechanics use the maximum values of stress, strain or strain energy resulting from finite element analyses, against a chosen failure criterion which uses the critical values of the material and indicates if a material has failed. Examples of such failure criteria are Von Mises and Drucker-Prager. Using continuum mechanics in failure analysis has proven successful and are still used today, although it has a shortcoming when applied to composite lamina.

Within cracks, a stress discontinuity exists at the beginning of the crack tip. In reality, the y-stresses at the crack tip are actually finite instead of infinite as derived by continuum mechanics. Further along the crack towards the end, the y-stresses are zero, due to free surfaces where crack propagation has already occurred. This creates a discontinuity between the head of the crack and the remaining crack length. The stresses are required to be continuous, and so the stresses at the crack tip are not defined, being infinite. This is called a singularity. These singularities are always present in crack angles smaller than 180 degrees [4].

Continuum mechanics are simple and easy to use, very suitable for brittle material, but it is not suitable material with discontinuous structure and ductile material. It is sensitive to stress singularities and mesh which can increase computation time for accuracy.it can give inaccurate and overestimation due to use of only one or few variable.

1.1.3. Fracture mechanics

Fracture mechanics can be divided in Linear Elastic Fracture Mechanics (LEFM) and Elasto-Plastic Fracture Mechanics (EPFM). LEFM neglects non-linearity while EPFM takes non-linearity and plasticity into Account.

Linear Elastic Fracture Mechanics

LEFM was the first introduced form of fracture mechanics and is still used today. As the name suggests, it assumes linear elastic behavior in brittle materials up till the point of failure and uses simple failure criteria to indicate crack growth once reached, such as Griffith's criterion and Irwin's modification of Griffith's criterion, Griffith's energy balance is based on the 3rd law of thermodynamics which states that a system that goes from a state of non-equilibrium to a state of equilibrium will have a net decrease in energy [5]. The interpretation of the application on cracks

is that a crack can only grow if the fracture process results constant or decreased total energy. On the atomic scale, fracture occurs when the applied stress and work are sufficient to sever the atomic bonds. The bond between atoms is caused by the attractive electrostatic force between opposite charges. The cohesive strength can be derived in terms of the cohesive stress. Irwin also followed with a method to predict fracture initiation with a so-called stress intensity factor [6], which is based on the stress field of the crack tip within a radius and involves a small surrounding volume of the crack tip, and was widely adapted. A disadvantage when using the stress intensity factor is that the factor itself is not easily determinable when cracks grow near or at an interface. To counter this, methods were introduced using the strain energy release rate and critical value of fracture toughness and applied to laminates. Another method that was to improve the use of stress intensity factors was the generalized stress intensity factor. This improved version was able to predict damage initiation for bonded joints at interface corners [7, 8] and for a variety of adhesive thickness these methods work well enough for standard simple joints, although they are questionable for more complex geometries and joints.

Elasto-Plastic Fracture Mechanics

LEFM is not applicable for ductile material as these materials tend to plastically deform before fracturing and thus rendering the assumption of linearity untrue. To analyze ductile material, or material subject to plastic deformation before failure, EPFM was introduced. The first theories to incorporate plasticity in crack behavior were using the crack tip opening displacement as an important parameter and a plastic radial or spherical zone which incorporated the crack [9]. Modifications and improvements were made to improve the method by correcting the actual crack length, plastic zone and assumption that the stress is not singular at the boundaries but zero [10]. Although the method took care of the stress singularity, a strain singularity is still invoked for ductile materials. within non-linear fracture mechanics with the introduction of the J-integral [11].The J-integral is used as an energy contour line integral, and the independent integral path can be used to travel from one crack surface to another and encloses the crack tip. In each point of the contour

A modified version of the J-integral is the Hutchinson, Rice and Rosengren solution, applied to material that behave. The J-integral has given good results in cracked bonded joints [12], although the J-integral comes with disadvantages. Even though the integral itself is path-independent, it is

limited by joint geometry. The development of the plastic zone field is limited by the adherents and the interfaces, seeing as the adhesive is often very thin in bonded joints. This ultimately makes the fracture toughness dependent of the geometry of the joint and interface length [13]. Because of this, the integral must be extrapolated against interface length where by a mesh refinement is required, which increases computational time. An initial crack tip should be present in the structure if J-integral is used. Aside from this, the J-integral also has some issues when applied in finite element codes regarding crack propagation. Nodal variable and topological information from the nodes ahead and behind the crack front are required for the calculation of fracture parameters, such as the energy release rates or stress factors, and these calculations can be difficult when these codes are applied to progressive crack propagation.

Virtual Crack Closure Technique

Perhaps the most widely and successfully used technique for the delamination propagation is the Virtual Crack Closure Technique (VCCT) [14] . Also, since VCCT can be thought as representative‖ of FM type methods, in order to compare damage mechanics method with fracture mechanics type methods, it would be convenient to discuss VCCT in more detailed manner.

As an application of FM have developed VCCT in which the procedure is mainly based on the calculation of the strain energy release rates at the crack tip [13]. VCCT is based on the same assumption of Irwin's crack closure integral [6], in which the energy released in the process of crack expansion is equal to work required to close the crack to its original state as the crack extends by a small amount. Actually, the direct application of the Irwin's crack closure integral is generally referred as *crack closure method*

1.1.4. Damage mechanics

Damage mechanics follow cracks, or damage, progressively in a finite region, starting at an arbitrary point or a pre-defined crack, up to complete structural failure. This technique monitors and allows damage growth progressively while taking continuous stiffness degradation into account, from damage initiation till propagation. Damage models incorporate a so-called damage variable *D* or tensor D, which decreases the stiffness properties in elements.

These damage variables and tensor, or collectively called damage laws, can be expressed in many ways and dependent on a variety of material properties such as moduli, strain, strain rates, stresses, Poisson ratios and more.

A unique damage model is cohesive zone modelling. It can be divided into two approaches: local and continuum approach. In the local approach, damage in a finite element region is confined to a zero volume or zero surface area, which allows simulation of interfacial failure between materials in 3D or 2D respectively. In the continuum approach, the damage is modelled over a finite element region, non-zero volume or surface area elements. The elements used in both approaches that are subjected to damage mechanics can use the theories of Dugdale and Barenblatt [10, 15], and are called cohesive elements. CZM works with the strain energy release rate, which acts as the fracture toughness, and the cohesive traction in an element as a function of the relative displacement of opposing nodes. This function is called a constitutive relation, or separation-traction law, whereby the area of the function is the fracture toughness. The traction law starts with reversible or elastic behavior, allowing no penalty to its stiffness for unloading and reloading, and after the maximum traction has been reached it shows irreversible or softening behavior, lowering the stiffness for unloading and reloading after the maximum traction. Since the early nineties, the first applications of CZM were done in a local approach in brittle materials. The first applications of CZM on composites were performed in the last decade around the turn of the new millennia, with the advances in finite element software packages contributing a major part around half the decade [16]. CZM relates the relative displacement of two opposing associated points in a finite region to the force per unit of area, also known as traction. In cohesive elements, the relative displacement is often expressed as changes in surface normal and the traction as a function of the displacement with a stiffness tensor. Cohesive zone elements do not necessarily have to represent any physical material, yet they still describe the cohesive forces that exists when material elements separate from each other. Cohesive zone elements can also be modelled with an initial zero-thickness

CZM projects all damage mechanisms in and around a crack tip, leading to a constitutive relation, or cohesive zone law. There are many ways to define the criteria and laws for a cohesive zone model

Traction laws

A cohesive zone law, also known as a traction-separation law, describes the constitutive behavior between the relative displacement between two points and traction T as a curve. There are many varieties of traction laws, with the majority of them being piece-wise linear or non-linear and continuous or discontinuous A traction law can be divided into two parts. The first part is the

interval between zero displacement and traction up till the damage initiation criterion. The damage initiation criterion is where maximum traction of a mode at a certain displacement occurs. The interval can be seen as an initial stiffness which the structure possesses. The damage initiation criterion is described as the maximum traction *T max* or the displacement at the maximum traction of a pure mode, based on known material properties. Once the damage initiation criterion has been reached and displacement increases, damage starts to occur and the initial elastic behavior disappears, and the behavior goes into the second part of the traction law. This part is the interval between the damage initiation criterion and the damage propagation criterion. The damage propagation criterion is described as a critical energy release rate *Gc* . The energy release rate, often called cohesive energy, is in fact the area between the traction law curve, governed by the simple integral for a pure mode and critical energy release rate *Gc* , max traction *Tm*, energy release rate *G* and opening displacement . The critical energy release rate is often based on pure mode fracture, such as tension or shear. When the critical energy release rate is reached, it coincides with zero or near-zero traction. By then, full damage has been achieved, the cohesive zone disappears and crack growth occurs, hence the traction being reduced to zero as no cohesive forces are available to keep the material together. For a pre-determined crack path that has been designated as a cohesive zone, every opposing point or node pair along the interface or bulk material will find itself at a certain point on the traction law.

The damage remains zero in the part with reversible behavior, or in other words, until the damage initiation criterion *T max*. Within the irreversible damaged part, damage starts to become non-zero and increases till the value of 1, indicating damage propagation and thus failure in the element. The damage law can be expressed in many forms to attain a damage Mode I; a damage variable can be set up as a scalar function ranging from 0 to 1.

The traction σ is exerted by the interface until the interfacial separation reaches a critical value. σ is a function of c given by traction-separation law. As the element becomes damaged, the area beneath the traction-separation law is the mechanical work needed to separate the element. Thus, the area beneath the traction-separation law is equivalent to G_C. Several shapes of CZ law are available for describing material behaviors, as seen in Fig. 1, such as bilinear, exponential, trapezoidal, and trilinear. Such laws allow for cohesive zone elements to model a wide range of

material behavior, including the potential for modeling nonlinear behaviors that cannot be captured with fracture mechanics.

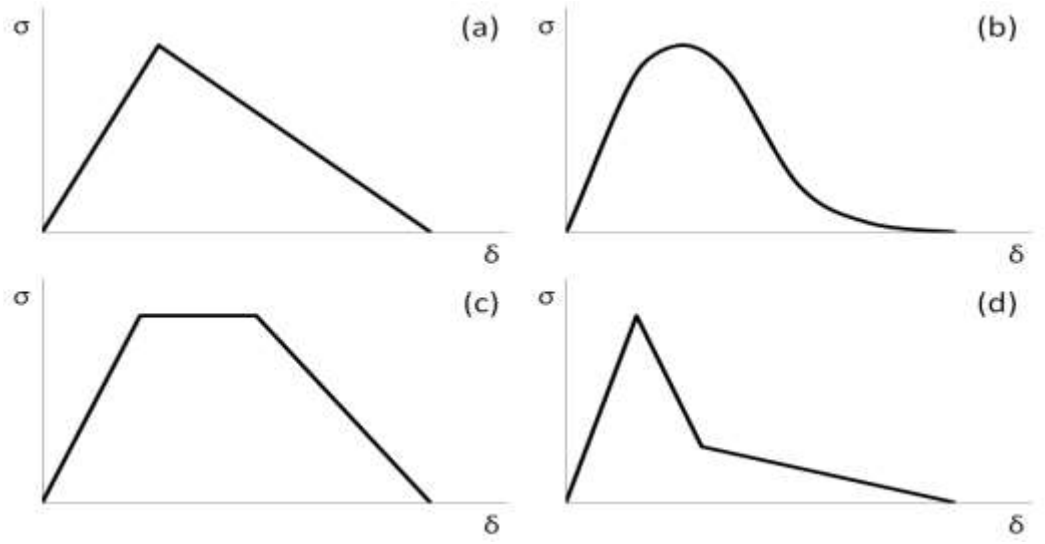

Fig 1. 2. Available traction-separation laws for cohesive zone models, including (a) bilinear, (b) exponential, (c) trapezoidal, and (d) trilinear laws [17]

Traction-separation laws shown in Fig 1.2 a , (b), (c), and (d) require four or more parameters to fully define the cohesive zone behavior bilinear traction-separation law (Fig. 1.2,a) is used because the curve is defined by only three parameters. Most common used traction laws in literature and experimental validation are the bilinear law, the trapezoidal law and the exponential law [17]. The selection of traction laws dependent on the type of experiment, geometry and material. A bilinear model is often preferred for brittle materials and delamination, which offers a good compromise between numerical performance, computational cost and accuracy of results. For ductile adhesives, a trapezoidal law is preferred [18]. In simple coupon tests like a double cantilever beam test, the exponential law offers the most accurate results at the expense of computational cost [17].

The cohesive model does not model the real physical fracture process and there is no evidence for which traction-separation law is the right one to use. In the literature there are several different approaches found.

A. Bilinear law

The bilinear, or triangular, traction law is a popular choice because of its simplicity. The bilinear law was redesigned from a simple rigid linear softening relationship to include an initial stiffness. The shape as it suggests is triangular and the function is piece-wise linear and discontinuous. It is described by the following uncoupled relation:

A typical stress-displacement diagram for a cohesive element, taken from. The bilinear traction-separation law was proposed by Alfano and Crisfield for modeling interfacial separation. Several bimaterial interfaces have been simulated using this law, though properly defining a mixed-mode law for such interfaces remains a challenge. The bilinear law shows interfacial traction σ versus interfacial separation δ. As CZ elements undergo deformation, they exhibit elastic loading for $\delta < \delta^*$. In this region, no damage is accumulated in the interface, and unloading returns CZ elements to their initial configuration, a critical traction $\sigma\ max$ is reached and damage is initiated. Delamination is tracked by a damage parameter D. When $\delta > \delta^*$, D increases, and when $\delta \geq \delta C$, D reaches a maximum value of 1, Regardless of the current magnitude of δ, the damage value D can never decrease. In other words, unloading will not reduce the damage that has accumulated. Therefore, if a CZ element is unloaded while partially damaged.

When the damage parameter $D = 1$, the CZ element is said to be fully damaged, and the stiffness of the cohesive zone element is zero. Thus, a fully damaged element has been completely separated and will not produce interactions between layers. As mentioned previously, the area under the traction-separation profile is the critical strain energy release rate.

B. Exponential law

The exponential law is also used often. This function is continuous and smooth. It was first introduced by Xu and Needleman. Exponential traction - separation curve Their relation includes coupling and calculates directly with the energy release rates, equalizing modes II and III, with max traction Tm, critical energy release rates Gc , critical opening displacement $\pm c$, traction T and opening displacement.

C. Trapezoidal law

Tvergaard and Hutchinson developed a model for an idealized traction-separation law specified on the crack plane to characterize the fracture process in 1992 [19]. The relation is built on an increase of traction in the cohesive element until it reaches the peak traction, $\hat{\sigma}$, at δ_1. The traction

will stay the same for further separation until δ_2 is reached. Then damage evolution is modeled until reaching δ_c where fracture occurs.

In order to implement a CZM in its simplest form, two parameters are required: a fracture toughness (or energy) and a cohesive strength. The choice of these parameters and how they are measured and/or calibrated depends on the problem that is being addressed. In general, the CZM parameters are ‘‘system’’ parameters and are related to the material system that is being studied. The fracture toughness can be obtained from coupon level tests of the material system under study. This measured toughness value in conjunction with a CZM/FE. Simulation of the test can be used to back out the cohesive strength. Alternatively, both the toughness and strength can be measured from coupon level tests for subsequent use in prediction of crack growth in other structural configurations.

In the CZM, an existing crack starts to grow when the stress at the crack tip attains the cohesive strength and when there is sufficient energy supplied from the system to create new cracked area associated with the advancing crack. Thus, unlike LEFM, which requires one parameter, a CZM strategy requires two parameters for predicting crack growth. A cohesive law combines fracture energy and cohesive strength to describe the resistance offered to crack advancement within the cohesive zone.

Compared to VCCT, a major advantage of cohesive zone modeling is its capability to predict both onset and propagation of cracking without the need for a pre-existing crack [19]. Furthermore, it does not require the topological information for the crack front (or the exact crack front shape) in FE implementation. However, the softening portion of the cohesive law, in certain instances can give rise to difficulties leading to mesh sensitivity, lack of convergence, computing inefficiency, sensitivity to element aspect ratio and so on. These difficulties, if not properly resolved, may prevent CZM from being widely used by practicing engineers. There are two major approaches in implementing a cohesive zone model: smeared cohesive element and an interface cohesive element. In a smeared cohesive element, the cohesive zone model is applied as a part of the stress vs. strain relation like a conventional continuum element [20]. The smeared cohesive element is not suitable to study interfacial crack growth. First, when they are placed between the two surfaces of initial zero separation that need to be decohered, a very thin layer must be inserted between the two surfaces to accommodate the smeared cohesive elements. This leads to large aspect ratio

elements that may prevent the FE analysis even to proceed, let alone the hardship in the mesh generation. Second, severe convergence difficulties may also be encountered. Depending on the formulation, the stiffness matrix of these smeared elements may contain off-diagonal terms. A comprehensive overview of the different smeared elements and their finite element formulation is provided in. In particular, it is noted that smeared elements lead to a fully populated stiffness matrix. To overcome the limitations over the smeared cohesive element, the interface cohesive element with the zero-thickness was introduced. The procedure is developed in a similar way to the smeared cohesive element except that the cohesive zone model is applied as stress vs. displacement separation.

A common feature of previously developed elements for CZM is that they treat the process zone ahead of crack tip as a continuous compliant layer and therefore, it is continuum cohesive zone model (CCZM). An alternative way to implement a CZM is to use point-wise elements and we refer to such an approach as the discrete cohesive zone model (DCZM). The central idea of DCZM is to treat the process zone as a discrete spring type foundation that is attached to adjacent node pairs of the surfaces to be decohered, Thus, a non-linear ‘‘spring type’’ discrete interface element is placed between interfacial node pairs to model cohesive interactions between surfaces instead of using continuum type elements along the crack path. A generalization is to use 1D rod type elements in which case the DCZM has a finite thickness. Such an approach finds utility in the modeling of adhesively bonded join

Damage mechanics has more advantage than fracture mechanic approach in order to know delamination. Onset and propagation. It can be used both ductile and propagation. It can be used both ductile and brittle material with good accuracy. We are able to monitor crack propagation progressively for any bulk ok interface element by accounting both reversible and irreversible behavior but it has its own limitation like mesh sensitivity which can increase computation time for accuracy and traction low depends on material type and failure modes.

1.1.5 Modes of delamination

Delamination has three modes of loading as shown by the Fig.1.2. In mode I the forces act perpendicular to the crack. The Mode I loading condition is also called the opening mode. In Mode II the forces act parallel to the crack plane. One force is pushing the top half of the crack back and the other force is pulling the bottom half forward. This creates a shear crack. Since the forces do not cause

the material to move out of its original plane this is also called in-plane shear. In mode III the forces are perpendicular to the crack and pull the top half left and the bottom half right or vice versa. This causes the material to separate out of its plane. It is also called out-of-plane shear.

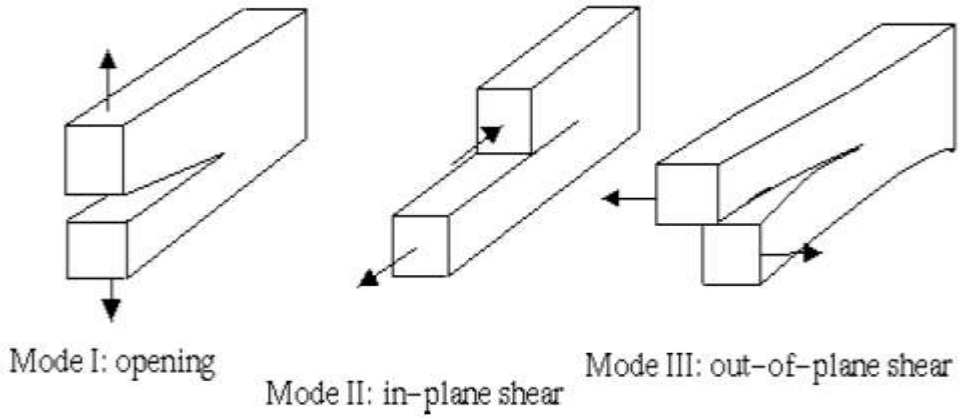

Fig 1. 3. Three Mode of loading

1.2. Purpose

As mentioned in the introduction, delamination failure is a vital phenomenon that should be investigated deeply. From initiation to propagation, VCCT and CZM promises visualization, accuracy and performance. In this sense, the capability of CZM and VCCT makes it a senior candidate for the delamination finite element analysis.

However, there are many interface element types, approaches, models and artificial modifications that are all struggling to reach the most effective and accurate VCCT method and CZM interface element. On the other hand, in industry, engineers, who would like to apply this method, cannot always know the best way to use CZM. Therefore, a single CZM element, with both accurate and showing high performance in convergence issue, should be reached. Material is developed using AUTODESK COMPOSIT DESIGNIG software and DCB are modeled and analyzed on ABAQUS$^{@}$ 10.14. Therefore, the main motivation behind this study is to reach most effective and accurate interface element addressing VCCT and CZM.

1.3. Literature review

1.3.1. Damage in laminated composites

Glass fiber reinforced composite generate complex damage zones at stress concentration, with damage progression in the form of, matrix cracking, delamination and fiber fracture or fiber/matrix de-bonding. Research on the failure mechanism of composites started in close relation to the utilization of such composite materials in aerospace industries. Countless efforts have been made in this area and substantial breakthroughs have been made with constant improvements of existing theories still on-going, to lead the way towards a better understanding of the essence behind the various failure behaviors of lamina/laminate [21]. Since fiber reinforced composites are comprised of two materials with distinct mechanical and thermal properties, if geometric inhomogeneity is taken into account, fiber and matrix play different roles under different loading conditions. Fibers are longitudinally continuous and contribute more to the development of longitudinal modulus and strength, indicating that the fiber supports almost the entire longitudinal tensile load applied to a ply and compressive load without consideration of fiber buckling [21]. The matrix on the other hand, binds fibers together and contributes more to the development of transverse strength and modulus [22].

With the longitudinal modulus of laminated composites being always greater than the transverse modulus, minimizing the transverse stresses of laminated composite materials therefore is a critical design consideration. Load transfer between adjacent layers in a fiber reinforced laminate takes place by means of inter-laminar stresses which develop due to mismatch in Poisson's ratios and coefficients of mutual influence between various layers [21].

Generally, tensile normal stresses applied to an isotropic material cause's elongation in the direction of the applied stresses and contraction in the two transverse directions, a more complex response however, is experienced in laminated composites where a combination of extensional and shear deformation may be produced. To minimize extension-shear coupling therefore laminates are designed to be balanced and symmetric about the mid-plane with examples being unidirectional and cross-ply laminates.

1.3.2. E-Glass and epoxy

The cost of composite materials is usually much higher up to 10 times higher when using carbon fibers than those of conventional metals. A comparison of the cost elements for the glass fiber composites and carbon fiber composites show less coasty. Therefore, the main targets for future development must be the use of hybrid composites (low-cost fibers to be used where possible and aramid and carbon fibers to be used only where they are required for damage tolerance or stiffness reasons), the evaluation of highly automated and rapid manufacturing processes including the application of intelligent preforms or half-finished goods, and the full use of the potential of composites for parts integration. Either glass or carbon, reinforced in the matrix of thermoset or thermoplastic polymer materials. The glass-reinforced thermoset composites are the most commonly used composite in automotive applications today [23].

Glass fibers fall into two categories, low-cost general-purpose fibers and premium special-purpose fibers. Over 90% of all glass fibers are general- purpose products. These fibers are known by the designation E-glass [24].

The first level of classification is usually made with respect to the matrix constituent. The major classes include organic Matrix Composite, Metal Matrix Composites and Ceramic Matrix Composites. The term organic Matrix composite is generally assumed to include two classes of composite, namely polymer Matrix Composite and carbon matrix composite commonly referred to as carbon-carbon composite. For polymer matrix ideal materials as they can be processed easily, possess lightweight, and desirable mechanical properties.

Two main kinds of polymers are thermosets and thermoplastics. Thermosets have qualities such as a well-bonded three-dimensional molecular structure after curing. They decompose instead of melting on hardening. Merely changing the basic composition of the resin is enough to alter the conditions suitably for curing and determine its other characteristics. They can be retained in a partially cured condition too over prolonged periods of time, rendering Thermosets very flexible. Thus, they are most suited as matrix bases for advanced conditions fiber reinforced composites [25].

Thermosets are the most popular of the fiber composite matrices without which, research and development in structural engineering field could get truncated. Aerospace components, automobile parts, defense systems etc., use a great deal of this type of fiber composites

Epoxy resins they are reasonably stable to chemical attacks and are excellent adherents having slow shrinkage during curing and no emission of volatile gases. These advantages, however, make the use of epoxies rather expensive [26].

HexPly® 8552 is an amine cured, toughened epoxy resin system with unidirectional or woven carbon or glass fibers. HexPly® 8552 is recommended for structural applications requiring high strength, stiffness, and damage tolerance. HexPly® 8552 was developed as a low flow system to operate in environments of up to 250°F [27]**,** HexPly® 8551-7 is an amine cured, toughened epoxy resin system supplied with unidirectional graphite and glass fibers, typical reinforcement is continuous intermediate modulus graphite. HexPly 8551-7 was developed to operate in a temperature environment of up to 200^{o}F (93^{O}C). IM7/8551-7 is an extremely damage- resistance system, recommended for structural application requiring high strength, stiffness, and damage tolerance [28]. OUDRACure™ 5505 Amine Hardener is a medium viscosity adducted cycloaliphatic amine used as a curing agent for liquid and solid epoxy resins. OUDRACure™ 5505 Amine Hardener is used to cure resins liquid epoxy resins such as D.E.R ™ 331 Liquid Epoxy Resins, solid epoxy resins such as D.E.R.™ 674 Solid Epoxy Resins, or epoxy solutions such as D.E.R. 671 X-80 Epoxy Solutions [29].

1.3.3. Virtual crack closure technique

A delamination can be assimilated to a fracture process between anisotropic layers (interlaminar damage). Thus, fracture mechanics principles can be used to study the behavior of composite structures in presence of interlaminar damage and to determine the conditions for the delamination growth initiation. Under the assumption of considering the delamination growth process as crack propagation phenomenon fracture mechanics concepts can be generally transferred to the analysis of delaminated composite structures. The propagation of a crack is possible when the energy released for unit width and length of fracture surface (named Strain Energy Release Rate, G) is equal to a threshold level or fracture toughness, characteristic for each material. Starting from the earlier analytical works by Chai et al., [30] delamination in composites has been studied by evaluating the Strain Energy Release Rate. Nowadays, the G calculation is generally performed

by means of techniques used in conjunction with the finite element method, such as the Virtual Crack Closure Technique. According to the Virtual Crack Closure Technique, the evaluation of the Strain Energy Release Rate can be obtained starting from the assumption that for an infinitesimal crack opening, the strain energy released is equal to the amount of the work required to close the crack. Therefore, the work W required to close the crack can be evaluated by performing two analyses. Alternative approaches to compute the strain energy release rate based on results obtained from finite element analysis have also been published recently. For delamination in laminated composite materials where the failure criterion is highly dependent on the mixed mode ratio and propagation occurs in the laminate plane, the virtual crack closure technique has been most widely used for computing energy release rates because fracture mode separation is determined explicitly [14].

1.3.3.1. *Crack closure method using two analysis steps*

The crack closure method or two-step crack closure technique. The terminology in the literature is often inexact and this two-step method is sometimes referred to as VCCT. It may be more appropriate to call the method the crack closure method because the crack is physically extended, or closed, during two complete finite element analyses. The crack closure method is based on Irwin's crack closure integral [6]. The method is based on the assumption that the energy ΔE released when the crack is extended by Δa is identical to the energy required to close the crack. Index 1 denotes the first step depicted and index 2 the second step. For a crack modeled with two-dimensional four-nodded elements, the work ΔE required to close the crack along one element side can be calculated. The crack closure method establishes the original condition before the crack was extended. Therefore, the forces required to close the crack are identical to the forces acting on the upper and lower surfaces of the closed crack. The forces X_1, and Z_1, may be obtained from a first finite element analysis where the crack is closed, by summing the forces at common nodes from elements belonging either to the upper or the lower surface. Forces at constraints may also be used if this option is available in the finite element software used [14].

1.3.3.2. *Modified crack closure method*

The modified, or virtual crack closure method VCCT Is based on the same assumptions as the crack closure method described above. Additionally, however, it is assumed that a crack extension of Δa form $a+\Delta a$ to $a+2\Delta a$ does not significantly alter the state at the crack tip. Further, the energy ΔE released when the crack is extended by Δa, from $a+\Delta a$ to $a+2\Delta a$ is identical to the energy required to close the crack between location i and k. For a crack modeled with two-dimensional, four-nodded elements, the work ΔE required to close the crack along one element side therefore can be calculated. Thus, forces and displacements required to calculate the energy ΔE to close the crack may be obtained from one single finite element analysis [14].

In fracture mechanics approach linear elastic fracture method can be used for brittle (elastic) material, but it cannot be used for material with plastic behavior or material which deform plastically before failure, instead of LEFM, Elasto-plastic fracture mechanics (EPFM) were used, EPFM, J-integral, VCCT can be used for both linear, nonlinear and plastic material. Fracture mechanics are suitable for multiple material structure like, joint and laminas, but it is limited by joint geometry. Stress are not singular at the boundary but zero, strain singularity is not taken care of it. Necessary to have initial crack, unable to grow crack and, it is mesh sensitive, which can increase computation time for accuracy [14].

1.3.3.3. *Delamination by virtual crack closure method*

Strain energy release rate calculation for a major delamination front of arbitrary shape based on the virtual crack closure technique. Efficient algorithm to trace a moving delamination front with on arbitrary and changing shape so that delamination growth can be analyzed by using stationery meshes. Based on the algorithm a delamination front can be defined by two vectors that pass through any point on the front. The normal vector and the tangent vector for the local coordinate system can be obtained based on the two delamination front vectors. 3D-VCCT is applied with finite element models, the orthography meshes can be easily achieved when the delamination front is fixed and adjusting FEA meshes to fit pre-existing shape of the crack front, though this is kind of matching between meshes and the geometry may require fine mesh patterns for coupled delamination shape, most of the research/study used assumption of the delamination front remains straight across the width during its growth. By imposing orthogonal meshes that edges parallel or perpendicular to the original delamination shape without tracing the actual delamination front

during the growth. Delamination growth is limited in the direction to the normal direction defined by orthogonal mesh. The assumption of delamination on straight across the width during its growth is correct in prediction the initiation of the delamination growth. However immediately after growth initiates at a certain point, the releasing of some but not all nodes pairs on the delamination front makes its shape differ from the original [31].

Delamination in the composite structure using orthogonal mesh pattern becomes problem due to the change position and shape of the delamination from the required mesh adjustment, together with the associated non-linear iterations, makes the analysis prohibitively large in the most case. Equation on the analysis are checked its validation by using three different condition. For the first case taking one quarter of the solid are models by the three dimensional ABAQUS standard element "C3D8" taking the result and comparing with analytical solution. Since the mesh is orthogonal and nodes lie exactly on the track front, 3D-VCCT approximation almost coincides with the analytical solution. For the second case with circular crack and mixed mode problem of homogeneous quasi-isotropic material symmetrical stacking sequence was selected and it shows good agreement between 3D-VCCT employed by Whit comb and his 3D-VCCT method, especially in region where G_1 and G_{11} values are maximum. For the third case with embedded elliptical crack in a solid rectangular prism. Two mesh patterns were used, nodes on defined to be precisely along the crack front but the mesh is not orthogonal to the crack front. Mesh is unrelated to the smoothly curved delamination shape and the crack front is approximated by a Zig-Zag line with the same general shape as the quarter delamination [14].

A Zig-Zag approximation to the smooth curve can be defined as best compromise between on inner and on outer boundary to give a model that best approximate the curved shape. The 3D-VCCT with best Zig-Zag approximation shows accuracy with the analytical solution being just over 1% even without on orthogonal mesh [32]. The difference in the two solutions may be reduced by increased mesh requirement. At last mesh orthogonally to the delamination front is shown not to be a requirement for good accuracy in computation of the strain energy release rate. When a very simple mesh is defined in which the model nodes do not lie precisely on a specified delamination front but rather surround that front in a Zig-Zag pattern, the method can be used with good accuracy to analyze on approximation to a specified delamination shape [31].

Prediction of delamination growth initiation in composite structure, the effectiveness of the VCCT has been proved through the delamination growth initiate lead for composite plate with an elliptical delamination and the comparison of this value with the Benchmark results [33].

Introducing interface element for 2D-VCCT suitable for implementing in to commercial FEA. The procedure can be used to any FEA such as ABAQUS @. The interface element is developed based on the original modified crack closure integral technics by introducing stiff spring on the crack tip to calculate the interface force and dummy loads are introduced to investigate displacement opening behind crack tip and the virtual crack jump ahead of crack tip. Three classic example are done on the stationary crack and crack growth. The interface element shows some advantages. it does not require extra post processing to extract fracture parameters nor does in place any special burden on definition of the body mesh, but it is limited on crack with self-similar manor like crack kinking which is not crack with self-similar manor [34].

Simulation of mode 1 delamination propagation in multidirectional composite using VCCT method with the Timoshenko beam element with the displacement degrees of freedom is first formulated for a laminated composite beam and maximum deflection of a simple supported beam are compound with conventional plane element available in the commercial software it shows more advantage it shows numerical procedure for DCB specimens based on fracture mechanics using the virtual crack closure technique (VCCT). If there is small scale fiber bridging, the VCCT method with constant value of initiation fracture toughness predicts experimental data very well. In the case of large-scale bridging the fracture mechanics approaches alone are not suitable for delamination growth modeling. Therefore, the variable R-curve is proposed to link with the formulated finite element code [35].

Formulation developed for modeling crack propagation with an element without additional degrees of freedom DOFs, done by introducing constraint equation to extrapolate the strain fields of adjacent element to the element containing a crack. The extrapolation gives the transformation matrix to eliminate the slave nodes DOF from the global matrix, considering global stiffness keeps the same DOFs. The constraint equation are used to eliminate degree of freedom of slave node located at the crack face. While introducing new slave nodes for modeling cracks. The crack growth simulation doesn't increase the numbers of DOFs regardless of increased number of slave

nodes. Additional DOF elimination procedure for model I the cracked faced is named assumed displacement discontinuity finite element method (ADD-FEM) it compare with VCCT and show similar behavior especially under mode I and mode II, slight difference in mixed mode [36].

General condition of applying the VCCT in conjunction with commercial programs are presented, equation for three-dimension brick element and Algorithms of applying the VCCT are presented, general condition and limitation for using the VCCT with commercial software are provided. The complexity of the user sub routine depends on the output of the commercial FE solver. If all needed data are available FE analysis only little effect has to be made to calculate SIF [37].

Modified virtual crack closure technique (MVCCT) in the corporates with in the finite element method (FEM) is applied to investigates the delamination behavior between stacked copper bumps in 3D chip stacking packaging at package level and board level and the energy release rate at the delamination front is evaluated at the criterion of the crack expansion [38].

Fracture mechanics principle can be used to study the behavior of composite structure in presence of interlaminar damage and determine the condition for the delamination growth initiation. Crack closure method or two-step crack closure technique, two-step method referred as VCCT. Crack are extended or closed during two complete finite element analysis [14]. The method is based on the assumption the energy ΔE released when the crack is extended from a - Δa is identical to the energy required to close the crack. The Two-Step procedure is modified, to modified or virtual crack closure method (VCCT) with the assumptions as CCT & MVCCT is found to be more accurate to use for delamination of composite material [34]. Able to investigate displacement opening behind crack tip by developed interface element based on original modified crack closure integral. [31]Shows effectiveness of the VCCT to determine delamination of composite with an elliptical delamination front. Timoshenko beam element with displacement degree of freedom, with small scale of fiber bridging, it predicts very wall. Delamination behavior between stacked copper bump in 3D- chip staking packing. Using the formulation of VCCT to predict delamination of composite [38]. I am able to use VCCT or MVCCT on the characterization of delamination fracture of composite which is proven to be effective method [33].

1.3.4. Cohesive zone parameter

1.3.4.1. Stiffness of the cohesive zone model

Different guidelines have been proposed for selecting the stiffness of the interface, Calculating the stiffness in terms of the thickness and the elastic modulus of the interface. The resin-rich interface between plies is of the order of 10^{-5} m. Therefore, the interface stiffness obtained from the Daudeville et al [39]. Equations are very high. Zou et al. [40], Based on their own experience, proposed a value for the interface stiffness between 10^4 and 10^7 times the value of the interfacial strength per unit length. Camanho et al. [41] Obtained accurate predictions for graphite/epoxy specimens using a value of 10^6 N/mm3. For this paper A. Turon proposed equation is used （equ.23） a new equation for the selection of the interface stiffness parameter K was derived. The new equation is preferable to previous guidelines because it results from mechanical considerations rather than from experience. The approach provides an adequate stiffness to ensure a sufficiently stiff connection between two neighboring layers, while avoiding the possibility of spurious oscillations in the solution caused by overly stiff connections [42].

1.3.4.2. Length of cohesive zone

The length of the cohesive zone l_{cz} is defined as the distance from the crack tip to the point where the maximum cohesive traction is attained. Different models have been proposed in the literature to estimate the length of the cohesive zone. Irwin [43] estimated the size of the plastic zone ahead of a crack in a ductile solid by considering the crack tip zone where the von Mises equivalent stress exceeds the tensile yield stress. Dugdale [10]estimated the size of the yield zone ahead of a mode I crack in a thin plate of an elastic–perfectly plastic solid by idealizing the plastic region as a narrow strip extending ahead of the crack tip that is loaded by the yield traction. Barenblatt [15]. Provided an analogue for ideally brittle materials of the Dugdale plastic zone analysis. Hui et al. Estimated the length of the cohesive zone for soft elastic solids, Rice estimated the length of the cohesive zone as a function of the crack growth velocity. Studied the length of cohesive zone extensively [44]. It is pointed that there are many analytical cohesive zone length approximations variable from specimen to specimen. It is also stated that the main characteristics of all proposed length approximations have the same structure that is given as in equation 2.5 and suggested the minimum number of elements required for reaching converged solution should be more than two element concept from Turon are used for this study.

1.3.4.3. Traction model

Cohesive zone behavior bilinear traction-separation law (Fig. 1, a) is used because the curve is defined by only three parameters. Most common used traction laws in literature and experimental validation are the bilinear law, the trapezoidal law and the exponential law [18]. The selection of traction laws dependent on the type of experiment, geometry and material. A bilinear model is often preferred for brittle materials and delamination, which offers a good compromise between numerical performance, computational cost and accuracy of results. For ductile adhesives, a trapezoidal law is preferred [19] .

1.3.4.4. Delamination using CZM

The effective elastic properties of the whole laminate depend on the properties of both the cohesive surfaces and the bulk constitutive relations of the plies. Although the compliance of the cohesive surfaces can contribute to the global deformation, its only purpose is to simulate fracture. Moreover, the elastic properties of the cohesive surfaces are mesh-dependent because the surface relations exhibit an inherent length scale that is absent in homogeneous deformations [45].

Simulation of low velocity impact on fiber laminates using a cohesive zone based delamination, an existing delamination model is further developed for use in transverse impact simulations [45]. An algorithm is developed making it possible to determine the propagation direction of the delamination front. Using this it is possible to determine relative orientation of the delamination front with respect to the fibers above and below the interface. It develops the existing delamination for use of transverse impact simulation computing the direction of the delamination growth. It determines local fiber orientation how fibers above and below the interface are oriented relative to the propagation direction of the delamination front. In the analysis of the cross-ply laminated shaved that several different properties affected the size and shape of the delamination. The analysis is done on three and eight-layer laminate both show similar result. The cross-ply shows that several different properties affected the size and shape of the delamination. Size of the delamination depended mainly on the magnitude of the critical energy release rates while the shape of the delamination depends on several different properties. The orientation of the fibers below each interface makes the delamination extend in these directions. A slight peanut Shape is obtained if the interface was mad tougher perpendicular to the fibers below each interface. The delamination showed a better alignment with fiber orientations and also more characteristic peanut shapes were

obtained but general conclusions cannot yet be made without considering study including more materials layers' impact energies [45].

Discrete cohesive zone model for mixed-mode fracture using finite element analysis. The discrete cohesive zone model (DCZM) is implemented using the finite element (FE) method to simulate fracture initiation and subsequent growth. When material non-linear effects are significant. Different from the widely used continuum cohesive zone model (CCZM) where the cohesive zone model is implemented within continuum type elements and the cohesive law is applied at each integral point, DCZM uses rod type elements and applies the cohesive law as the rod internal force vs. nodal separation (or rod elongation). These rod elements have the provision of being represented as spring type elements and this is what is considered. A series of 1D interface elements was placed between node pairs along the intended fracture path to simulate fracture initiation and growth. Dummy nodes were introduced within the interface element to extract information regarding the mesh size and the crack path orientation. To illustrate the DCZM, three popular fracture test configurations were examined. In this study discrete cohesive zone model (DCZM) for mixed –mode fracture using finite element analysis [46].

An engineering solution for simulation of delamination using coarse mashes was developed, the methodologies proposed are relevance for the use of cohesive zone models in the simulation of delamination in large composite structure in the industry where the requirement of extremely fine mash cannot be meet. Coarse mashes in the simulating delamination is proposed by Turon [31], the procedure is procedure is based on an artificial strength while keeping the fracture toughness constant. A new equation for the selection of interface stiffens parameter K was derived. The equation is based on mechanical consideration rather than experience. the approach provides an adequate for ate stiffness to ensure a sufficiently stiff connection between two neighboring layers while avoiding the possibility of spurious oscillations in the solution caused by overly stiff connection. It was showed that a minimum number of element with in the cohesive zone is necessary for accurate simulation.by reducing the maximum interfacial strength the cohesive zone spans more element. The results show by reducing the maximum interface strength show that accurate results can be obtained with a mash ten times coarser than by using normal interface strength. The drawback the crack in using a reduced interfacial strength value is that the stress concentration in the bulk material near the crack tip are less accurate [42].

A.B.de Morais consider Williams mode crack length correction accounting crack root rotation and displacement in to considering to model the DCB specimen leg as beam. It discarding the shear foundation in pure mode specimen allows much simpler implementation of a cohesive beam model, and its application of FEA [47].

Discrete cohesive zone model for mixed fracture using finite element analysis material used for unidirectional fiber reinforced laminate consisting of 0◦ plies with their orientation aligned with the global x director. Mesh sensitivity are checked by using both biased meshes of 400 and 100 element and uniform meshes of 400 and 100 element bias factor of 1.05 and 1.15 respectively, from the analysis it concludes the DCZM is insensitive to the mesh size same for biases and uniform mesh all parameters are kept, with displacement increment (0.1mm, 0.01mm) where studied. As the displacement increment becomes fine the result appears to converge, therefore the current DCZM is also not sensitive to the displacement increment. At last simulation using DCZM is requires much simulation time that DCZM to implement in ABAQUS [46]

It shown that the bilinear CZM does not capture the model I delamination of laminated DCB specimen in the presence of large scale bridging and a three linear traction-separation is obtained for the unidirectional DCB specimens following procedure that only requires the experimental R-curve parameter i.e the initiation fracture toughness (G_i) ,the fracture process zone length (l_{FPZ}) and the steady state toughness (G_{ss}).Three-linear cohesive zone model is introduced for the simulation of fiber bridge phenomena [48].

Gaussian integration (GI) method and Newton Cotes integration (NCI) method are improved by considering increased number of integration points and various improved cohesive stress integration schemes. The improved integration methods can greatly improve the numerical accuracy, stability and roughness especially when mesh sizes are comparable to the cohesive zone size. Maximum cohesive element size as large as the cohesive zone size without significant compromise of the numerical accuracy [49].

Most of the delamination model was based on a cohesive zone model combination with an adhesively penalty contact for solid elements. The proposed model of delamination is based on a cohesive zone model in combination with an adhesive penalty contacts for shell elements, modifying this for shell elements only affected the adhesive penalty contact leaving the cohesive

zone model unchanged. The new model capable or useful tool for simulation of delamination initiation and growth on Double Cantilever Beam (DCB), End Notch Flexural (ENF) and Mixed Mode Bending (MMB) specimen, although applied to quasi-static conditions its intended use is for low velocity impacts on laminated plates. In such simulations it will be possible to model each individual lamina in a laminate with separate layers of shell element. Considerable time saving with respect to computing time is expected as well as detailed information on the delamination patterns. Reliable results will of course also need a constitutive equation for the in-plane response of the lamina material. Finally, being able to handle quasi-static conditions, it will be possible to examine residual strengths by simulation compressive tests on damaged laminates [50].

A discrete cohesive zone model has been developed and implemented in an explicit FE program. The model defined such that the allowable adhesive force are reduced by the amount of dissipated work. When a fracture criterion in terms of fracture energies is met the adhesive forces have been reduced to zero. Dissipated work is used to control the unloading path in the process zone (the model is defined such that the allowable adhesive forces and reduced by the amount of dissipated work) instead of using Damage formulation of discrete cohesive crack model. The normal Couse of mesh dependency in FE model is the localization of the softening behavior to an increasingly smaller region as the element size shrinks. While this model is based on a cohesive zone formulation no mesh dependency behavior of this kind is expected and none has been observed. The proposed model is capable of simulating delamination subjected to mode I, mode II and combined loading [51].

Delamination initiation and growth are analyzed by using discrete cohesive crack model. The delamination constrained to grow along a tied interface. Developing mathematical model for simulating delamination under simpler and combined loading in order to model delamination using discrete cohesive zone and damage formulation. Governing equation are based on a damage formulation. The delamination model has been implemented in the FE code LS-DYNA by explicit time integration. Using developed damage formulation leads for simpler and more robust implementation [52].

Effect of delamination in composite laminated have been considered in the context of continuum damage mechanics. Make use of appropriately constructed damaged surface. The damage evaluation law and incremental interfacial constitutive law on established. In this model does not require any new material properties other than those involved in conventional stress-based and fracture mechanics based failure criteria [53]**.**

Utilizing spring elements on the fracture presence zone to consider the residual strength of the damaged material in the fracture presence zone proposed model called multi- linear cohesive zone model I. using variable stiffness springs consider fracture proses zone (FPZ) affects the simulation of the initiation as propagation of model I delamination in laminated composite [54].

Delamination test have been modelled by means of TSEM (Two Stop Extension Model) implicit solver and CZM (Cohesive Zone Mode) explicit solver has been used. If the critical load is known the two stop extension model method is better than CZM to analyze and solve mixed model problems and if the critical energy release rates in the pure model I&II are known at the critical load unknown the proposed method to calculate the initiation (critical load) and crack propagation would be the CZM [55]**.**

Damage mechanics follow cracks or damage CZM works with the strain energy release rate, which acts as the fracture toughness and the cohesive fracture in an element as a function of relative displacement of opposing nodes. Cohesive law (traction- separate law) Constitutes behavior of displacement between two points and traction T as a curve. There are five mostly known traction law, bi-linear exponential trapezoidal and tri-linear laws [19, 18]. For this case bi-linear or triangular fracture is better option due to its simplicity and it is also recommended to predict delamination of composite [18]. CZM has two form smeared cohesive element and interface cohesive element, for those of the two interface cohesive element are preferred due to the zero thickness element, it treat the process zone head of crack trip as a continuous compliant layer therefore, a continuum cohesive zone model (CCZM). CCZM is useful for the pure mode of crack. CZM with combination with an adhesive penalty contact for stiff element used for law velocity impacts [35]. Multi-linear cohesive method utilizing the spring element on the fracture process zone to consider radial strength of the damage material [35]. Two step extension model with implicitly solver and CZM explicit solver can be used for critical load and critical energy release rates in the pure model are known respectively [55]. By artificial strengthening, where keeping the

fracture toughness constant, and reducing the maximum interface strength it shows that accurate results can be obtained with a mesh ten times coarse, it can be used when there is large composite structure, so our composite structure is not large, we can use dense mesh [50] . Discrete cohesive zone model (DCZM) it treat process zone as a discrete spring type foundation. DCZM are more important for adhesively bonded joint. DCZM are capable for mixed mode fracture [46], DCZM is not sensitive to the mesh size for bias mesh and uniform mesh develop DCZM has implemented in an explicit FE program [51]. For this study continuum cohesive zone is selected due to the above reason like useful for pure mode and our material assumed to have linear-effect continuum type of element and cohesive law is applied [46], dense mesh can be used because our composite material is not large [42].

1.3.4.5. Numerical method of delamination

using solid- shale element is particularly suitable to achieve the required accuracy especially in the thin shell like application are considered and he conclude the proposed method is capable of predicting the initiation of delamination of fiber reinforced composites in shell-like structure accounting for the anisotropic material behavior made solid-shell formulation for orthotropic behavior of fiber composites with woven fabric accounting for different fiber direction [56]**.**

It present influence of fiber bridging on fiber delamination growth, Fiber bridging has an influence on fatigue delamination resistance. Increase of fiber bridging crack growth rate da/dn verifying at a given G will decrease significantly and the corresponding resistance curve will shift from the left to the right in the resistance graph. The resistance is different from those of quasi- static delamination growth. The bridging criteria in fatigue delamination is different from that of quasi-static delamination of the same crack length,R-curve should not be used to normalize fatigue delamination However, there appears to be a steady state of bridging in fatigue delamination similar to the plateau state in quasi-static delamination growth after the bridging is fully developed. This means that the most right-hand resistance curve in the delamination resistance graph represents the crack growth resistance in the plateau state, with fully developed bridging. It is therefore recommended to investigate and establish the fatigue curves similar to quasi-static R-curves for fatigue delamination growth [57].

Influence of ply orientation on the resistance to model I delamination of multidirectional composite lamina is assessed by Double Cantilever Beam Using special staking sequences that allow the assessment of the influence of the fiber orientation without changing the whole elastic behavior of the specimen. Multidirectional DCB specimens were designed so as to obtain an uncoupled quasi-isotropic and quasi-homogeneous (QIQH) elastic behavior, with the same properties for the entire laminate and the two arms separated by the pre crack at mid-plane, The result shows the toughness in terms of G_{ic} is slightly affected by the variance of the ply orientation at the crack interface even with the same orientation at the crack interface, different subsequent ply orientations can also lead to different crack resistance behavior. The effect of ply orientation variations of both plies at the crack interface and the subsequent plies are more obvious in the crack propagation behavior after the initiation point [58].

Virtual crack closure technique is made for three dimensional finite element method for circular delamination embedded in woven and non-woven composite lamina. Computation of delamination and the prediction of delamination growth in laminated composite is proposed a methodology for prediction delamination growth in woven fabric composites using fatigue evaluation criteria. The direction of delamination growth generally coincides with the direction of maximum strain energy release rate; Sub-laminate lay-up sequence plays an important role in the distribution of local strain energy release rate components along the delamination front. The use of one-quarter models is popular because of significant reduction in computational effort, but will generally lead to erroneous results, particularly when material property symmetry is incompatible with symmetry conditions imposed on the boundaries. Even in the case of quasi-isotropic sub-laminates, the use of one-quarter models can lead to over-prediction of the values of SERR components. In cases where it is not possible to impose correct boundary conditions in one-quarter models, full models must be used instead and method for predicting delamination fatigue growth is proposed and illustrated, taking into account the accumulated damage along the delamination front. It is found that propagation criteria employing strain energy release rate components rather than total strain energy release rate give closer predictions [59].

During the experimental characterization of the mode I interlaminar fracture toughness of multidirectional composite laminates, the crack tends to migrate from the propagation plane (crack jumping) invalidating the tests. This problem could be eliminated by choosing the appropriate

bending stiffness of the beam arms. Using six multidirectional configurations were checked for crack jumping under mode I loading. The results showed that by increasing the flexural stiffness of the crack arms the crack jumping under mode I propagation can be avoided. The fracture toughness values were more affected by the fiber bridging than by the mismatch angles between the layers interfacing the crack plane. The measured effect of fiber bridging is 47% whereas the effect of the mismatch angle is 29%. The optical microscope images show that the delamination are not a truly interlaminar fractures. Instead, the fiber tearing is more common along the crack propagation path [60].

Predicting the delamination propagation in multidirectional laminates under model I and mixed model I/II loading using the cohesive elements. Three kind of multidirectional laminate with different interface $0^0/5^0$, $45^0/-45^0$ and $90^0/90^0$ were designed and both DCB and MMB experiment were carried out to investigate the simulation of delamination growth in multidirectional laminate and simulated with new proposed numerical model, the action of modeling parameter about martial, interface and computational aspect in the definition of cohesive element with bilinear constitutive law and reviews on their determination guidelines are depicted. Based on the parameter studies on unidirectional DCB specimen, a basic parameter choose element with large interface stiffness $1*10^{15}$, a small viscosity coefficient $1*10^{-5}$ and at least 3 cohesive elements in the cohesive zone is presented and it shows good agreements between the numerical and experimental results are obtained [61].

Experimental investigation on the test method for model II interlaminar fracture testing of carbon fiber reinforced composites are carried out. Model II interlaminar fracture testing of unidirectional composite of carbon/epoxy (T800/#3631) are conducted using end notched (ENF), end loaded split (ELS) test, four-point bend end notched flexural (4ENF) test and over notched flexural (ONF) tests. Experimental result show that ENF test gives reliable initiation value of fracture toughness with a small scatter and that the average value of fracture toughness obtained from 4ENF test is about 2% higher than that obtained from ENF test. The effect of friction between crack face in ONF test is serious and it increases as the crack grows. However, the effect of fracture predicted based on present analytical model is not sufficient to explain the larger difference of the experimental results between the ONF and ENF test. Friction between crack face is the present of

4ENF test has a slight influence on the evaluation of model II interlaminar fracture toughness of fiber reinforced composite [62].

In this paper he made three experiment on spray applied fire resistive material (SFRM) for modeling delamination of fire insulation from steel structure for characterizing cohesive stress displacement relationships in both model 1 and mode II delamination. It indicates noticeable strain softening zone verifying that SFRM is not a completely brittle material rather it is quasi brittle [63].

Compressive delamination model is developed with in the CDM frame work that accounts for the influence of sheer stress and hydraulic stress effects.as well as the fracture mode- mixed effects. Developed continuum level damage models with enhanced failure criteria that can capture progressive delamination in FRPs and eliminate the mesh dependency of ill posed constitutive reactions. It formulates CDM model for temporary sensitive for delamination analysis of FRPs and develop model is capable of applying model I, mode II and mixed –mode delamination with coinciding dynamic loading effects on the progressive delamination [64].

Ted Diehl presented impressively accurate simulations of failure in surface-bonded structures using the new cohesive element technology in ABAQUS A rationale has been shown for how to relate classical energy release methods which assume zero cohesive compliance to the compliance-based method implemented in ABAQUS. A practical approach has been derived and demonstrated to address the problematic issue of determining numerous cohesive element properties when only a single input is known, the critical fracture energy G_c and a penalty parameter defining the cohesive ductility. It was further shown that sizing cohesive ductility penalty must be done relative to the level of detail desired in the model [65].

Fiber bridging on fiber delamination growth investigation due to influence of fatigue shows bridging critics in fatigue delamination is different from quasi- static delamination (R-curve). But at steady state of bridging in fatigue delamination R-curve can be used [57]for our case R-curve can be used without considering fatigue delamination. Taking accumulated damage along the delamination front it is found that propagation critical strain energy release rate gives closer production than total strain energy release rate [59]. For circular delamination embedded in a woven and non-woven composite lamina Quasi-isotropic, sub-lamina the use of one-quarter models that can lead to over prediction of the value of SERR, full models must be used for

prediction of delamination [59]. Numerous model proposed to investigate multidirectional under model I and mixed model I/II load using the cohesive element [61] and experimental challenges of model I inter laminar fracture toughness of multidirectional composite lamina choosing the appropriate bending stiffness of the beam arms and can eliminate crack jumping [60]. Experimental investigation on the test method for mode II interlaminar fracture of using four test methods ENF, 4EN, ON & ELS. ONF shows friction between crack face is serious and it increases as the crack grows [62]. Ply orientation slightly affected crack interface and it's lighter for crack propagation than initiation [58] and sub-laminar layup sequence play on important role in the distribution of local strain energy release rate components along the delamination front.

1.5. Problem statements

From the Literature review we can have brief discussion of composite material for automotive application, due to light weight, high stiffness composite is used to benefit from those behavior. There was plenty development on delamination of composite using analytical and numerical analysis, But there exist significant difference between theoretically determined and numerically found [30,38,39], due to complex behavior of composite it still need more research on delamination of composite material, so it is important to performing numerical analysis on delamination of composite, major problem of composite material for different automotive application. For This specific research fiber glass epoxy composite are developed and delamination is conducted using VCCT and cohesive zone method.

1.6. Objectives

1.6.1. General objectives

The general objective of this research is developing Composite material for automotive application and Mode I delamination of composite by Virtual Crack Closure Technique and Cohesive method.

1.6.2. Specific objectives

The specific objectives of the research are

- Developing Composite Material using Autodesk simulation software
  - Material 3D and 2D material development
  - Material stress to strain behavior development
  - Material first ply failure
  - Material progressive ply failure
- Mode I delamination of composite by VCCT method
  - Finding lode-displacement relation
  - Finding suitable dumping and viscosity
- Mode I delamination of composite by cohesive zone method
  - Extracting the traction separation behavior of the cohesive element
  - Investigating delamination growth
  - Finding appropriate cohesive interface element
  - Finding suitable penalty stiffness and interface strength
  - Finding lode-displacement relation

1.7. Scope of the study

As limitation we can have more points:

- Time limitation of working on Mode II and mixed mode.
- Even though there are different material used for automotive application we are limited on the selected one of the material

Composite in automotive industry there are more than two applications, but we are limited on one of application used on the automotive industry

1.8. Organization of the paper

This thesis work is organized in to five chapters. The first chapter, includes introduction which gives some background information on the overall idea behind this work, a review of literatures relevant to this thesis work, which can lay the background for the work to be done, statement of the problem based on the existing gap that is observed, general and specific objectives to be achieved at the end of this work.

In chapter two developing composite material and delamination modeling the methodology applied, the assumptions considered, the materials selected and designing composite lamina, analytical methods in modeling of double cantilever beam, characterization of delamination using virtual crack closure technique and characterization of delamination using cohesive zone method.

In chapter three all necessary step to model double cantilever beam on detail in ABAQUS @ 10.14 for both cohesive zone method and for virtual crack closure method.

In chapter four the results and discussion of the analysis, Quas-isotropic 2D and 3D material property as the well stiffness of the material from Autodesk Simulation composite Design @ 2014, Abaqus 10.14 simulation result. It also includes different plots to illustrate the results and the meaning of the results is discussed comparing it to a previous work and result.

In chapter five, conclusions based on the result are made and future works to be done on this area are suggested

Chapter Two

2. Developing Material and Numerical Modeling of Delamination

2.1. Developing composite material using Autodesk composite design

2.1.1. Fiber Glass property

For the purpose I have selected E-Glass fiber in order to have good tensile and compressive strength and stiffness, good electrical property and relatively low cost. E-Glass fiber with mechanical property specified on table 2.1 are taken. Glass fibers are among the most versatile industrial materials known today.

Table 2. 1. E-Glass fiber mechanical property [23].

Name:	E-Glass
Title	Value
E11 (MPa)	7.24E+04
E22 (MPa)	7.24E+04
G12 (MPa)	3.03E+04
G23 (MPa)	3.03E+04
NU12	2.00E-01
NU23	2.00E-01
CTE1 (mm/mm/C)	4.90E-06
CTE2 (mm/mm/C)	4.90E-06
+S1 (MPa)	2.15E+03
-S1 (MPa)	-1.45E+03
K1 (W/mm/K)	1.28E-03
K2 (W/mm/K)	1.28E-03
Density (g/mm3)	2.60E-03

2.1.2. Matrix Property

Polymer thermosetting type of matrix are used in order to gain higher mechanical property and resistance to environment degradation. Standard 8552 Epoxy are used with mechanical property of listed on table 2.2. 8552 is an amine cured, toughened epoxy resin system with unidirectional or woven carbon or glass fibers.8552 is recommended for structural applications requiring high strength, stiffness, and damage Tolerance. 8552 was developed as a low flow system to operate in environments of up to 250°F, Impact Tolerant and Low Flow.

Table 2. 2 Epoxy mechanical property [27].

Name:	8552 Epoxy
Title	Value
E11 (MPa)	7.24E+03
E22 (MPa)	7.24E+03
G12 (MPa)	2.68E+03
NU12	3.50E-01
NU23	3.50E-01
+S1 (MPa)	7.09E+01
-S1 (MPa)	-2.12E+02
S12 (MPa)	8.32E+01
K1 (W/mm/K)	0.00E+00
Density (g/mm3)	1.26E-03

2.1.3. Lamina stacking sequence

Lamina stacking sequence are organized In order to get homogenous lamina stacking sequence. Lamina stacking sequence have four distinct evenly distributed ply angle through lamina thickness and laminate contains equal numbers of plies in each orientation (balanced) and laminates are arranged to have the plies 0n either side of a mid-plane matching in both material and orientation (symmetric).Quasi-Isotropic material with stacking sequence of $[(-45^0,45^0,90_2^0, 0_2^0)_2]_s$ and V_f=60 are developed table 2.3.

Table 2. 3. Lamina stacking sequence

Name:	quasi isotropic tem
Thickness (mm)	Angle
1.25E-01	4.50E+01
1.25E-01	4.50E+01
1.25E-01	-4.50E+01
1.25E-01	-4.50E+01
1.25E-01	0.00E+00
1.25E-01	0.00E+00
1.25E-01	0.00E+00
1.25E-01	0.00E+00
1.25E-01	9.00E+01
1.25E-01	9.00E+01
1.25E-01	9.00E+01
1.25E-01	9.00E+01
1.25E-01	9.00E+01
1.25E-01	9.00E+01
1.25E-01	9.00E+01
1.25E-01	9.00E+01
1.25E-01	0.00E+00
1.25E-01	0.00E+00
1.25E-01	0.00E+00
1.25E-01	0.00E+00
1.25E-01	-4.50E+01
1.25E-01	-4.50E+01
1.25E-01	4.50E+01
1.25E-01	4.50E+01

2.2. Numerical characterization of delamination using VCCT

2.2.1. Virtual crack closure technique

A delamination can be assimilated to a fracture process between anisotropic layers. Thus, fracture mechanics principles can be used to study the behavior of composite structures in presence of delamination damage and to determine the conditions for the delamination growth initiation. VCCT is advantageous as it allows the strain energy release rate to be determined with simple

equations from a single (FE) analysis, but pre-existing of the initially debonded surface along a predefined delamination front is compulsory.

Crack closure method or *two-step crack closure technique*. The terminology in the literature is often inexact and this two-step method is sometimes referred to as VCCT. It may be more appropriate to call the method the *crack closure method* because the crack is physically extended, or closed, during two complete finite element analyses. VCCT approach was based on two assumptions 1st Irwin's assumption that the energy released in crack growth is equal to the work required to close the crack to its original length, and 2nd, that crack growth does not significant alter the state at the crack tip (self-similarity state), this mean the energy ΔE released when the crack is extended by Δa from a [Fig.2.1.a] to $a+\Delta a$ [Fig. 2.1.*b]* is identical to the energy required to close the crack between location, and i [Fig 2.1.*a]*. Index 1 denotes the first step depicted in Fig.2.1 *a* and index 2 the second step as shown in Fig 2.1.*b*. For a crack modeled with two-dimensional four-nodded elements as shown in Fig.2.1 the work ΔE required to close the crack along one element side can be calculated as

$$\Delta E = \frac{1}{2}[X_{1\ell}\Delta u_{2\ell} + Z_{1\ell}\Delta w_{2\ell}] \text{.....Eqn 2. 1}$$

Where $X1_{\ell}$, and $Z1_{\ell}$, are the shear and opening forces at nodal point, to be closed [Fig. 2.1*a*] and $\Delta u2$, and $\Delta w2$, are the differences in shear and opening nodal displacements at node, as shown in Fig. 2.1.*b*. The crack closure method establishes the original condition before the crack was extended. Therefore, the forces required to close the crack are identical to the forces acting on the upper and lower surfaces of the closed crack. The forces $X1_{\ell}$, and $Z1_{\ell}$, may be obtained from a first finite element analysis where the crack is closed as shown in Fig. (2.1*a*) by summing the forces at common nodes from elements belonging either to the upper or the lower

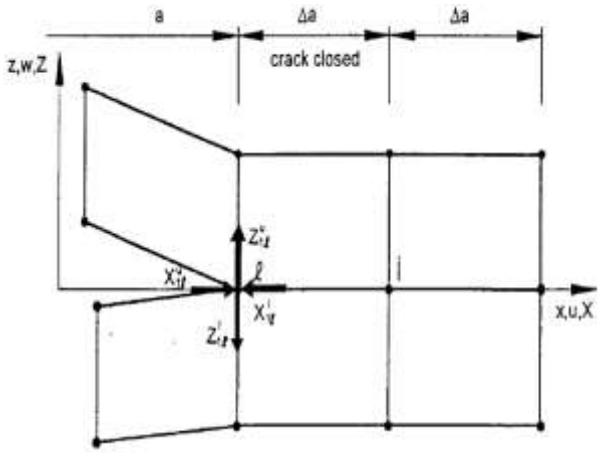

Where $Z^1{}_{1\ell} = Z^u{}_{1\ell}$ and $X^1{}_{1\ell} = X^u{}_{1\ell}$ from equilibrium

a. First step-crack closure

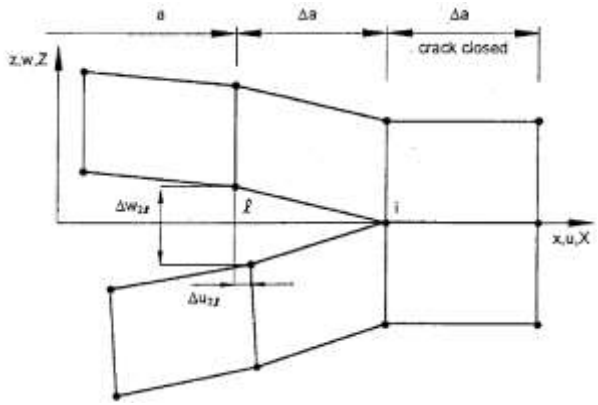

a. Second –Step crack closure

Fig 2. 1. Crack closure method -two-step method! a, first step-crack closed and b, second step crack extended [14].

The calculation of the Energy can be simplified by adopting an alternative approach the one step Virtual Crack Closure Technique (VCCT). The VCCT is based on the assumption that an infinitesimal crack extension has negligible effects on the crack front therefore both stress and displacement can be evaluated within the same configuration by performing only one analysis. It is assumed that a crack extension of Δa from a+Δa (node i) to a+2Δa (node k) does not significantly alter the state at the crack tip Fig.2.2.

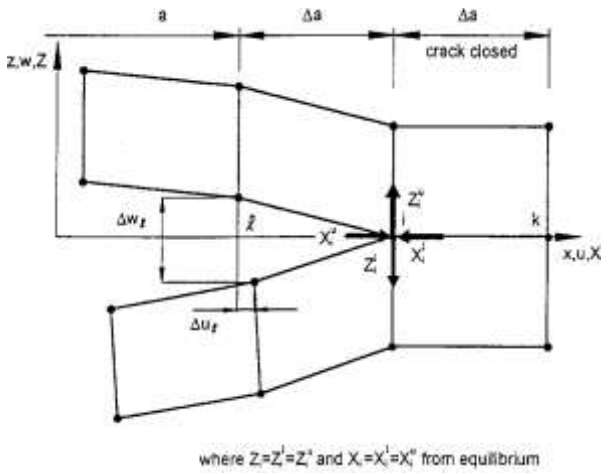

Fig 2. 2. Modified crack closure method (one step VCCT) [14].

2.2.2. Formula for two-dimensional analysis

In a two-dimensional finite element plane stress, or plane strain model, the crack of length a is represented as a one dimensional discontinuity by a line of nodes as shown in Fig.2.3a

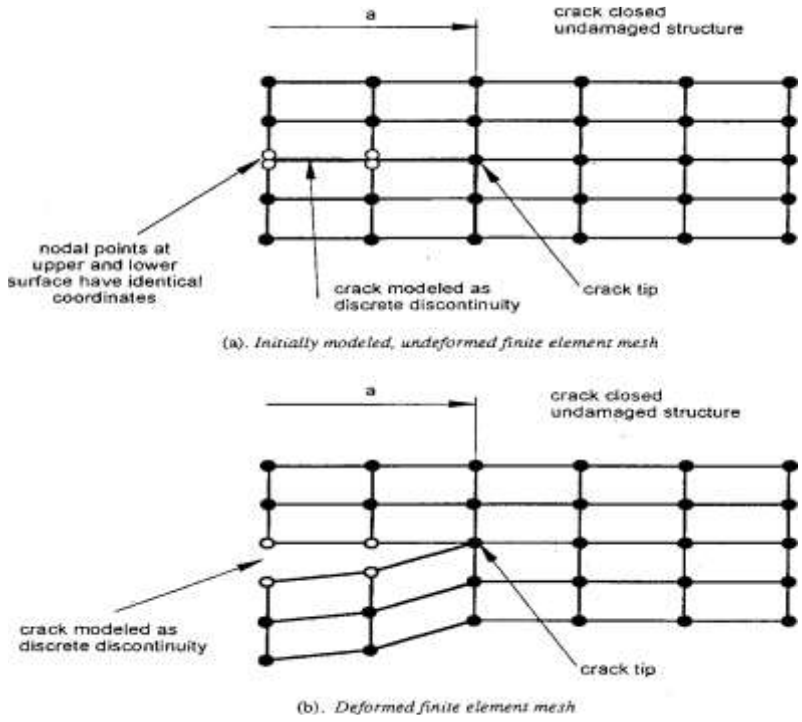

Fig 2. 3. Crack modeled as one-dimensional discontinuity. A, initially modeled, unreformed finite element mesh and deformed finite element mesh [42]

2D finite element model in the X-Y plane imposes the out of plane stresses to be zero

$\sigma_{zz}= \tau_{xy}= \tau_{yz}=0$ and allows the displacement to be the free parameter. Plan strain imposes the out of plane strains to be zero,$0 = \varepsilon_{zz}=\gamma_{zy}=\gamma_{yz}$ which excessively constrains the plies

For a crack propagation analysis, it is important to advance the crack in a kinematically compatible way. Node wise opening/closing, where node after node is sequentially released along the crack, is possible for the four-noded element. It is identical to element wise opening in this case as the crack is opened over the entire length of the element. Node wise opening/closing, however, results in kinematically incompatible interpenetration for the eight-noded elements with quadratic shape functions, which caused initial problems when eight-noded elements were used in connection with the virtual crack closure technique. Element wise opening-where edge and midside nodes are released-provides a kinematically compatible condition and yields reliable results. The mode I and mode II components four-noded elements as shown in the fig.2.4 a

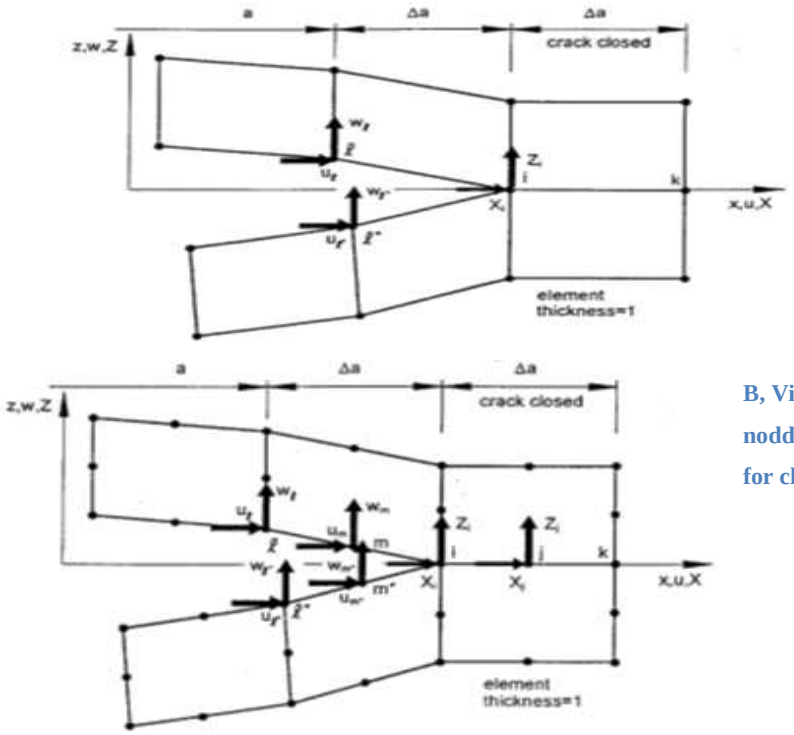

A, Virtual Crack Closure Technique for four nodded elements (lower forces are omitted clarity)

B, Virtual Crack Closure Technique for eight-nodded element (lower surface forces are omited for clarity)

Fig 2. 4. Virtual crack closure technique for 2D solid elements. a! Virtual crack closure technique for four-noded element (lower surface forces are omitted for clarity) and b (virtual crack closure technique for eight-noded element) lower surface forces are omitted for clarity [42]

Element length Δa for the element in front of the crack tip and behind are identical once automatic mesh generator are used.

2.3. Numerical characterization of delamination using CZM

2.3.1. Cohesive zone model

Cohesive zone (CZ) modeling is an emerging technology capable of simulating crack initiation in addition `to crack propagation. Therefore, a major advantage of cohesive zone theory over fracture mechanics theory is that CZ analysis does not require knowledge of starter crack size and geometry. CZ models have been used to simulate several types of interfaces, including integrated thin-film structures, adhesively bonded polymers, glass/elastomer, and on-chip interfaces. Here I have applied a CZ technique to model delamination between lamina of quasi-isotropic E-glass epoxy.

2.3.2. Cohesive zone approach

The formulation of the cohesive finite elements is based in the Cohesive Zone Model (CZM) approach. The CZM approach is one of the most commonly used tools to investigate delamination. The CZM approach assumes that a cohesive damage zone develops near the crack tip. The CZM links the microstructural failure mechanism to the continuum fields governing bulk deformations. Thus, a CZM is characterized by the properties of the bulk material, the crack initiation condition, and the crack evolution function.

Cohesive damage zone models relate cohesive surface tractions, τ, to displacement jumps, Δ, at n interface where a crack may occur. Damage initiation is related to the interfacial strength, τ^0, the maximum traction on the traction–displacement jump relation. The area under the traction–displacement jump relation is equal to the fracture toughness, G_c. There are several types of constitutive equations used in cohesive elements: trapezoidal law, perfectly plastic rule, polynomial law and later an exponential law. The law used in this paper is a bilinear relation between the tractions and the displacement jumps Figure 2.5. The slope of the constitutive equation before damage initiation, K, is refereed as the interface stiffness.

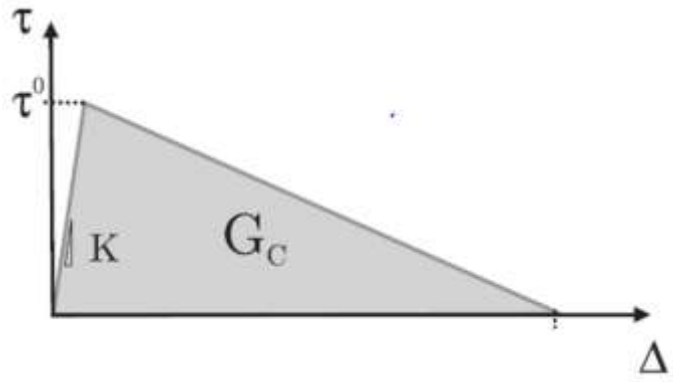

Fig 2. 5. Bilinear relation traction–separation law

2.3.3. Cohesive zone model and FEM

In a finite element model using the CZM approach, the complete material description is separated into fracture properties captured by the constitutive model of the cohesive surface and the properties of the bulk material, captured by the continuum regions. To obtain a successful FEM simulation using CZM, two conditions must be met: (a) The cohesive contribution to the global compliance before crack propagation should be small enough to avoid the introduction of a fictitious compliance to the model, and (b) the element size must be less than the cohesive zone length.

2.3.4. Stiffness of cohesive zone model

Different guidelines have been proposed for selecting the stiffness of the interface. Daudeville et al. [26] calculated the stiffness in terms of the thickness and the elastic modulus of the interface. The resin-rich interface between plies is of the order of 10^{-5} m. Therefore, the interface stiffness obtained from the Daudeville et al. equations is very high. Zou et al. [27], based on their own experience, proposed a value for the interface stiffness between 10^4 and 10^7 times the value of the interfacial strength per unit length. Camanho et al. [9] obtained accurate predictions for graphite/epoxy specimens using a value of 10^6 N/mm^3.

The effective elastic properties of the whole laminate depend on the properties of both the cohesive surfaces and the bulk constitutive relations of the plies. Although the compliance of the cohesive surfaces can contribute to the global deformation, its only purpose is to simulate fracture. Moreover, the elastic properties of the cohesive surfaces are mesh-dependent because the surface relations exhibit an inherent length scale that is absent in homogeneous deformations. If the

cohesive contribution to the compliance is not small enough compared to that of the volumetric constitutive relation, a stiff connection between two neighboring layers before delamination initiation is not assured. The effect of compliance of the interface on the bulk properties of a laminate is illustrated in the 1D model. The equilibrium condition requires

$$\sigma = E_{3\epsilon} = k\Delta \quad \text{.....Eqn 2. 2}$$

Where σ is the traction on the surface, t is the thickness of an adjacent sub-laminate, ε= δt/t is the transverse strain, K is the interface stiffness that relates the resulting tractions at the interface with the opening displacement Δ, and E_3 is the through-the-thickness Young's modulus of the material. For a transversely isotropic material $E_3 = E_2$. The effective strain of the composite is

$$\epsilon_{eff} = \frac{\delta t}{t} + \frac{\Delta}{t} = \varepsilon + \frac{\Delta}{t} \quad \text{.....Eqn 2. 3}$$

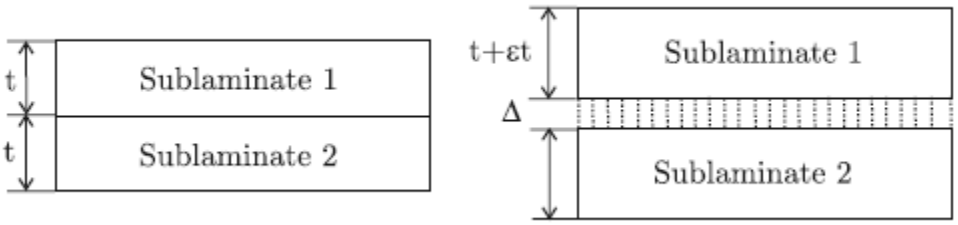

Fig 2. 6. Two sub laminate are connected by cohesive element

Since the equilibrium condition requires that r = Eeffeeff, the equivalent Young's modulus E_{eff} can be written as a function of the Young's modulus of the material, the mesh size, and the interface stiffness. Using Eqs. (2.2) and (2.3), the effective Young's modulus can be written as

$$\varepsilon eff = E_3\left(\frac{1}{1+\frac{E_3}{K_t}}\right) \quad \text{.....Eqn 2. 4}$$

The effective elastic properties of the composite will not be affected by the cohesive surface whenever $E_3 \ll K_3$, i.e.,

$$k = \frac{\alpha E3}{t} \quad \text{.....Eqn 2. 5.}$$

Where α is a parameter much larger than 1 (α » 1). However, large values of the interface stiffness may cause numerical problems, such as spurious oscillations of the tractions.

Thus, the interface stiffness should be large enough to provide a reasonable stiffness but small enough to reduce the risk of numerical problems such as spurious oscillations of the tractions in an element. For values of α greater than 50, the loss of stiffness due to the presence of the interface is less than 2%, which is sufficiently accurate for most problems.

The use of Eq.2.5 is preferable to the guidelines presented in previous works, because it results from mechanical considerations, and the resulting value of K does not significantly affect the compliance of the composite.

The spurious oscillations of the tractions resulting from an excessively stiff interface and Gauss integration scheme are avoided by calculating the interface stiffness using Eq.2.5, using linear shape functions and Newton–Cotes integration scheme.

2.3.5. Length of cohesive zone

The boundary of cohesive zone was implied the distance from the maximum attained traction to the zero traction. It is shown as Γ, defining the cohesive zone as the detailed view given on a DCB specimen in **Fig**.2.5 Hence, the region bounded by the points 2 to 4 defines the softening of the interface; the cohesive zone. The length of the cohesive zone l_{CZ} is defined as the distance from the crack tip to the point where the maximum cohesive traction is attained.

$$\ell_{CZ=} ME \frac{G_C}{(\tau^0)^2} \quad \text{.....Eqn 2. 6}$$

ℓ_{CZ} Cohesive zone length

M Cohesive zone parameter

E Transverse module of material

τ^0 Maximum interfacial strength

In order to obtain accurate FEM results using CZM, the tractions in the cohesive zone must be represented properly by the finite element spatial discretization. The number of elements in the cohesive zone is, a minimum number of elements, Ne, is needed in the cohesive zone to get successful FEM results. Therefore, three elements in the cohesive zone were sufficient to predict the propagation of delamination in mode I. Studies in Refs. [68,71,75] using cohesive elements on delamination analyses have proven that 3 elements are sufficient to predict the delamination under mode I loading. Harper et al. [16] provided a more detailed investigation for mode I, mode II and

mixed-mode loadings and suggested the Ne, min between 1.2 and 2.4, between 2.05 and 2.73 for accurate analyses of the DCB and ENF specimens, respectively.

$$N_e = \frac{\ell_{CZ}}{\ell_e} \quad \text{.....Eqn 2. 7}$$

ℓ_e Mesh size in the direction of crack

N_e Number of element in the cohesive zone,

2.3.6. Interface strength

In the past, appropriate interface strength was mainly adopted to improve the computational efficiency without losing the simulation accuracy for the damage onset. However, this is only meaningful for supporting damage growth scenarios which have an initial crack and are governed by G_C values. Interface strength in the CZM cannot be completely validated by present approaches owing to the difficulties to accurately determine the very onset delamination traction follow from which the interface strength is usually replaced by the corresponding interlaminar strength. However, this replacement achieves good predictions only in few literatures while significant prediction deviations compared with test data have been reported in more literatures, especially for the structural load–displacement response. The strength of the resin is directly relevant to the interface strength. Usually, higher interface strength can be obtained if a tougher resin is used in laminates. Referring to the strength of typical epoxy matrix materials considered a reduction of the interface strength will enlarge the cohesive zone while a big one may even arrest the delamination growth. Thus they adopted the interface strength of 45 MPa for glass fiber/epoxy or 60Mpa

It is possible to develop a strategy to adapt the length of the cohesive zone to a given mesh size. The procedure consists of determining the value τ^o of the interfacial strength required for a desired number of elements Ne in the cohesive zone. The required interface strength is

$$\bar{\tau}^0 \sqrt{\frac{9\pi E G_C}{32 N_e{}^0 \ell_e}} \quad \text{.....Eqn 2. 8}$$

Finally, the interfacial strength is chosen as

$$\boldsymbol{T = min\{\tau^0 \bar{\tau}^0\}} \quad \text{.....Eqn 2. 9}$$

2.3.7. Viscosity coefficient

Material softening and stiffness degradation in the process of loading may lead to convergence difficulties when cohesive elements are used in the CZM. the viscosity makes the solution rate dependent and introduces additional energy dissipation into the computations, the effect of a value small enough compared with the characteristic time increment does not result in a compromising prediction, since for a value small enough the viscous energy dissipation can be ignored during a stable crack propagation. Computational costs, influences on predictions and the numerical solution convergence are three crucial aspects to determine the optimal viscosity coefficient. Obtained numerical results which were independent on the viscosity coefficient if a value ranging from 10^{-5} to 10^{-3} were recommended for delamination analysis.

2.3.8. Cohesive interface element

The cohesive elements are modeled as an own separate part of the model. Cohesive zone elements can be modelled as a flat interface element, having no volume in 3D or no surface in 2D, or bulk element, having a finite volume in 3D or finite surface in 2D. As a flat interface element, they are still modelled as eight-nodded element in 3D or as a four-noded element in 2D for example. A cohesive zone element can be approach analytically and be related to its traction, volume and body forces, the cohesive layer is one element layer thick in between the regions where the crack is to advance. For two-dimensional modeling, the four-node cohesive element COH2D4 is used. The cohesive element has a linear displacement formulation and the stress in the third direction does not act the element behavior and thus there is no deference between plane stress and plane strain condition. The separations and stresses in the cohesive elements are calculated in each increment at the integration points according to the traction-separation law.

When the critical separation energy is reached, the element has failed. The integration point which contributes to the stiffness obtains the status "failed". Once a integration point has lost its stiffness, it will never obtain another status.

2.3.9. CZM modeling in ABAQUS /EXPLISITE

The modeling approach essentially follows the described by Diehl (2005). The cohesive failure of the epoxy bond was modeled with zero thickness layer of cohesive element using a cohesive over meshing factor of 5. The traction separation characterization of cohesive elements is depicted in

fig…..the physical parameter governing the cohesive material law is $G_{c.}$ assuming isotropic cohesive behavior, this is defined in ABAQUS model via

*DAMAGE EVOLUTION, TYPE=ENERGY, MIXED MODE BEHAVIOR=BK, POWER=1.0

G_C,G_C, G_C

For isotropic behavior, the BK mixed mode behavior option (ABAQUS, 2013) is the easiest choice relative to be the same (isotropic), the value of the related power term (required input for BK, set to 1.0 here) will have no actual effect on the solution.

The ABAQUS cohesive element material law is described by the shape of triangle, and thus definition of G_c alone is not sufficient. Critical release energy is related to the cohesive material's effective ultimate nominal stress, T_{ul}, and cohesive ductility (failure separation) $\delta_{f\ via}$

$$G_c = \frac{T_{ult}\delta_f}{2} \text{.....Eqn 2. 10}$$

Fig…depicts an interpretation of a traction-separation law applicable to the classical Griffith energy release approach for which the bond is assumed to be infinitely rigid until failure, at which time a finite energy is released per unit crack growth. In this interpretation, taking the limit as the cohesive ductility, δ_f approaches zero results in an impulse function. This is deemed a reasonable interpretation of a classical Griffith energy criterion. Thus in the finite element cohesive material model, i view the cohesive ductility as a penalty parameter that we desire to make as small as possible until the numerical solution become ill-behaved. As stated by Diehl, mesh-relative cohesive ductility is the best measure of the penalty parameter intensity.

Having defined a range of $\delta_{f,}$ and knowing the value of G_c, we utilize Equ.2.10 To compute the effective ultimate nominal stress, T_{ult}, of the cohesive material. This data is entered via

*DAMAGE INITIATION, CRITERION = MAXS

Tult, Tult, Tult

Remember that this is not a physical material parameter,but rather a penalty term. It is not the ultimate stress of a bulk version of the bond material.

Initial material stiffness per unit area, K_{eff}, is simply

$$K_{eff} = \frac{T_{ult}}{\delta_o} \quad \text{.....Eqn 2. 11}$$

Defining the damage initiation ratio as

$$\delta_{ratio} = \frac{\delta_o}{\delta_f} \quad \text{.....Eqn 2. 12}$$

Provides a simple scalar variable ranging between 0 to 1for defining when damage initiates. Combining equation…..shows that

$$K_{eff} = \frac{2G_c}{\delta_{ratio}\delta_f} \quad \text{.....Eqn 2. 13}$$

The value of the effective elastic modulus of the cohesive material, E_{eff}, is related to K_{eff} via

$$E_{eff} = K_{eff} h_{eff} \quad \text{.....Eqn 2. 14}$$

Where h_{eff} is the initial effective constitutive thickness of the cohesive element. There are two options of how this thickness is defined in ABAQUS. One option is to have it defined by the actual geometric thickness derived from the nodal definitions defining the cohesive element (via *Cohesive Section, Thickness= Geometry). For many surface bonding application this approach is highly problematic because the actual physical thickness of the bond (or bond material) is ill-defined or unknown. Another option is to define the geometric thickness (via nodal locations) as zero or any value that is deemed appropriate and then to manually define a constitutive thickness on the *Cohesive Section card via the **Thickness= Specified** option. This later approach is the default method. A useful technique is to specify a unity constitutive thickness so that the effective modulus, which is entered on the *Elastic card, is actually the initial cohesive material stiffness per unit area. It also means that the strains reported in the output database for the cohesive elements are actually the separation values, δ.

From the Griffith energy release viewpoint, the cohesive element is simply representing the failure surface and thus has no thickness. Using the penalty framework for cohesive elements, it is best to directly modal bond compliance with solid elements and to utilize the cohesive elements to strictly modal an idealized zero-thickness peeling. Hence, we define the "nodal" cohesive thicknesses as zero and utilize a unity value for the user specified thickness h_{eff}.

*COHESIVE SECTION, RESPONSE=TRACTION SEPARATION, YHICKNESS=SPECIFIED,

ELSET=Glue, Material= Bond

1.0

Assuming a damage initiation ratio δ_{ratio}=0.5 and utilizing Equation…..and….., we can comput the effective elastic modulus, E_{eff}, which is then entered via

*ELASTIC, TYPE= TRACTION

E_{eff}, E_{eff}, E_{eff}

Since we have chosen an Explicit modeling approach, we must supply a material density for the zero-thickness bond surface. This is not the density of epoxy, but rather another numerical penalty parameter for the cohesive element. I simply compute an effective density so that the cohesive material does not, in general, unnecessarily constrain the solution time increment that the problem would otherwise require. The effective density, ρ_{eff} of the cohesive material is computed via

$$\rho_{eff} = E_{eff}\left(\frac{\Delta t_{stable}}{f_{t2D}h_{eff}}\right)^2 \quad \text{.....Eqn 2. 15}$$

Where the stable time scale factor for 2D cohesive elements in ABAQUS is f_{t2D}=0.32213(for cohesive elements whose original nodal coordinates relate to zero element thickness) and Δt_{stable} is the initial stable time increment without cohesive elements in the modal. The value of ρ_{eff} computed in this manner should be checked to make sure that it is not imposing too much mass in the bond area relative to the local mass of the surrounding structural materials. It is further noted that for ABAQUS version 6.13, additional density scale-up factors were utilized for certain cases to address some solution inefficiencies caused by an over-conservative time step estimation algorithm in ABAQUS. It is also noted the stable time scale factor which ABAQUS uses for

cohesive elements (f_{t2D}=0.32213) is potentially too conservative (making the solution unnecessarily inefficient). These problems have been identified to ABAQUS developers and should be addressed in a future release.

Lastly, upon complete material failure of a given cohesive element, it is desirable to direct the code to remove the failed element from the solution via

*SECTION CONTROLS, NAME = GLUE-CONTROLS, DELETION=YES

This option is the default behavior in ABAQUS. It is recommended that the user not override this setting to allow failed cohesive element to remain in the solution. Doing so can create excessively slow solution caused by inappropriate time increment estimates and can potentially create large numerical distortions caused by improper application of bulk viscosity damping on failed element.

2.4. Analytical method

The DCB test is compared with the analytically approximated solution in order to judge the accuracy of the study. From corrected beam theory and the definition of energy release rate. To start the analytical solution, one can consider one of the arms as a cantilever beam in which the length of initial crack length a_o as shown in Fig.2.7.

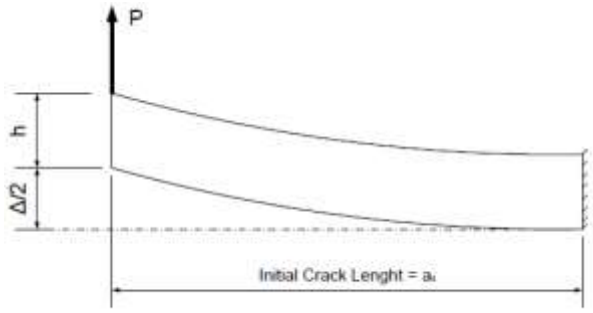

Fig 2. 7. One of arm is treated as cantilever beam.

One of arms is treated as cantilever beam. From fundamental elastic beam theory, one can find the deflection of the cantilever beam applicable for a DCB arm actually, modulus (*E*) in the above equation is the modulus works along the beam, therefore, $E = E_{11}$. Moreover, inertia (*I*) is for simple rectangular cross-section; $Bh3/12$ where *B* is the width and *h* is the thickness of the arm

$$\frac{\Delta}{2} = \frac{pa_0^3}{3EI} \quad \text{.....Eqn 2. 16}$$

In reality, the clamped surface is being rotated‖ during the loading due to the shear deformation of the assumed clamped‖ elastic arm. As a result, the fixed clamped arm assumption would result in stiffer results than the real case. Consequently, a corrected beam theory is proposed by Williams et al. [44] who modified the crack length with a *correction parameter*, χ_I (Noting the subscript x_I‖ which is used here is for defining the mode of the correction factor).

$$\Delta_I = \frac{2p(a_0 + X_I h)}{3E_{11}I} \quad \text{.....Eqn 2. 17}$$

Where, the correction parameter, χ_I can be found both by experimentally or analytically. *For this* study takes the analytical solution as follows

$$X_I = \sqrt{\frac{E_{11}}{11G_{13}}}\left[3 - 2\left(\frac{\Gamma}{1+\Gamma}\right)^2\right] \quad \text{.....Eqn 2. 18}$$

Where

$\Gamma = 1.18\frac{\sqrt{E_{11}E_{22}}}{G_{13}}$ ……..Eqn 2. 19

One can observe that the relation between tip load *P* and tip displacement Δ is linear. Actually, as the load *P* increases, the displacement increases linearly.

From the damage mechanics literature, the load can be increased until the cohesive element started to soften. Until the energy release rate *GI* reaches the mode I critical energy release rate, *GIc*. Therefore, the energy release rate is defined as and *GI using characteristics length (L_c) is shown on Equ. 2.21*.

$G_{Ic} = \frac{P^2(a+X_I h)^2}{BE_{11}I}$ ……..Eqn 2. 20

$G_{IC} = \frac{1}{2}\sigma_Y \epsilon_Y L_C$ ……..Eqn 2. 21

Noting that, the initial crack length a_0 in Eqn. 2.20 is replaced by the current crack length *a* due to the reason that the crack start to vary. As a result, since the modified‖ cantilever beam theory and the energy release rate definition holds throughout the delamination, one can combine Eqn. 2.18 and Eqn. 2.20 to obtain a unified solution. Since the delamination starts to propagate when *GI* = *GIc*, the unified solution curve after the failure can be written as

$\Delta_f = \frac{2(BE_{11}IG_{Ic})^{\frac{3}{2}}}{3E_{11}IP^2}$ ……Eqn 2. 1

By putting the initial crack length a_o and critical energy release rate *GIc* inside the Eqn. (2.20), the tip force at the crack growth regime becomes

$P_c = \frac{\sqrt{G_{Ic}BE_{11}I}}{a_0+X_I h}$ ……Eqn 2. 2

Following that, one can easily find the critical tip displacement at the crack growth just by putting the *Pc* inside one of the displacement equations above.

Chapter Three

3. Finite Element Modeling DCB on Abaqus @10.14

3.1. Modeling of DCB on ABAQUS by VCCT

3.1.1. Part *development*

Two part are sketched (lower and upper parts) the specimen has 150 mm length with 55 mm initial crack dimension. Each arm is 3mm in height with the stacking of $[(45,-45, 0_2, 90_2)_2]_s$. Figuring 6mm, while unit ply thickness is 0.1 mm. The dimensions of the DCB specimen and the material properties are summarized in Fig 3.1.

Fig 3. 1. Part drowing of DCB on ABAQUS 10.14

3.1.2. *Material properties*

Material properties of Quasi-isotropic composite with isotropic elastic type E_{11} of 30900Mpa and Poisson's ratio of 0.239 are taken from Table 4.1.

3.1.3. *Crating and assignment section*

Homogeneous solid sections consist of a material name comp. 1 section thickness are used. For both upper and lower part section 1 with solid homogeneous are assigned.

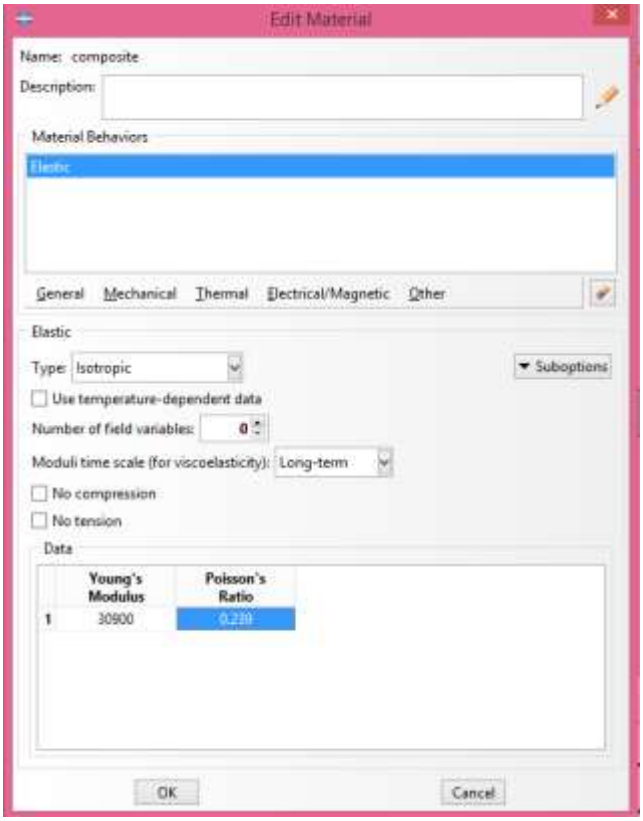

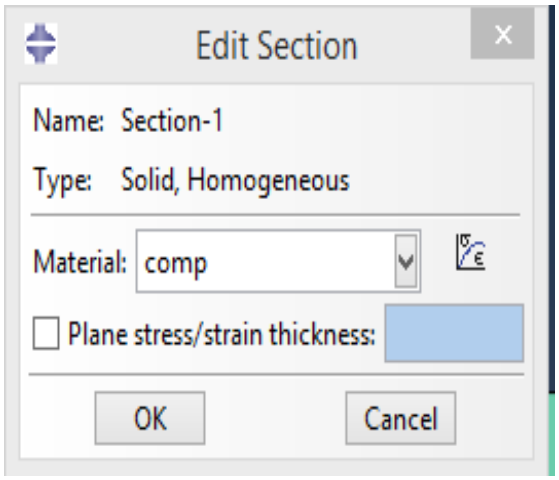

A, input material data for composite **B. Assigning section to composite material**

Fig 3. 2. Material and section assignment.

3.1.4. Crating assembly

Assembly module to create part instances and position them relative to each other in a global coordinate system. Top and bottom instance are crated in mesh dependent type, part position instances by sequentially applying position constraints that align selected face.

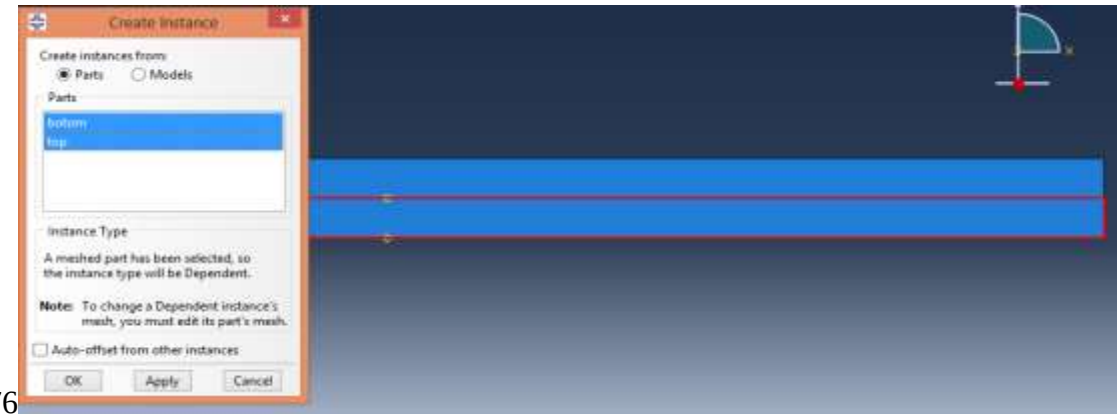

76

Fig 3. 3. Crating an assembly of top and bottom beam.

3.1.5. Crating step

Abaqus the process is composed of several distinct sections, or steps. Each of these provides the opportunity to define different boundary conditions (BCs), loads, constraints, and more in the Step module. This ability is integral to creating a realistic situation, and therefore accurate performance data. In this particular case, there is one steps defined from beginning to end: initial step, the purpose of initial step is to define boundary condition that form fundamental motion of the system.

Within this model there is only one analysis general static or dynamic nonlinear step having two bounders and loading condition. Nlgeom setting on if there is any geometric nonlinearity in the step.to diagnosis convergence problem I have used 2000 incriminations with time period of 10, initial step time of 0.01, minimum incrimination of 10e-15 and 0.1 maximum incrimination.

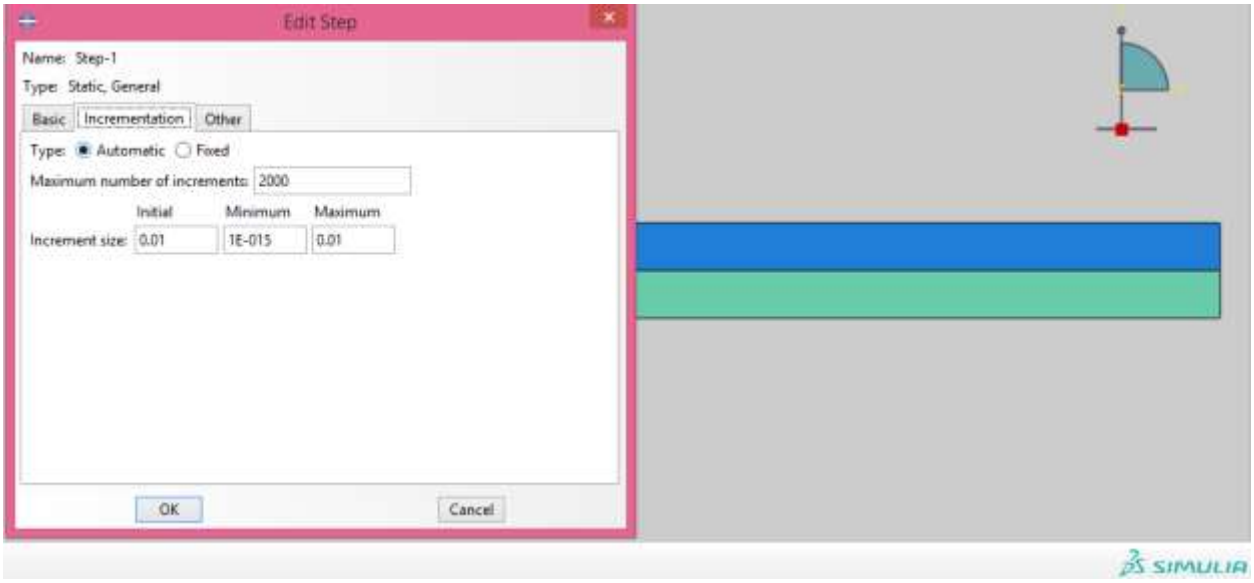

Fig 3. 4. Crating step and step increment.

3.1.6. Field output request

Field output request don for the whole model domain for every n increment, n=2, without put variable Displacement U_2, Force F_2 and DBT (time and bond failure), OPENBC (opening behind crack tip at bond failure).

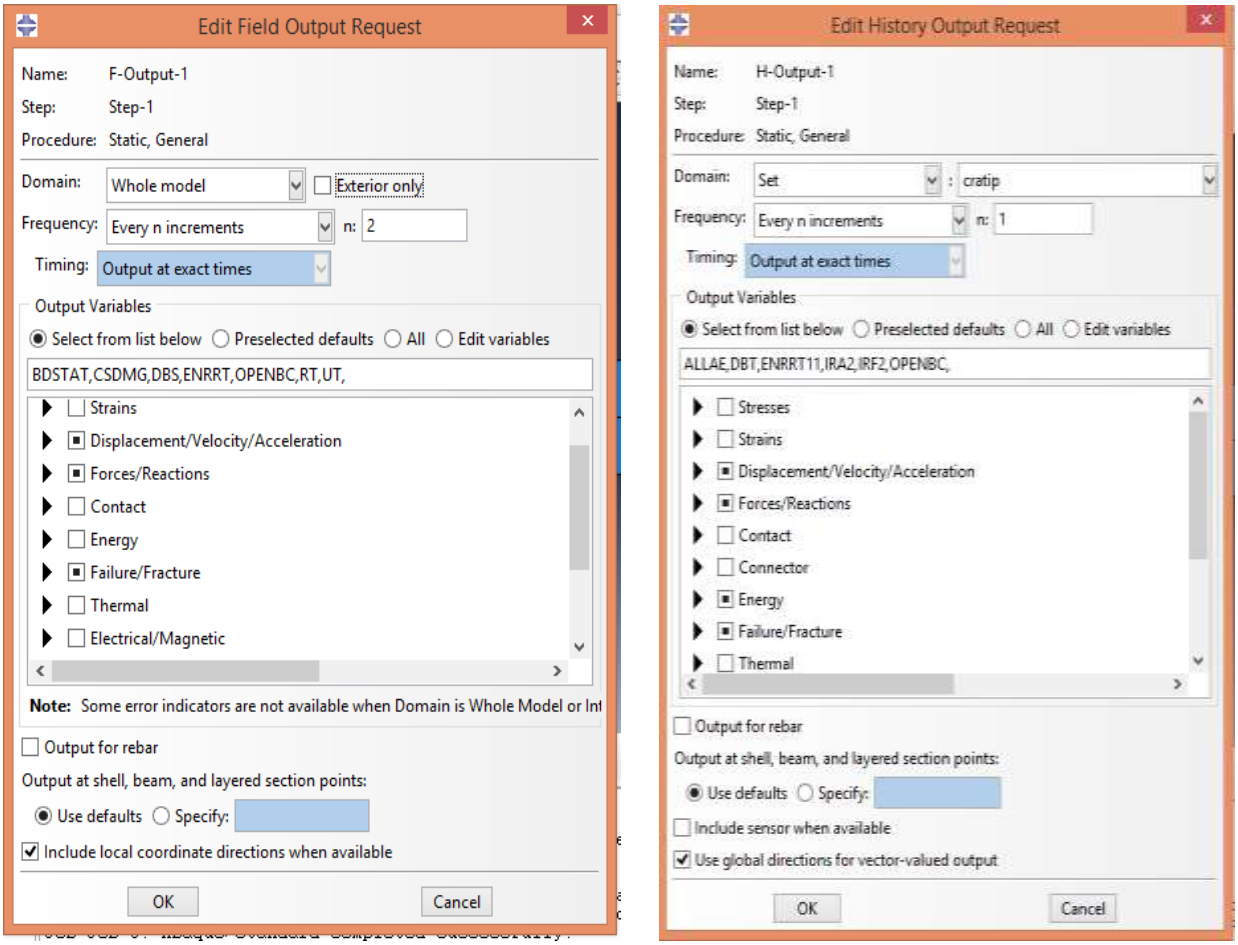

A. Editing field output request **B. Editing history output**

Fig 3. 5. Requesting output A. Editing field output request and B. Editing history output

3.1.7. History output request

History output request in don by setting on upward displacement and crack tip domain frequency of every increment n, n=2, without put variable displacement U2, force F2 and DBT (time and bond failure) and OPENBC (opening behind crack tip at bond failure).

3.1.8. Interaction and contact property

On defining Interaction property three contact property are assigned Tangential behavior of frictionless, Normal behavior of hard contact, this hard contact setting minimizes the penetration of the slave surface into the master surface and does not allow the transfer of tensile stress across the interface, and fracture criteria VCCT type are used. For VCCT type of fracture criteria direction

of crack growth relative to local 1- direction are maximum tangential stress, Mode independent behavior with tolerance 0.2 and viscosity 0 are taken. For BK criteria GI=0.7 j/mm^2 from Eqn 2.29.

Before selecting type of interaction we need to assignee master and slave surface. Type of interaction standard surface to surface interaction between the master and slave surface node to surface discretization with sliding formulation small sliding. Slave node is adjusted in set of BONDED contact interaction VCCT (from contact property) and bonding is limiting to slave nodes in subset BONDED

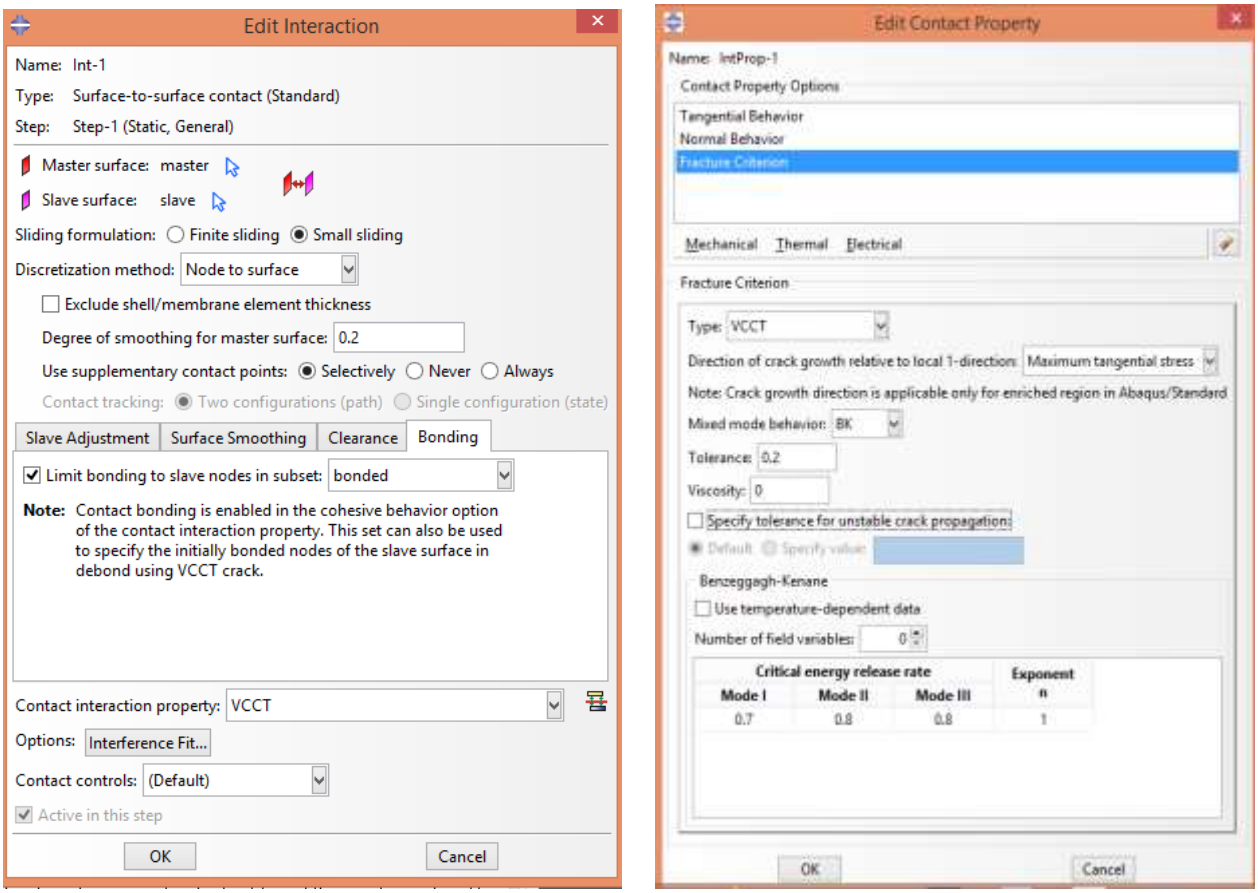

A. Edit interaction property **B. Edit contact property**

Fig 3. 6. Editing A. Edit interaction property B. Edit contact property

3.1.9. Create loads

Applying lode and boundary condition at located reference point (upper node, lower node, fixed node and bonded node). First set boundary condition, from step tree select initial then BC category assignee to mechanical, type displacement/ rotation. From previously set point fixed node is

selected it will prevent any movement in X and Y direction. Second use step menu set contact category assigned to mechanical, and type displacement/ rotation, from previously set point select upper node and apply +6 upward displacements and following the same procedure to lower node apply -6 downward displacement, both X and Z are taken to be zero.

3.1.10. Crating crack

Debond type of crack using VCCT is crated, initial step step-1 and contact pare interaction is Int-1 with stepped debonding force.

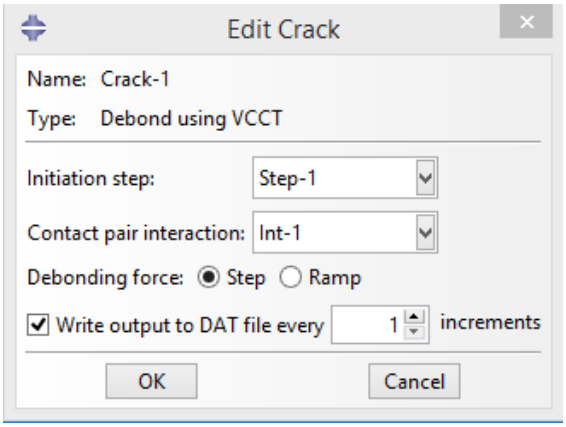

Fig 3. 7. Assgning VCCT Crack

3.1.11. Mashing

From part instance bottom and top part are meshed with different number of element. Mesh controller gives different meshing option mesh type is free technique, advanced front algorithm and quad-dominated element shape. Global seed with sizing control of 0.133, 0.2, 0.15, and 0.31M approximated global size with deferent curvature and minimum size controller.

Mesh element type standard, linear geometric order and plan strain family, quad reduced integral (CPE4R) are crated element size of four different.

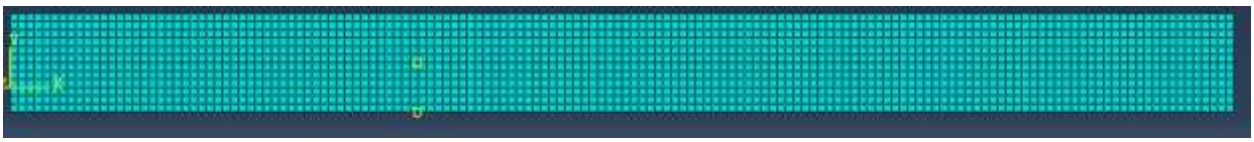

Fig 3. 8. Assigning Mesh density for DCB

3.2. Modeling of DCB on ABAQUS using CZM

Model setup

This problem has been identified to ABAQUS developers and should be addressed in a future release. Deleting the elements upon failure caused no ill effects on any of the solutions and avoided these problem.

3.2.1. Part development

Both bottom and top part has 150mm length and 3mm height, the cohesive layer has the same length and 10 μm height. Top and bottom layer has stacking sequence of $[(45,-45,0_2,90_2)_2]_s$, while unit ply thickness is 0.125 mm. The dimensions of the DCB specimen and the material properties are summarized in **Fig…**

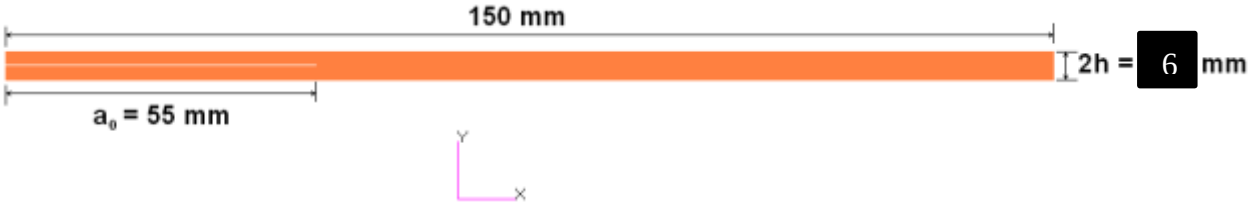

Fig 3. 9. Part drowing of DCB on ABAQUS 10.14

3.2.2. Material properties

Material composite properties of Quasi-isotropic composite with isotropic elastic type E_{11} of 30900Mpa and Poisson's ratio of 0.239 are taken from Table 4.1 and cohesive material property mechanical elastic type of traction with penalty stiffness K_0=2.8x10^6, Maximum traction t_n=40 And fracture energy G_Ic=0.7 j/mm^2 damage for traction separation low is Maxe Damage theory with Nominal-only mode I.

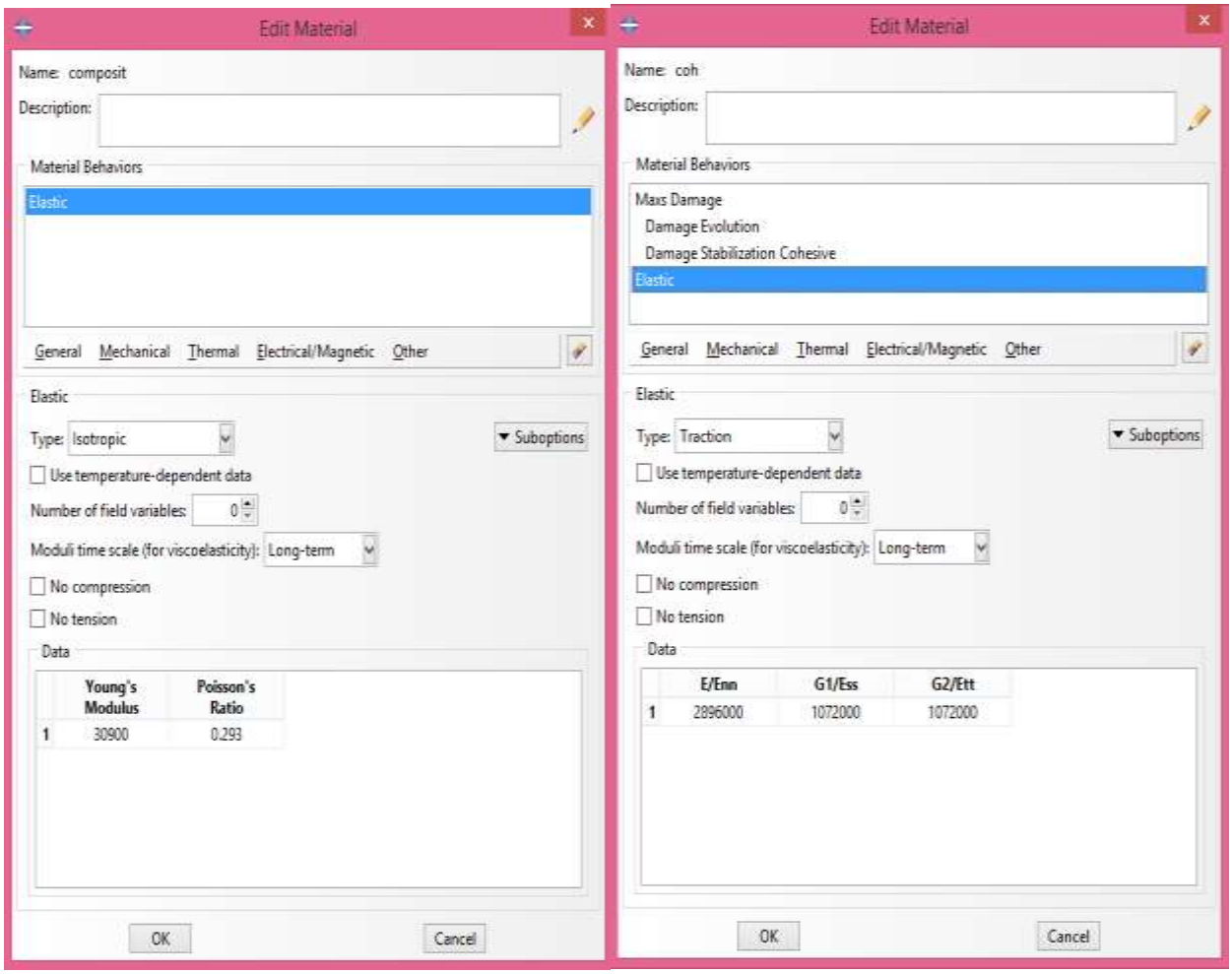

A, input material data for composite **b, input material data for cohesive**

Fig 3. 10. Material for A. input material data for composite B. input material data for cohesive

3.2.3. Crating and assignment section

Homogeneous solid sections consist of a material name composite section 1 is used for both bottom and top part. Solid homogeneous section one is assigned for top and bottom part. For cohesive part deferent section is used, cohesive section type cohesive with traction separation response and initial thickness of analysis default.

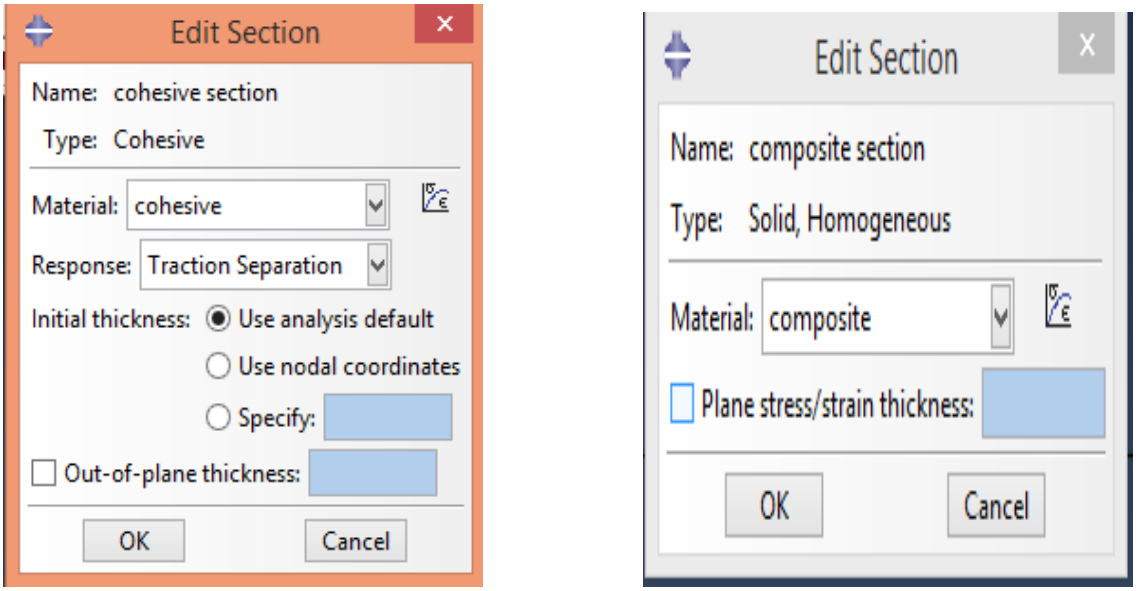

A. Assigning section to Cohesive material **B. Assigning section to composite material**

Fig 3. 11. Assigning section A. Assigning section to cohesive material B. Assigning section to composite material

3.2.4. Crating assembly

Assembly module create part instances and position them relative to each other in a global coordinate system. Top, bottom and cohesive layer instance are crated in mesh dependent type, part position instances by sequentially applying position constraints that align selected face of bottom, top and cohesive part.

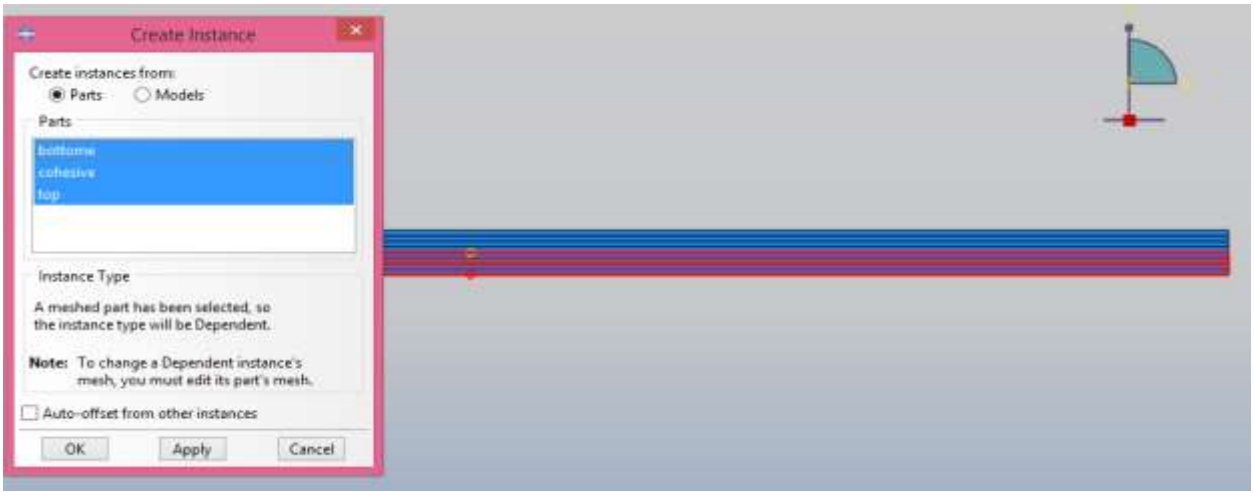

Fig 3. 12. Crating an assembly of top, bottom beam and cohesive element

3.2.5. Crating step

Abaqus the process is composed of several distinct sections, or steps. Each of these provides the opportunity to define different boundary conditions (BCs), loads, constraints, and more in the Step module. This ability is integral to creating a realistic situation, and therefore accurate performance data. In this particular case, there is one steps defined from beginning to end: initial step, the purpose of initial step is to define boundary condition that form fundamental motion of the system.

Within this model there is only one analysis general static or dynamic nonlinear step having two bounders and loading condition. Nlgeom setting on if there is any geometric nonlinearity in the step.to diagnosis convergence problem I have used 500 incriminations with time period of 10, initial step time of 0.01, minimum incrimination of 10e-15 and 0.1 maximum incrimination.

3.2.6. Field output request

Field output request don for the whole model domain for every n increment, n=2, without put variable Displacement U_2, Force F_2 and DBT (time and bond failure) and OPENBC (opening behind crack tip at bond failure).

3.2.7. History output request

History output request in don by setting on upward displacement and crack tip domain frequency of every increment n, n=2, without put variable displacement U2, force F2 and DBT (time and bond failure), OPENBC (opening behind crack tip at bond failure) and J-integral.

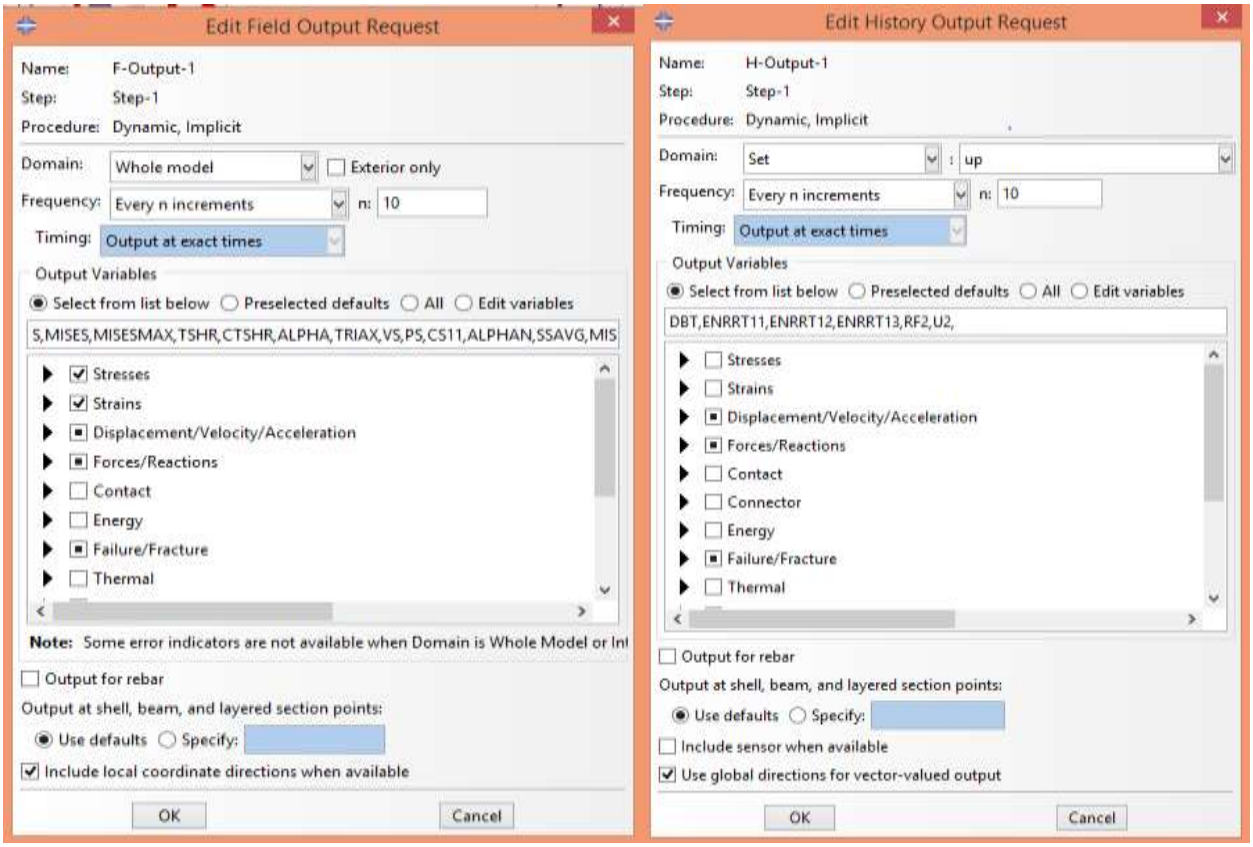

A. Editing field output request **B. Editing history output**

Fig 3. 13. Requesting output A. Editing field output request and B. Editing history output

3.2.8. Interaction and contact property

On defining Interaction property two contact property are assigned Tangential behavior of frictionless, Normal behavior of hard contact, this hard contact setting minimizes the penetration of the slave surface into the master surface and does not allow the transfer of tensile stress across the interface.

Before selecting type of interaction we need to assignee master (bottom) and slave (top) surface then Type of interaction standard surface to surface interaction between the master and slave surface node to surface discretization with sliding formulation small sliding. Tie constraint is used to produce connection with bottom, top and cohesive layer. Tie constraint 1 is used to connect the bottom surface (master surface) with cohesive surface (slave surface) and tie constraint 2 is used to make connection between the top surface (master surface) and cohesive surface (slave surface) with discretization of analysis default.

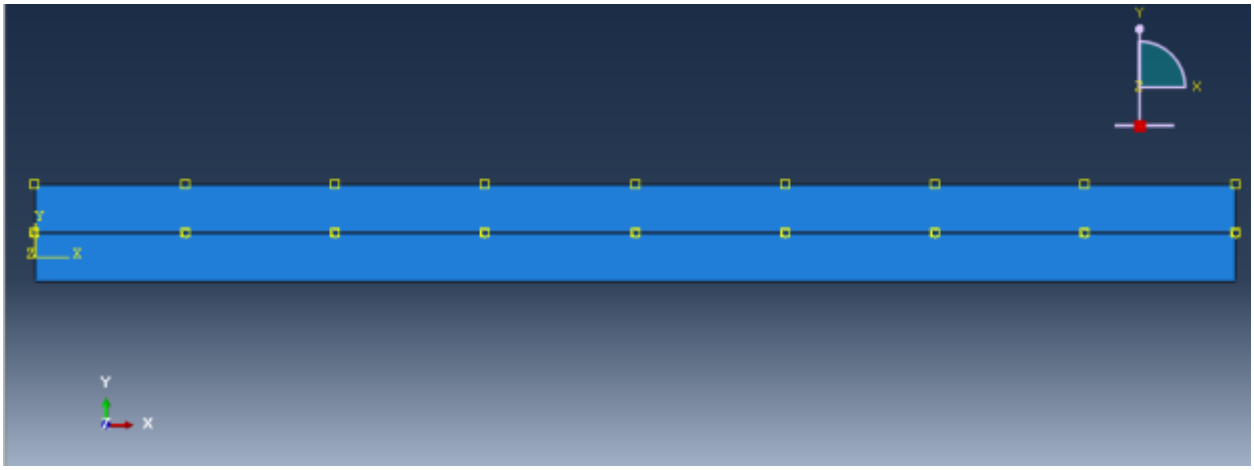

Fig 3. 14. Contact formation between top, bottom and cohesive layer

3.2.9. Create loads

Applying lode and boundary condition at located reference point (upper node, lower node and fixed node). First set boundary condition, from step tree select initial then BC category assignee to mechanical, type displacement/ rotation. From previously set point fixed node is selected it will prevent any movement in X and Y direction. Second use step menu set contact category assigned to mechanical, and type displacement/ rotation, from previously set point select upper node and apply +16 upward displacements and following the same procedure to lower node apply -16 downward displacement, both X and Z are taken to be zero.

3.2.10. Crating crack

Symmetrical crack is crated between cohesive layer and composite layer using q-vector

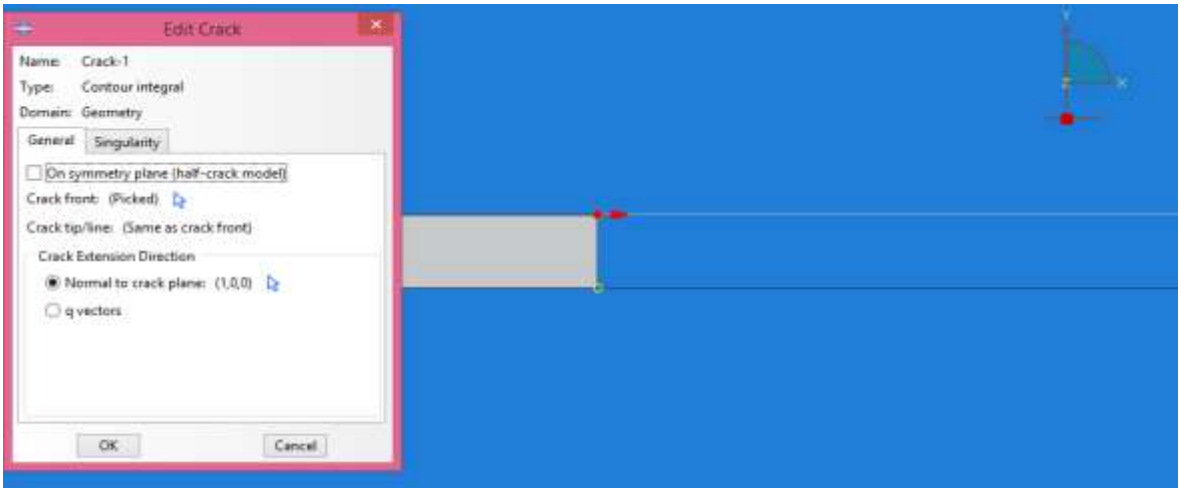

Fig 3. 15 Crating crack

3.2.11. Mashing

From part instance bottom and top part are meshed with different number of element. Mesh controller gives different meshing option mesh type is free technique, advanced front algorithm and quad-dominated element shape. Global seed with sizing control of 0.133, 0.2, 0.31 and 0.15 approximated global size with deferent curvature and minimum size controller. Cohesive part usually should be discretized with higher number of element, Global seed with sizing control of 0.026, 0.04, 0.062 and 0.03 respectively approximated global size with deferent curvature and minimum size controller.

Mesh element type standard, linear geometric order and plan strain family, quad reduced integral (CPE4R) are crated element size of 0.133x0.133for both bottom and top part. Cohesive Mesh element type standard, linear geometric order and cohesive family, quad reduced integral (CH2DR) are crated element size 0.026x0.026.

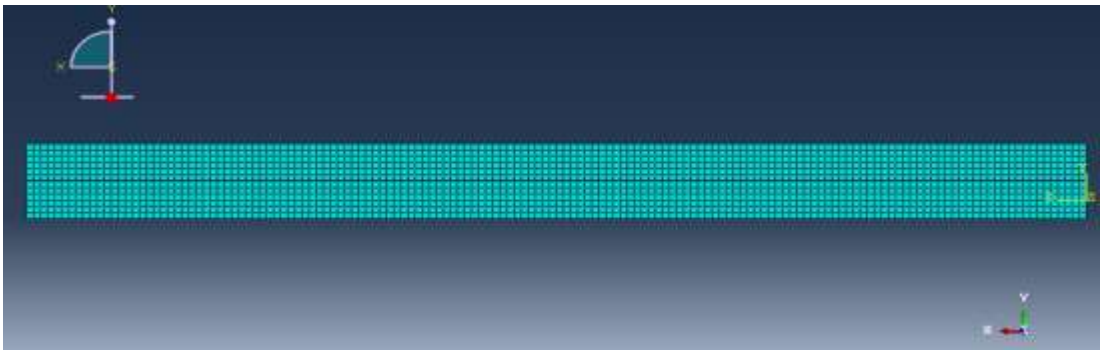

Fig 3. 16 . Assigning Mesh density for DCB

Chapter Four

4. Result and Discussion

4.1. Result and discussion of E-glass epoxy

Laminate 2D and 3D Material Property

Autodesk Simulation Composite Design @ 2014 software are used to calculate 2D and 3D mechanical properties of laminate. Lamination is the process by which composite material plies or "laminae" are stacked and cured together to form a layered material with unique stiffness and strength characteristics. E-Glass Fiber with fiber volume of 60% and 8552 Epoxy matrix *volume* 40% lamina are joint to form $[(-+45,90_2,0_2)2]_s$ stacking sequence of Quasi-Isotropic material with 2D and 3D mechanical property listed on table 4.1. Q-bars stiffness matrix expressed in the global coordinate system Q, [ABD], [ABD] Inverse **Appendix 3** Classical Laminate Theory (CLT) to compute the 6x6 laminate stiffness matrix fig 4.1.

Table 4. 1. Autodesk Simulation Composite Design @ 2014 2D and 3D mechanical property Quasi-Isotropic E-Glass/ Epoxy

2D Laminate Properties	
Title	Value
Ex (MPa)	3.09E+04
Ey (MPa)	3.09E+04
Gxy (MPa)	1.03E+04
NUxy	2.39E-01
NUyx	2.39E-01
NUxyb	-3.72E-01
NUyxb	-3.09E-01
Density (g/mm3)	2.07E-03
Thickness (mm)	3.00E+00

3D Laminate Properties	
Title	Value
Ex (MPa)	3.09E+04
Ey (MPa)	3.09E+04
Ez (MPa)	2.26E+04
Gxy (MPa)	1.03E+04
Gxz (MPa)	8.00E+03
Gyz (MPa)	8.00E+03
NUxy	2.39E-01
NUyx	2.39E-01
NUxz	2.94E-01
NUzx	2.14E-01
NUyz	2.94E-01
NUzy	2.14E-01
Density (g/mm3)	2.07E-03
Thickness (mm)	3.00E+00

Laminate stress and strength Analysis

Laminate load (in plan load) with load type stress for the axial load, transvers load and shear load are taken 65Mpa, 25Mpa and 35Mpa respectively applying this amount of load I am able find Global Stress Fig 4.1 **Appendix 1** stress and strain state in each ply of a laminate when the laminate is subjected amount of in-plane

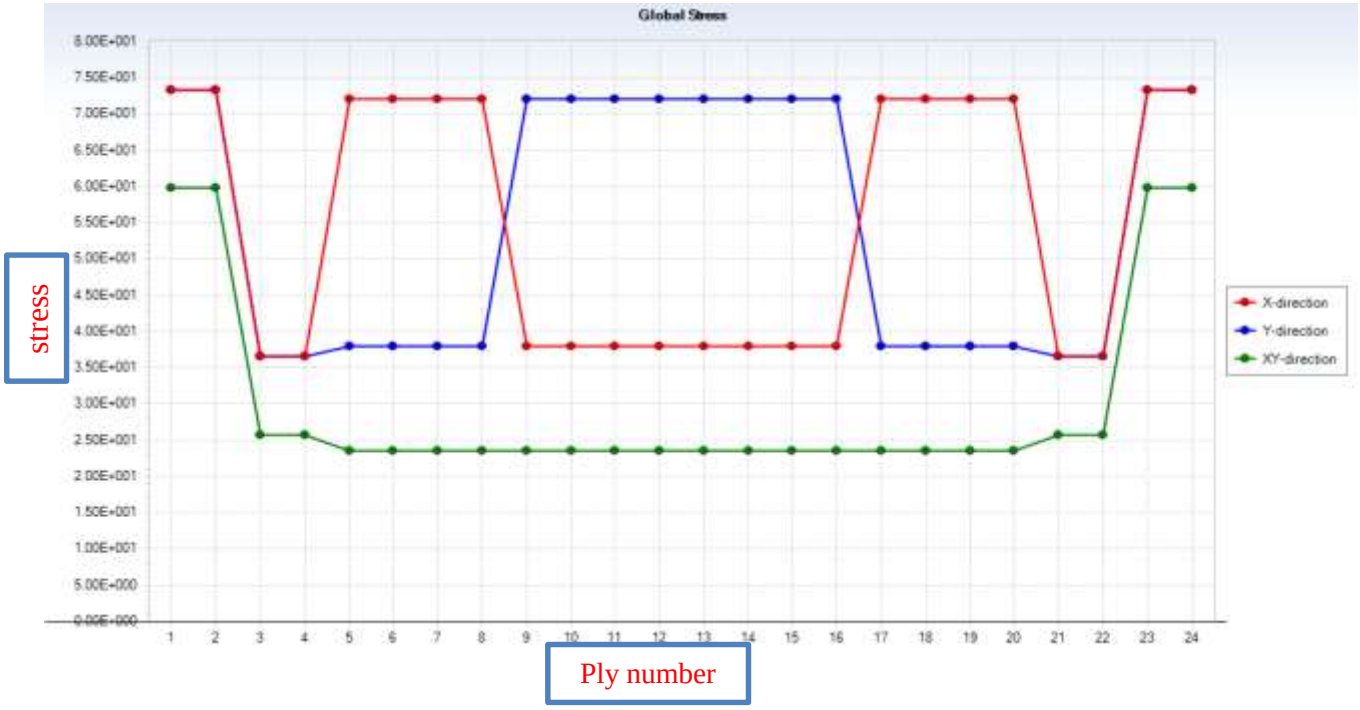

Fig 4. 1. Output of Autodesk Simulation Composite Design @ 2014 Stress of each Laminate

First ply failure analysis

First Ply Failure feature is used to identify the first ply that fails within a laminate as the laminate is subjected to Laminate load (in plan load) with load type stress for the axial load, transvers load and shear load are taken 65Mpa, 25Mpa and 35Mpa respectively, applying this amount of load I could find type of failure of the lamina as well the maximum amount of stress and strain the lamina capable of stand before failure. After lamina selection and applying in-plan load Hashin composite failure criteria Appendix 4 is used with default α and S23 parameter. In-plan load is iterated until failure index and safety factor is approximately unit. Hashin criterion identifies four different modes of failure for the composite material: tensile fiber failure, compressive fiber failure, tensile matrix failure and compressive matrix failure **Appendix 1**.

Progressive ply to failure

The maximum amount of stress and strain in longitudinal, Transvers and shear direction are shown in Fig 4.2, Fig 4.3 and Fig 4.4 Respectively. The progressive ply to failure is seen on ply 3, 4, 21, 22 with tensile mode of failure at stress and strain equal to 52Mpa and 0.00138mm/mm respectively in longitudinal direction, stress and strain in transvers direction is 42.8Mpa and 0.00098mm/mm respectively and stress and strain in shear direction is 33.5Mpa and 0.00327mm/mm all value is approximated.

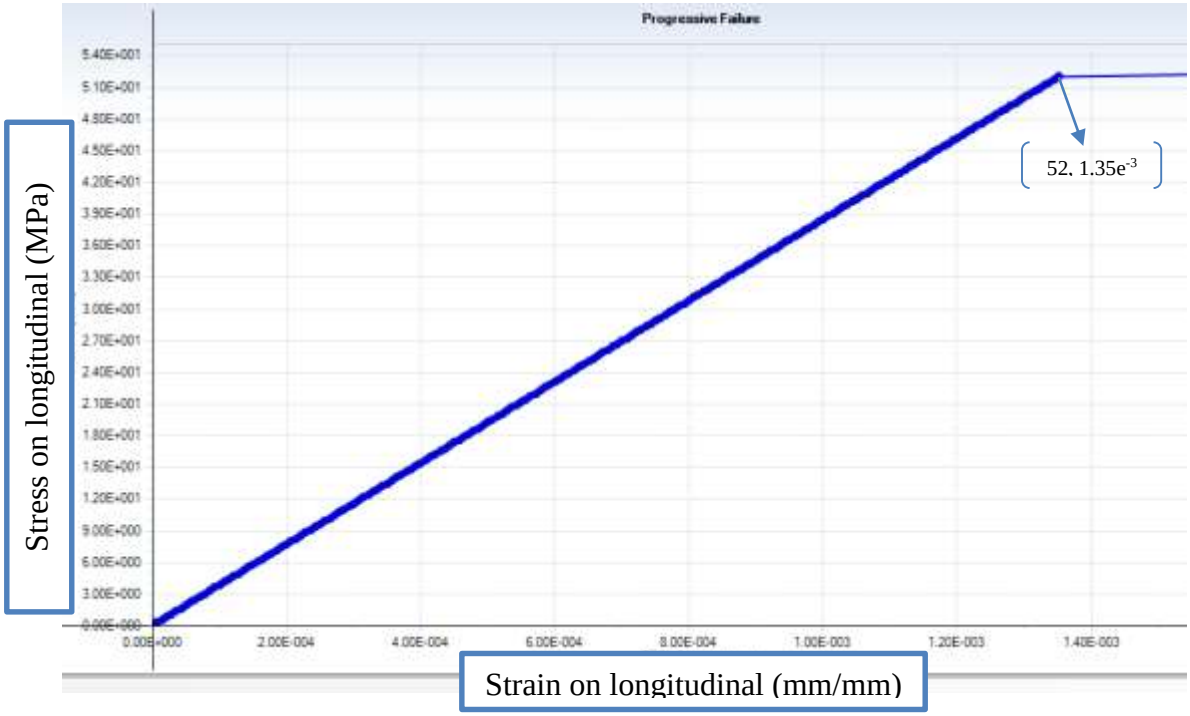

Fig 4. 2 stiffness of Quasi-Isotropic E-Glass/ Epoxy in longitudinal direction

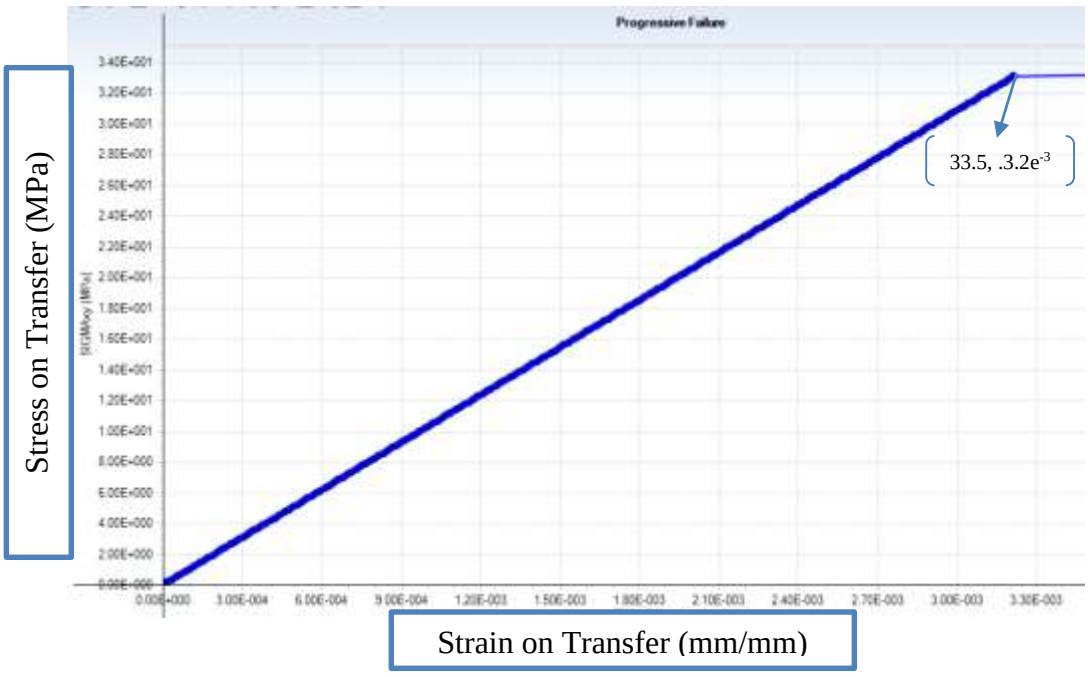

Fig 4. 3. Stiffness of Quasi-Isotropic E-Glass/ Epoxy in transfers direction

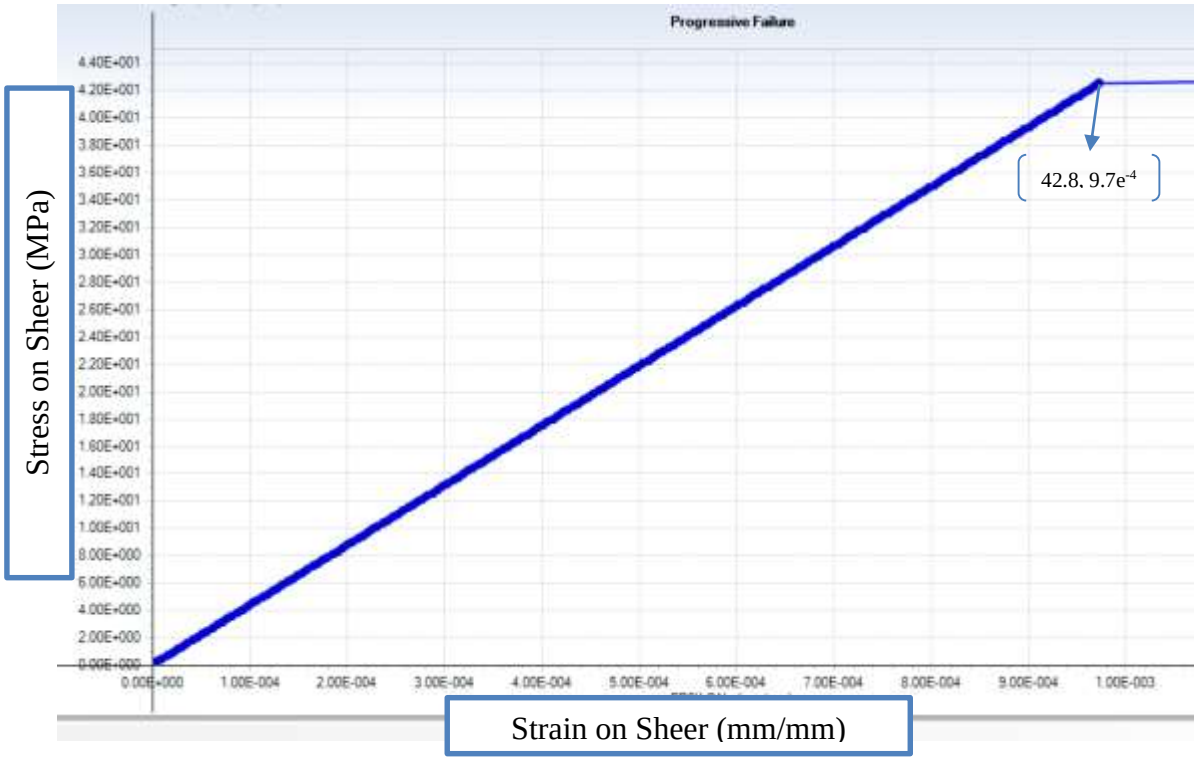

Fig 4. 4. Stiffness of Quasi-Isotropic E-Glass/ Epoxy in sheer direction

Failure envelope:

Simulation Composite Design computes a failure envelope for a laminate subjected to a pair of specified in-plane loads. The failure envelope concisely shows all possible combinations of the two selected in-plane loads that cause laminate failure

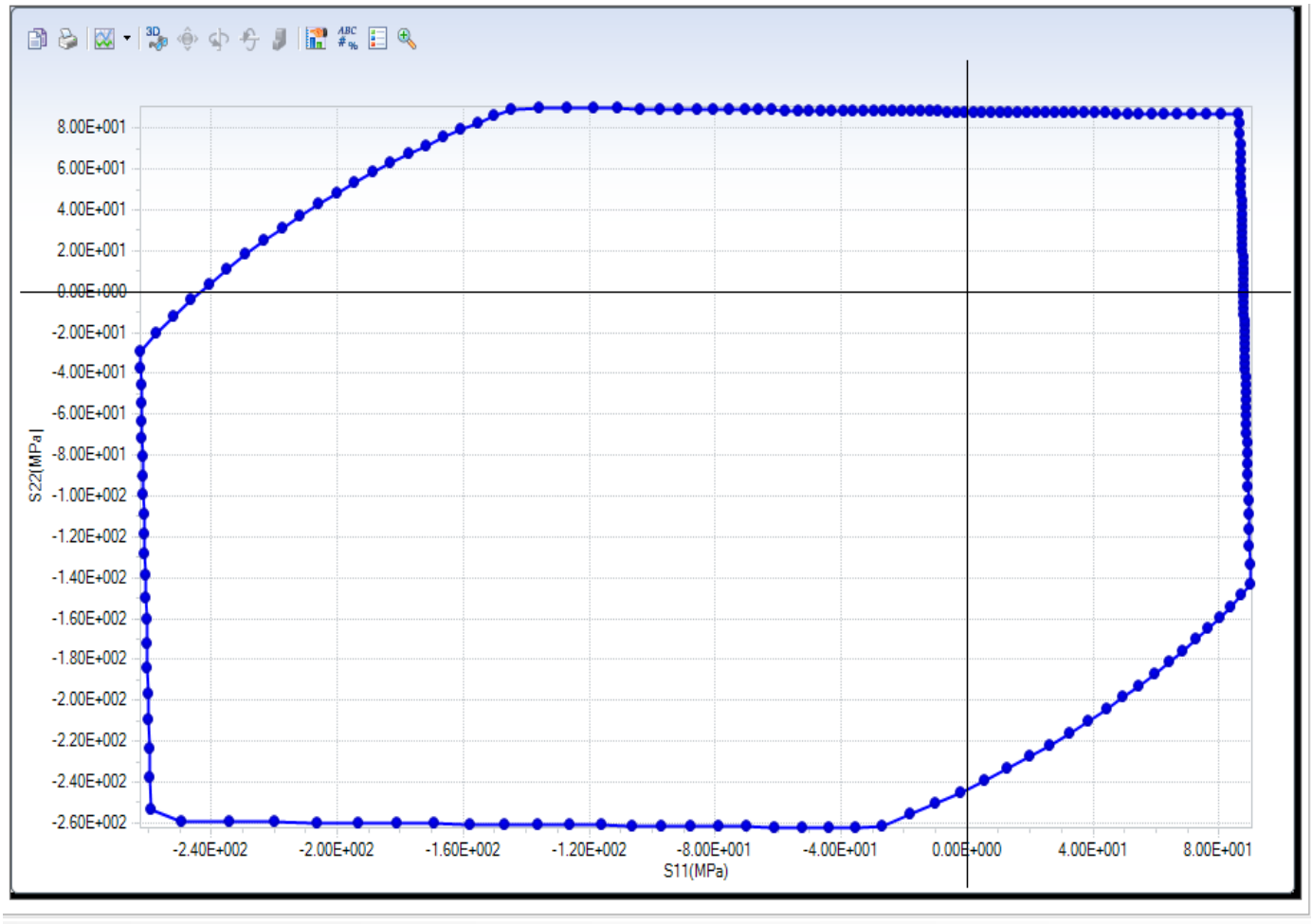

Fig 4. 5 Epoxy laminate failure envelop S11 vs S22

4.2. Result and desiccation of virtual crack closure technique

To initiate pure mode delamination, displacement increments are applied at mid-span as shown in the Fig.4.6 (A) Note that displacement control is applied in order to capture the load–displacement (P–Δ) curve. The VCCT crack is assigned between the two composite layers, which describes the expected delamination path. Fig.4.6(A) and Fig.4.6 (B) show the Misses contour plots on deformed shape at time step "A" when the crack propagates to the point of load application and at the final time step "B" simulation. All result of force and displacement are in Newton and millimeter respectively.

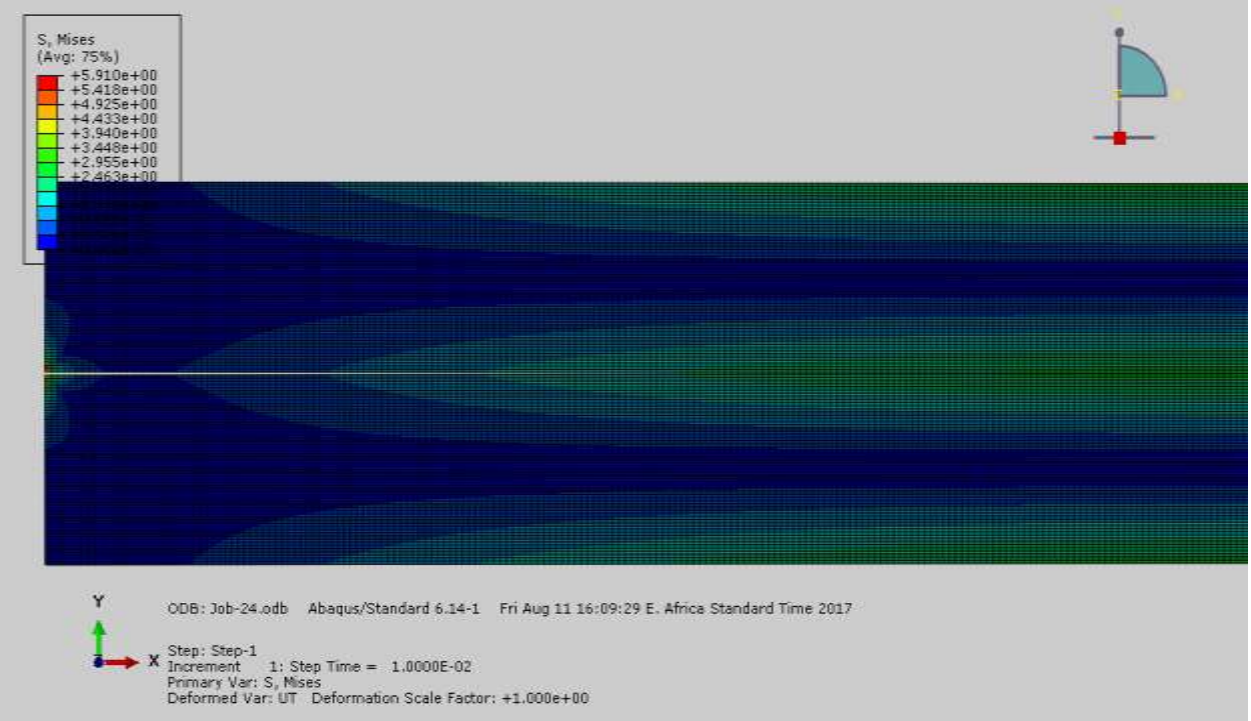

A, Delamination at the end of the first time step

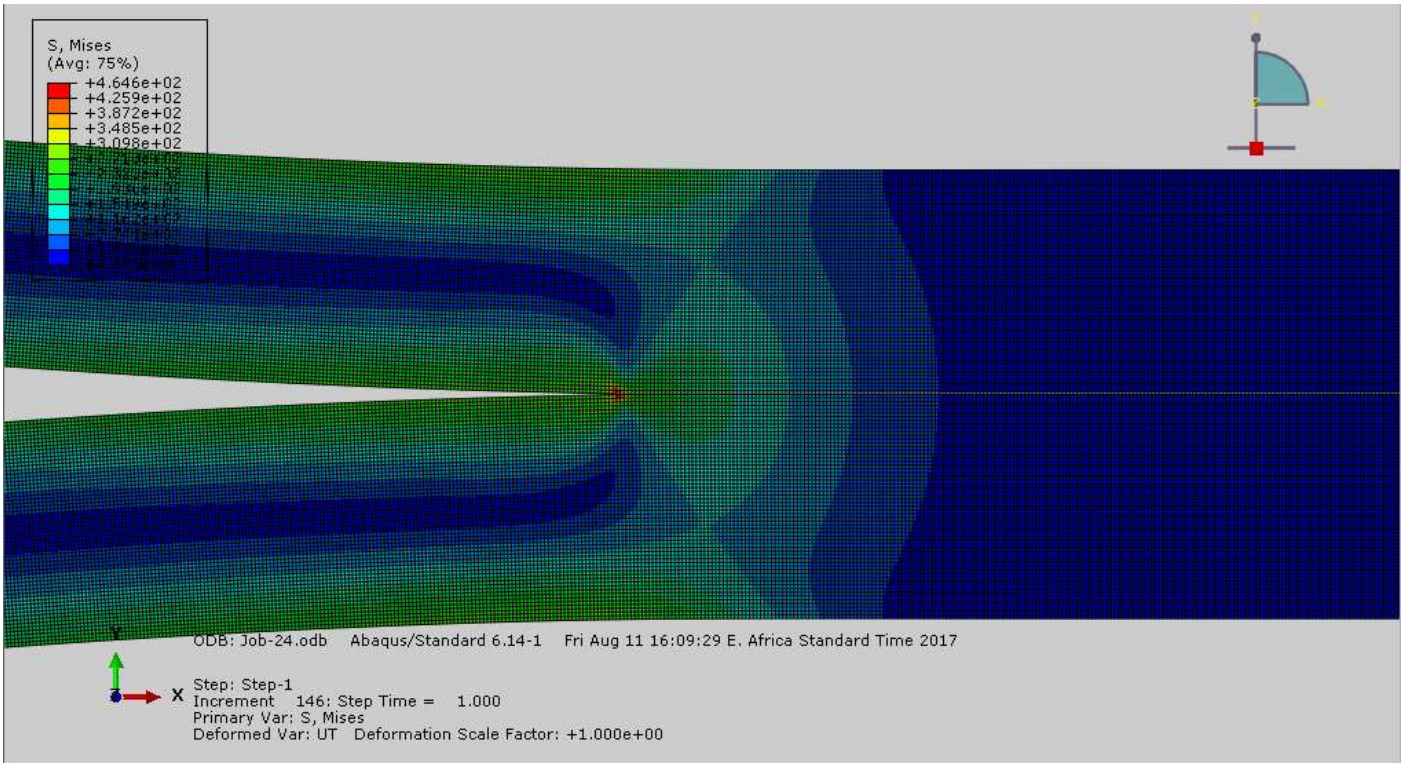

B, Delamination at the end of the final time step

Fig 4. 6 Delamination of DCB using VCCT, A. at the end of the first time step B. at the end of the final time step

Different element sizes and mesh patterns used in these five cases are shown in Fig 4.7, Fig 4.8, Fig 4.9, Fig 4.10 and Fig 4.11, while a much lower energy is consumed as the automatic stabilization energy (static dissipation). For these four DCB simulations under displacement control, reaction force verses time is shown in Fig 4.7, Fig 4.8, Fig 4.9, Fig 4.10 and Fig 4.11, and the response displays considerable oscillations during delamination propagation. In order to reduce the oscillations observed in the reaction force, a finer mesh has been utilized and another set of Simulations have been completed. When an analysis with small mesh is utilized with VCCT, it is necessary to maintain a small time increment. In order to understand the optimal mesh size and maximum allowable time Increment, five **c**ases have been studied with five different mesh sizes, viscosity, Damping Factor and with five Different maximum allowable time increments as given on Table 4.2.

Table 4. 2. VCCT load output for constant damping factor, different viscosity and five different mesh density

Case	Viscosity	Damping Factor	Element Size of Composite	Displacement	Critical Load (N)
Case 1	0.2	0.01	0.2156x0.2156	5.5	47.21
Case 2	0.2	0.01	0.2x0.2	5.51	44.1
Case 3	0.2	0.01	0.1x0.1	5.7	37.11
Case 4	0.2	0.01	0.08x0.08	4.5	35.69
Case 5	0.2	0.01	0.01x0.01	4.9	32.35

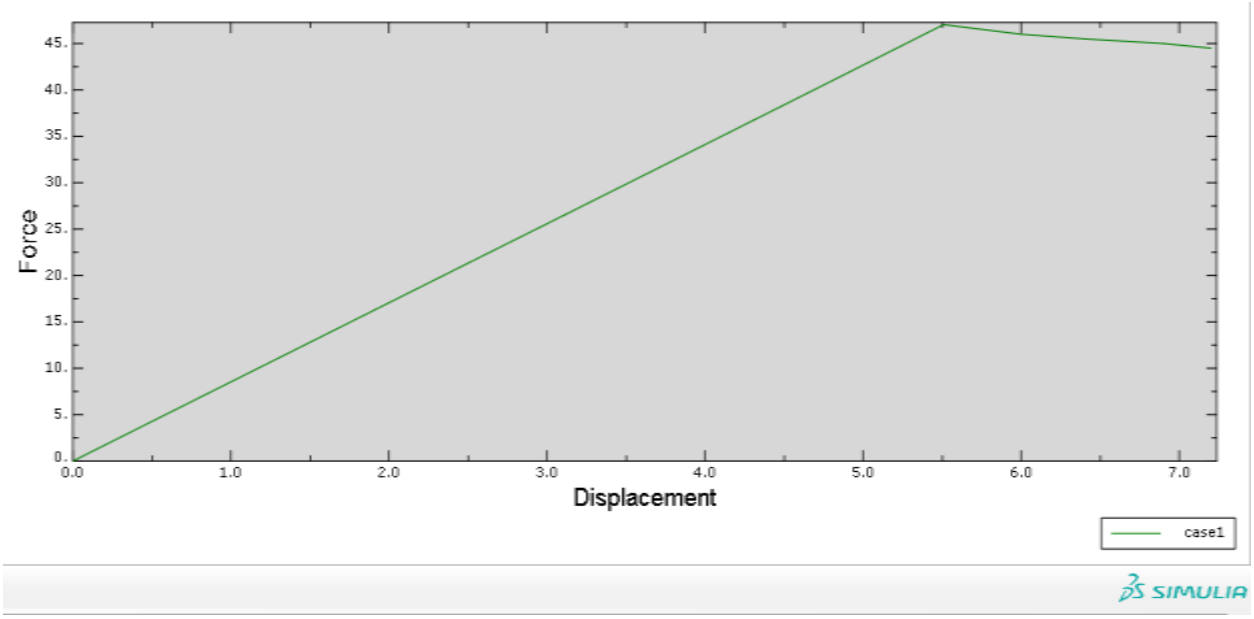

Fig 4. 7 . VCCT load-displacement output for case 1

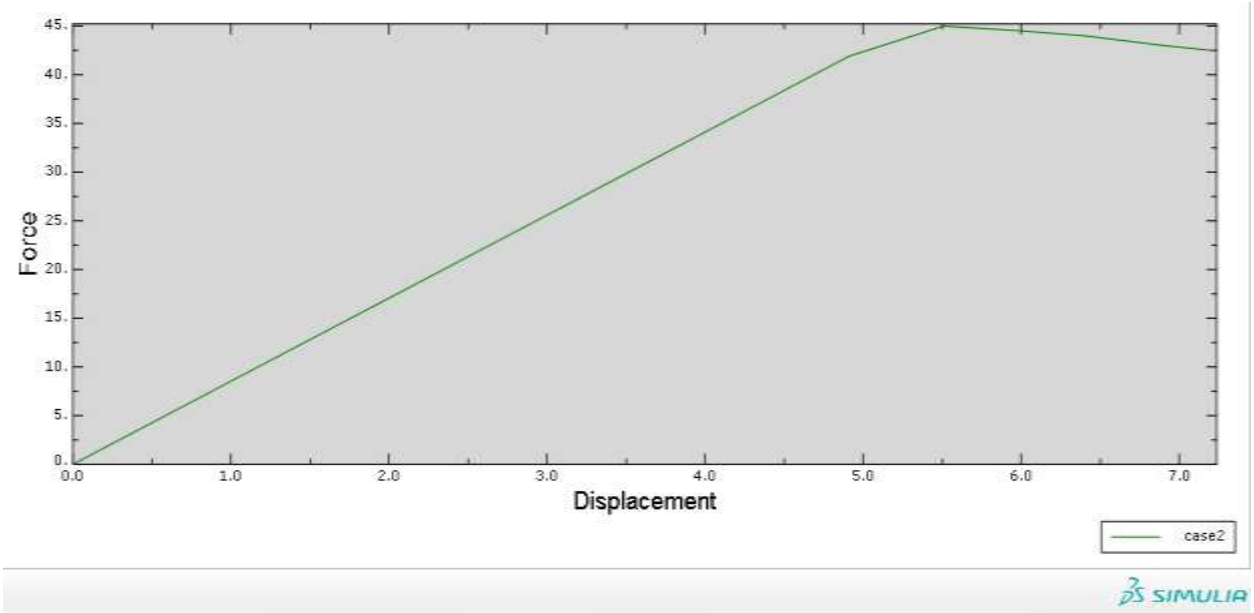

Fig 4. 8. VCCT load-displacement output for case 2

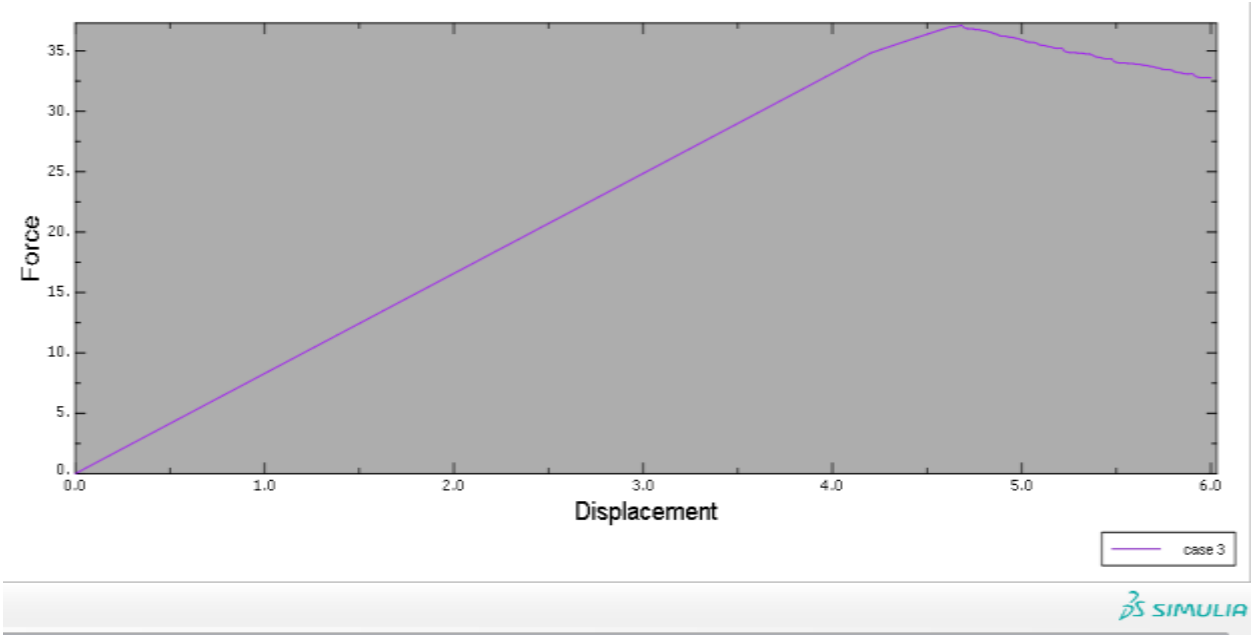

Fig 4. 9. VCCT load-displacement output for case 3

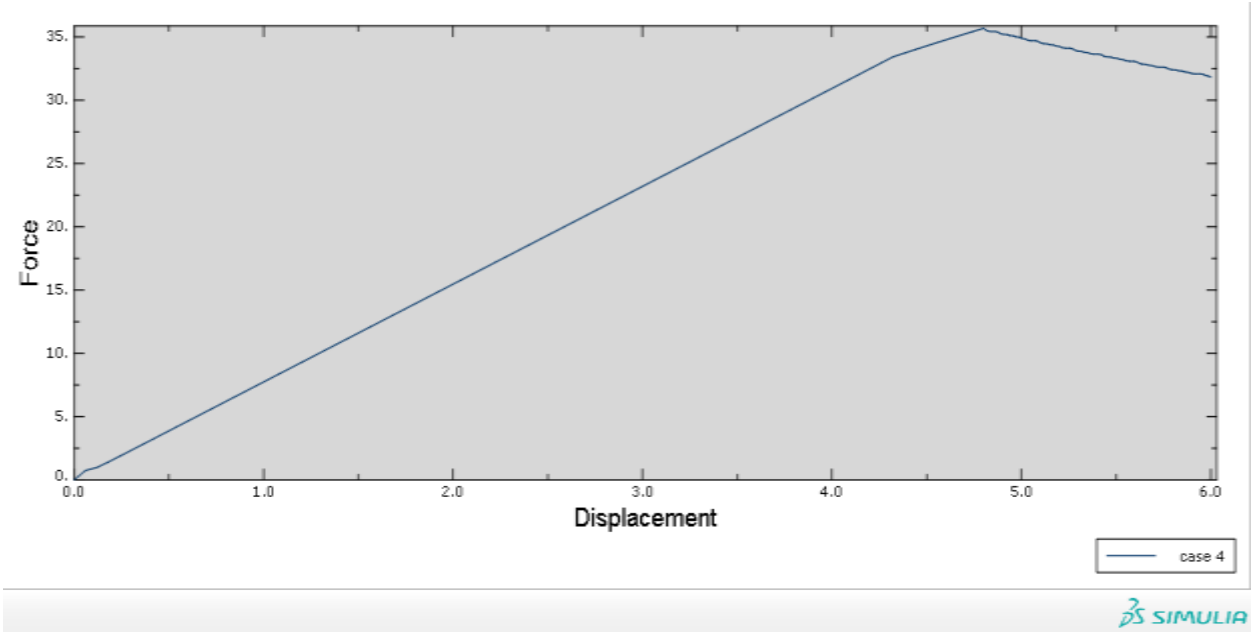

Fig 4. 10. VCCT load-displacement output for case 4

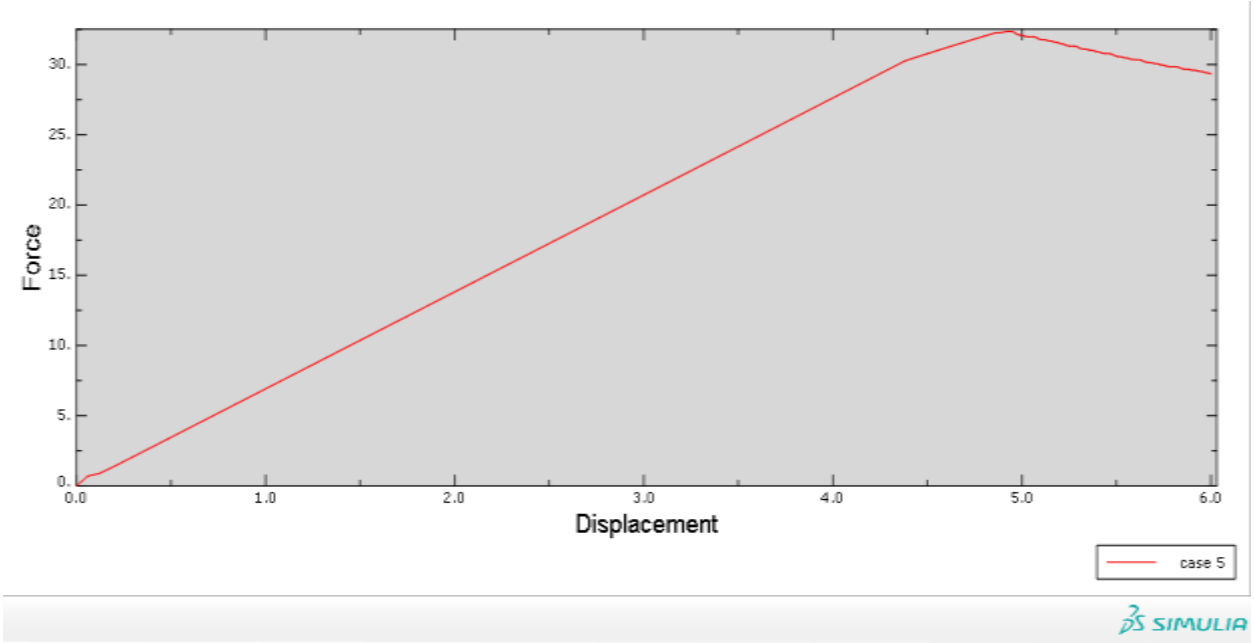

Fig 4. 11. VCCT load-displacement output for case 5

4.3. Result and desiccation of cohesive zone method

In this section the results from ABAQUS are presented. Running the DCB with traction-separation laws for the cohesive zone, a deformation of the beam similar as seen in Fig.4.12 (A, B) to initiate pure mode delamination, displacement increments are applied at mid-span. Note that displacement control is applied in order to capture the softening behavior of the load–displacement (P–Δ) curve. The COH2D4 cohesive elements are placed only between two layers, which describes the expected delamination path. Fig.4.12 (a) and (b) show the Mises contour plots on deformed shape at time step "A" when the crack propagates to the point of load application and at the final time step "B" of the simulation. All result of force and displacement are in Newton and millimeter respectively. The force-deflection curves are represented by values from the top node in the DCB which was subjected to a prescribed displacement. This node represents the behavior of the beam structure. The graphical illustrations of the traction-separation laws are constructed of values from a node in a cohesive element which is known to have collapsed.

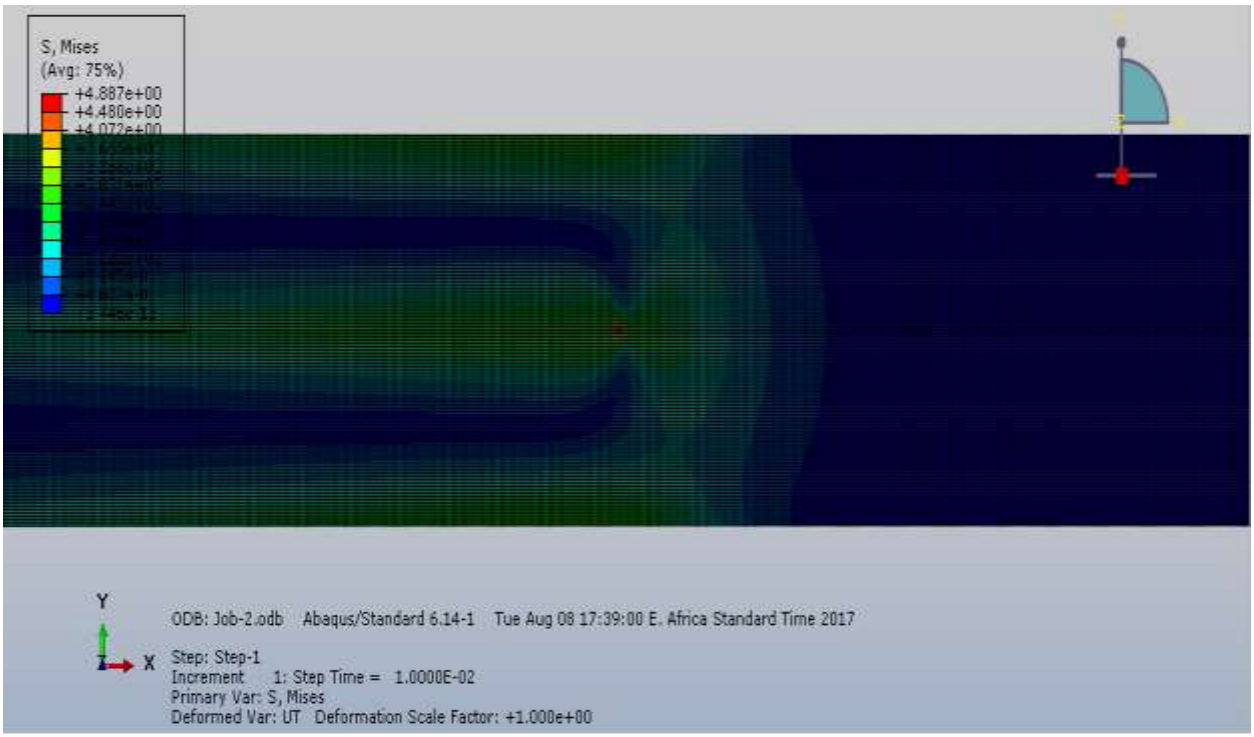

A. Delamination at the end of the first time step

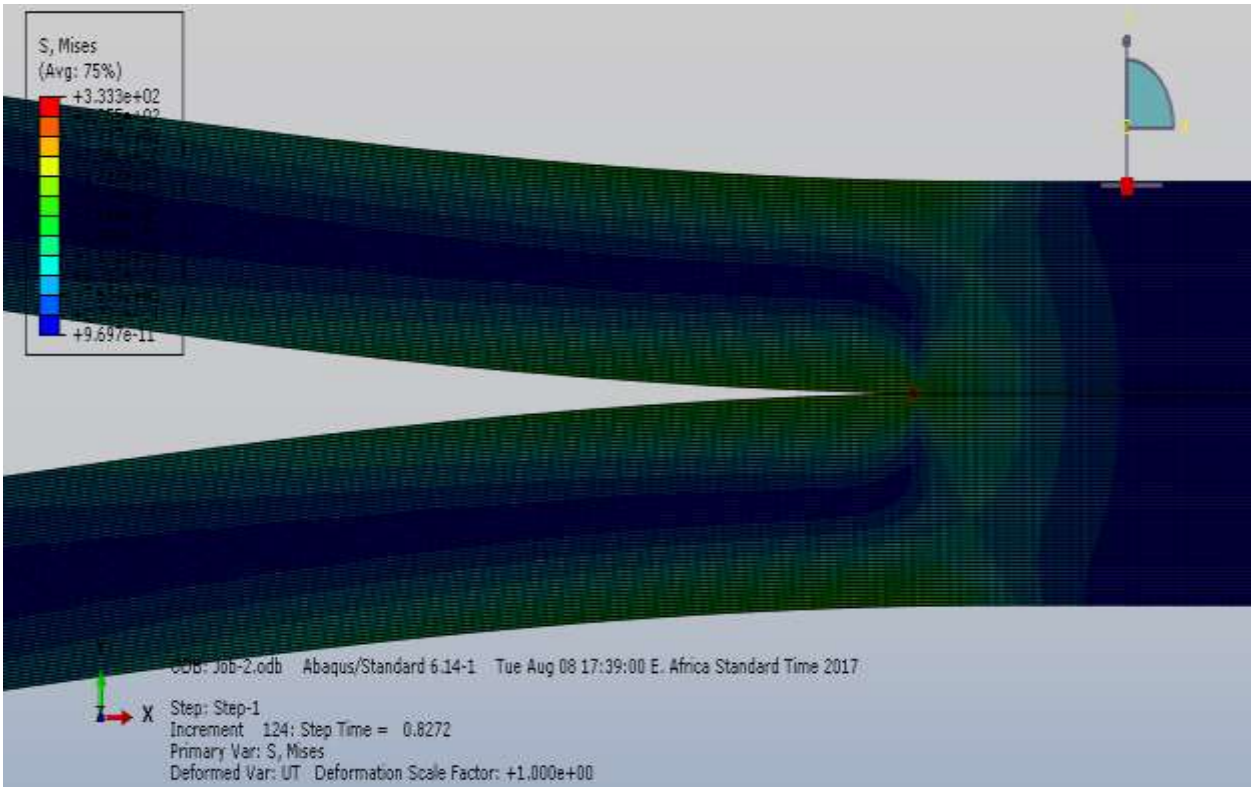

B. Delamination at the end of the final time step

Fig 4. 12. Delamination of DCB using CZM, A. at the end of the first time step B. at the end of the final time step

Effects of interfacial strength

The most struggling issue of the CZM method is the possibility to face with low convergence rates. As suggested in [42] the number of elements that stay inside the cohesive zone should be high in order to get improvement in the convergence. On the contrary, as the number of elements is increased, the solution time for finishing the run is peaked. To cope with this conflict, suggest to artificially reduce the interfacial strength to increase the cohesive zone

Therefore, by varying the interfacial strength as 20 MPa, 40 MPa 45MPa and 60 MPa, trials with penalty stiffness of 2.896x10^3 are performed table 4.3 in order to see the impacts on the results. Unless the interfacial strength was decreased excessively, the resulting response would be similar. Actually, this is exactly the same case that we currently have

Table 4. 3 CZM load output for different Maximum Traction with constant penalty stiffness.

Maximum Traction (Mpa)	Critical Load (N)
20	28
40	31.23
45	31.18
60	51

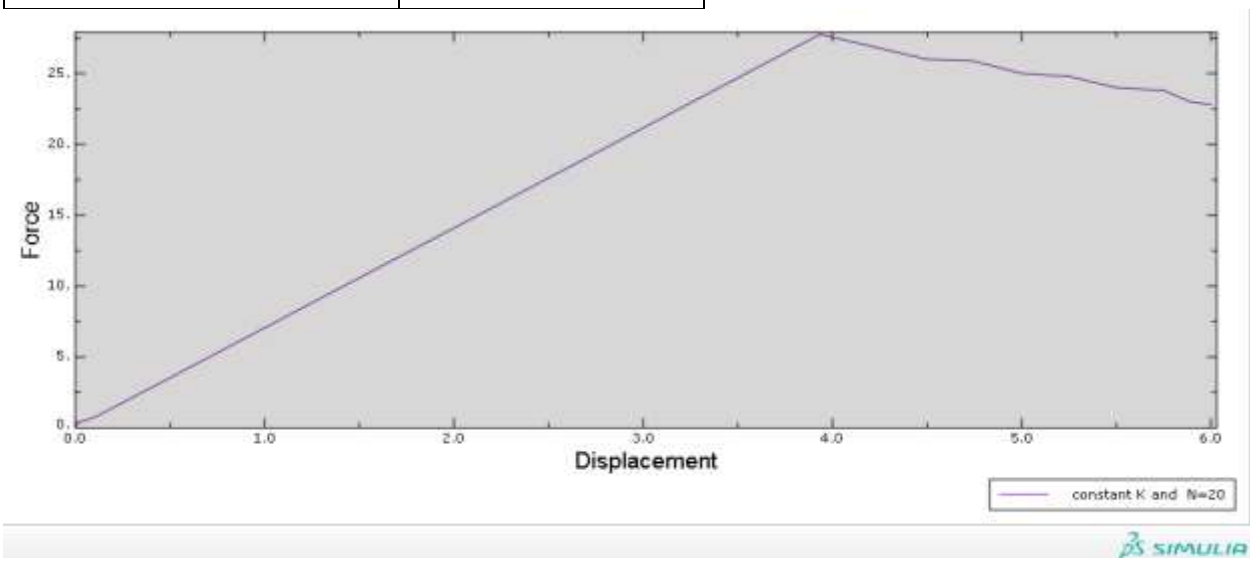

Fig 4. 13 CZM load output for 20MPa Maximum Traction with constant penalty stiffness

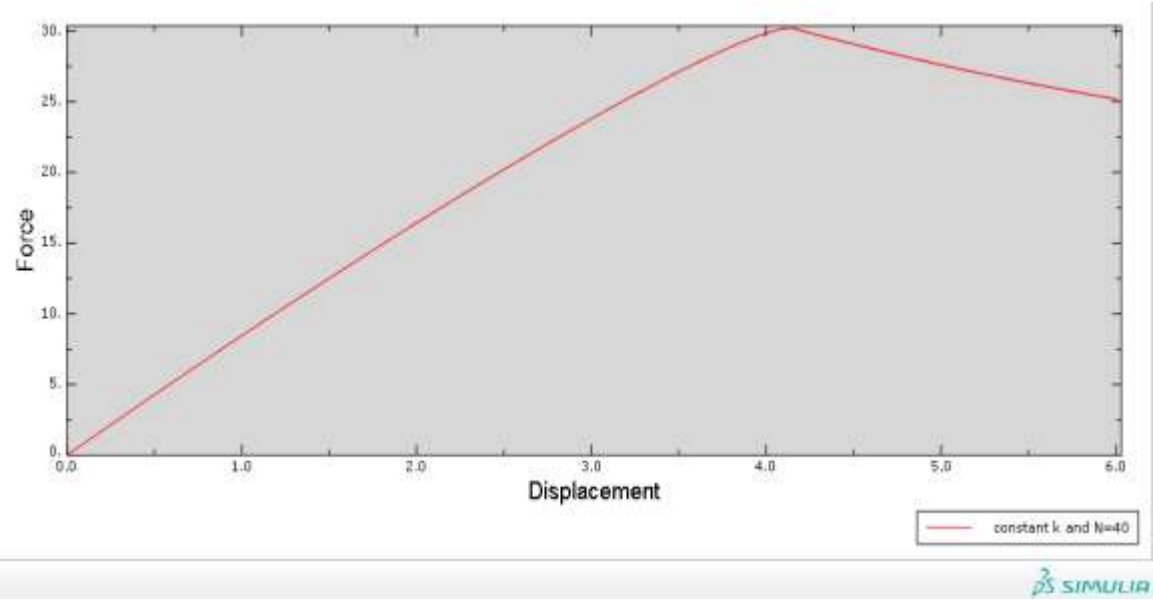

Fig 4. 14. CZM load output for 40MPa Maximum Traction with constant penalty stiffness

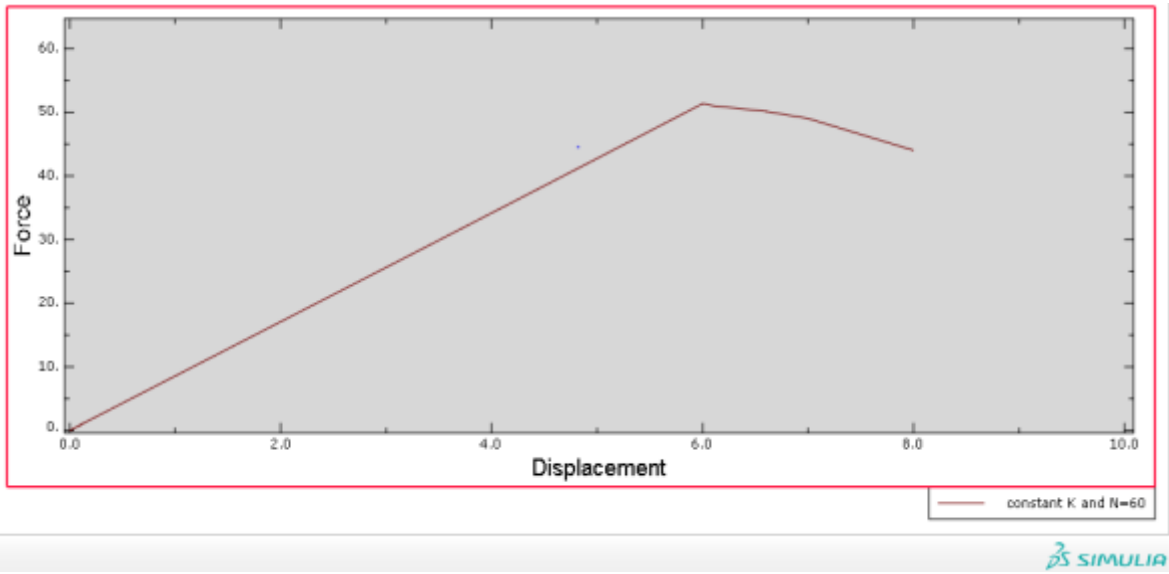

Fig 4. 15. CZM load output for 60MPa Maximum Traction with constant penalty stiffness

From Fig.4.15 it is seen that the trial with 60 MPa interfacial strength does not converge after theoretical value of Pc. On the other hand, 40 MPa case is converged after P_C. Finally, the interfacial strength of 20 MPa gives no convergence problem and without any high cyclic oscillations that shows better solution times. However, the result would be extremely

soft and hence; the solution was stopped manually to verify the effect of the interface strength on the numerical results.

Effects of penalty stiffness

The similar effect is observed, when the different penalty stiffness values is varied. As discussed before, penalty stiffness has a significant effect on convergence and the response of the structure. The load–displacement response curves obtained from simulations using an interface stiffness greater than 10^4 N/mm3 are virtually identical. However, smaller values of the interface stiffness have a strong influence on the load–displacement curves, since a stiff connection between the two neighboring layers is not assured. Moreover, the number of iterations needed for the solution when using an interface stiffness smaller than 10^4 N/mm3 is greater than the number of iterations needed for a range of the interface stiffness between 10^6 and 10^7 N/mm3. For values of the interface stiffness significantly greater than 10^7 N/mm3, the number of iterations needed for the solution increases. The stiffness that results from Eq. 2.4 with a = 50 is 2.896 10^6 N/mm5, which is ideal for a good convergence of the solution procedure.

The load–displacement response curves for higher values of interface stiffness show stable solutions. But values higher than 10^7 N/mm3 did not result in converged solutions and the simulation crashed. Lower values (e.g. 10^4 N/mm3), did not provide a stiff connection between two neighboring layers resulting in unstable load–displacement curves (Fig.4.16). Also the smaller values may induce large interpenetrations, which are not compatible with physical reality.

As a result of the sensitivity analyses and also from the (equation 2.4), the value for initial stiffness of the traction-separation law used throughout this work was chosen to be 2.896x 10^6 N/mm^3 which gave smoothly running simulations, and convergence was also achieved fairly easily, lode-displacement curve for different value of stiffness are show in Fig 2.16,Fig 2.17,Fig 2.18 and Fig 2.29.

The variation in calculated levels of the critical load due to the variation in the values of interface stiffness is presented in Table 4.4.

Initial Stiffness of cohesive K(N/mm3)	Critical Load (N)	Reference
2896x10^3	30.18	Eq.2.4
10^6	32.7	Comanche et [42]
2.6x10^4	29.71	Borg et
10^7	37.1894	

Table 4. 4. CZM load output for constant Maximum Traction and four different initial stiffness of

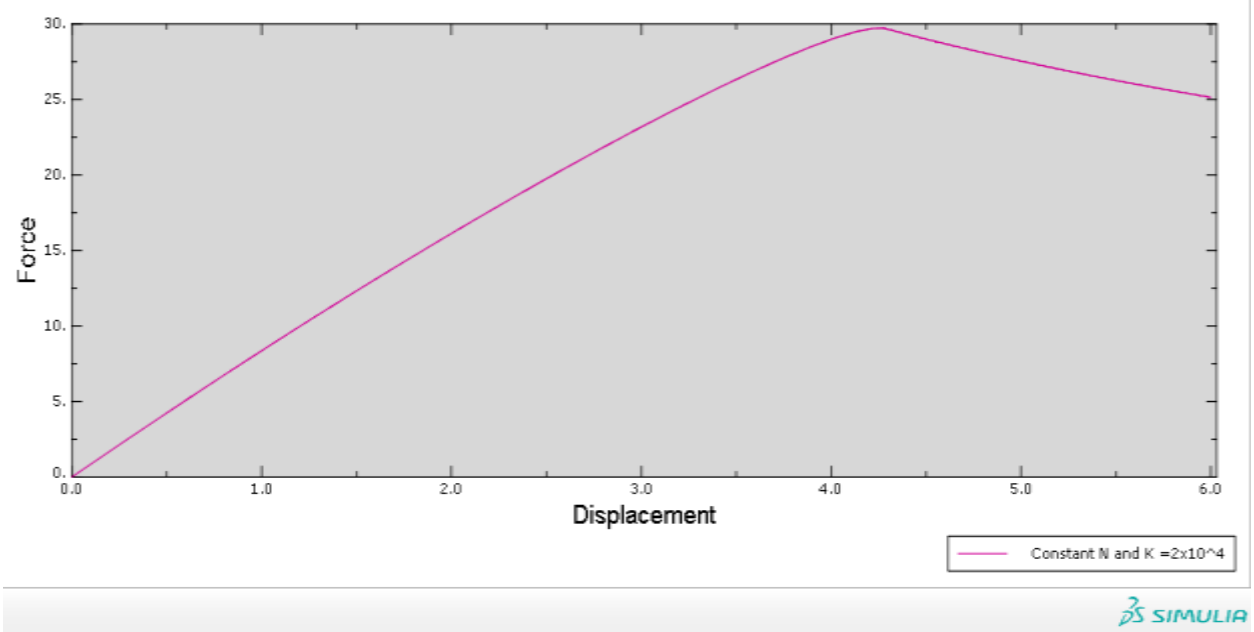

Fig 4. 16. CZM load-displacement output for 2.6x10^4 (N/mm3) initial stiffness and 40MPa Maximum Traction

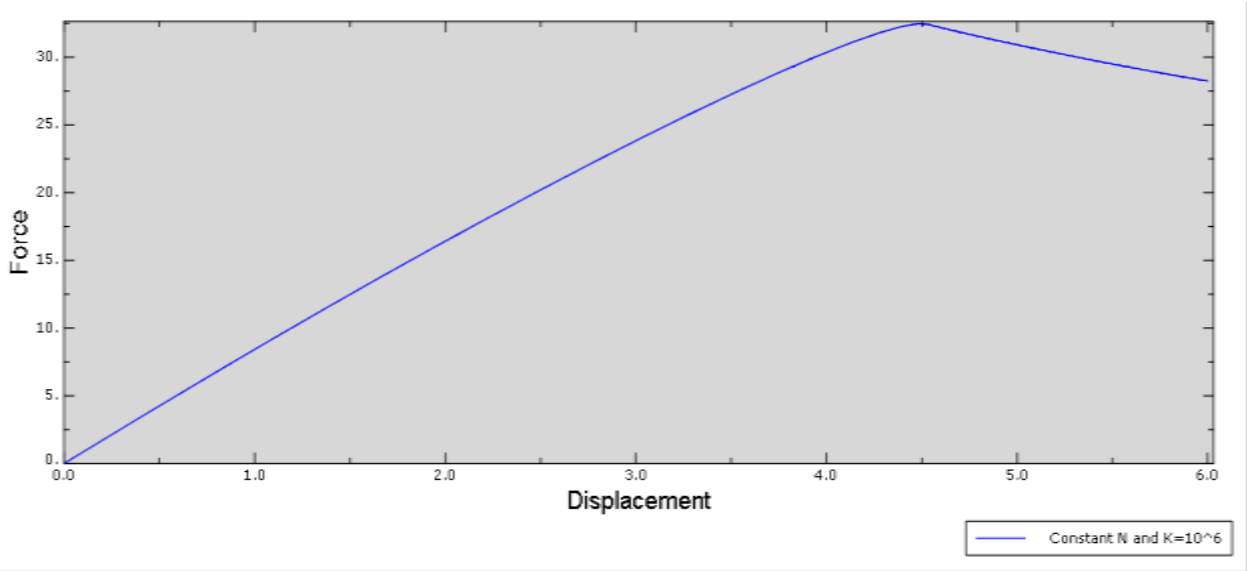

Fig 4. 17. CZM load-displacement **output for 10^6 (N/mm3) initial stiffness and 40MPa Maximum Traction**

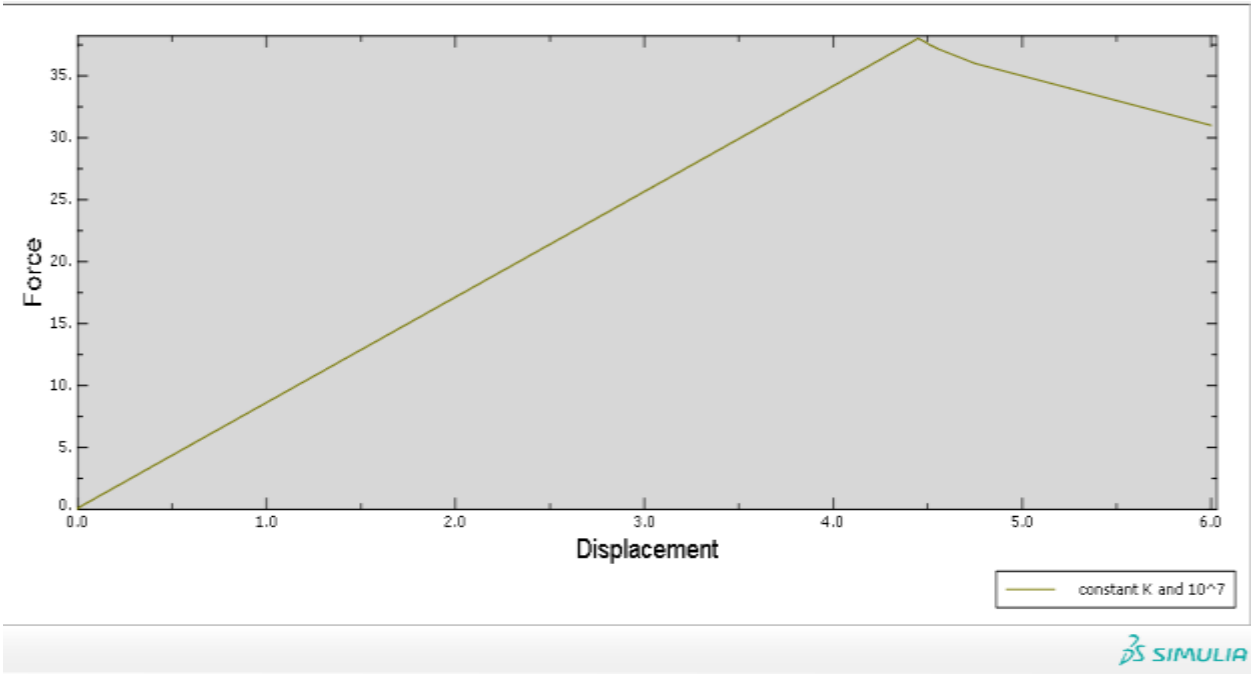

Fig 4. 18. CZM load-displacement output for 10^7 (N/mm3) initial stiffness and 40MPa Maximum Traction

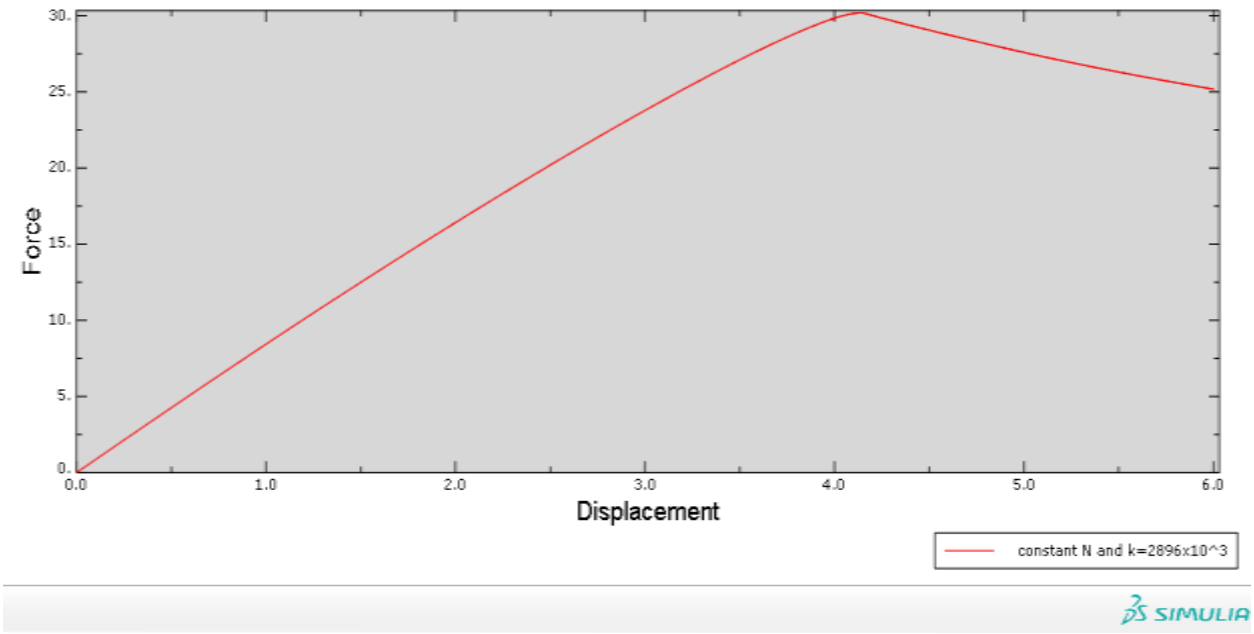

Fig 4. 19. CZM load-displacement output for 2896x10^3 (N/mm3) initial stiffness and 40MPa Maximum Traction

Mesh-size sensitivity

To highlight the mesh sensitivity of cohesive-zone problems, several numerical analyses were carried out with different mesh densities with element length varying from 0.310 mm (course) to 0.133 mm (fine). The calculated load-displacement graphs shown in Figure below. Show the variations in the critical values of load and opening displacement for various mesh densities

These results demonstrate that an increase in the mesh density leads to decrease in the critical load and opening displacement. For the pre-critical portion of the plot, all the cases nearly converge to a line, but in the post-critical behavior, due to the unstable crack growth, divergence was observed. In this work an element length of 0.133 mm was chosen to provide a balance between computational cost and accuracy. It should be noted that even the solution of 2D problems required the use of a high-performance multi-node computing cluster, with a large shared memory.

To study the effects of mesh refinement, several analyses were carried out for element sizes ranging between 0.133 mm and 0.31mm. The corresponding load–displacement curves are shown in Fig4.20, Fig4.21, Fig4.22 and Fig4.23. The results indicate that a mesh size of le ≤ 0.310 mm is necessary to obtain converged solutions. For applied lode the fine mash model capture the

softening region ahead of the crack tip while the coarse-mesh model does not. For different mesh density case using interface value of $2896x10^3$ and Traction of 40MPa (0.133, 0.15, 0.2 and 0.31) load -displacement are showmen in figure below and table 4.5.

Table 4. 5 . CZM load output for four different case of mesh density.

CASE	Element Size of Composite	Element Size of Cohesive	Critical Load (N)
Case 1	0.133x0.133	0.0266x0.0266	30.82
Case 2	0.2x0.2	0.04x0.04	42.2
Case 3	0.31x0.31	0.062x0.062	44
Case 4	0.15x0.15	0.03x0.03	32.5

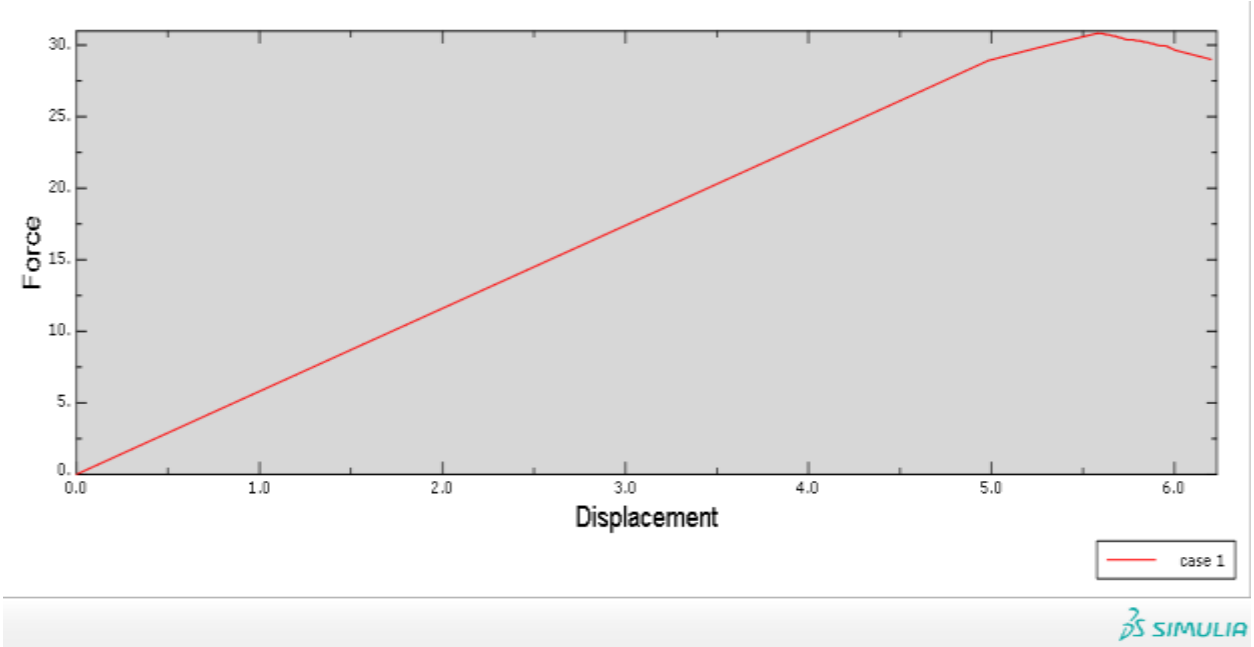

Fig 4. 20. CZM load-displacement output for case 1 of mesh density

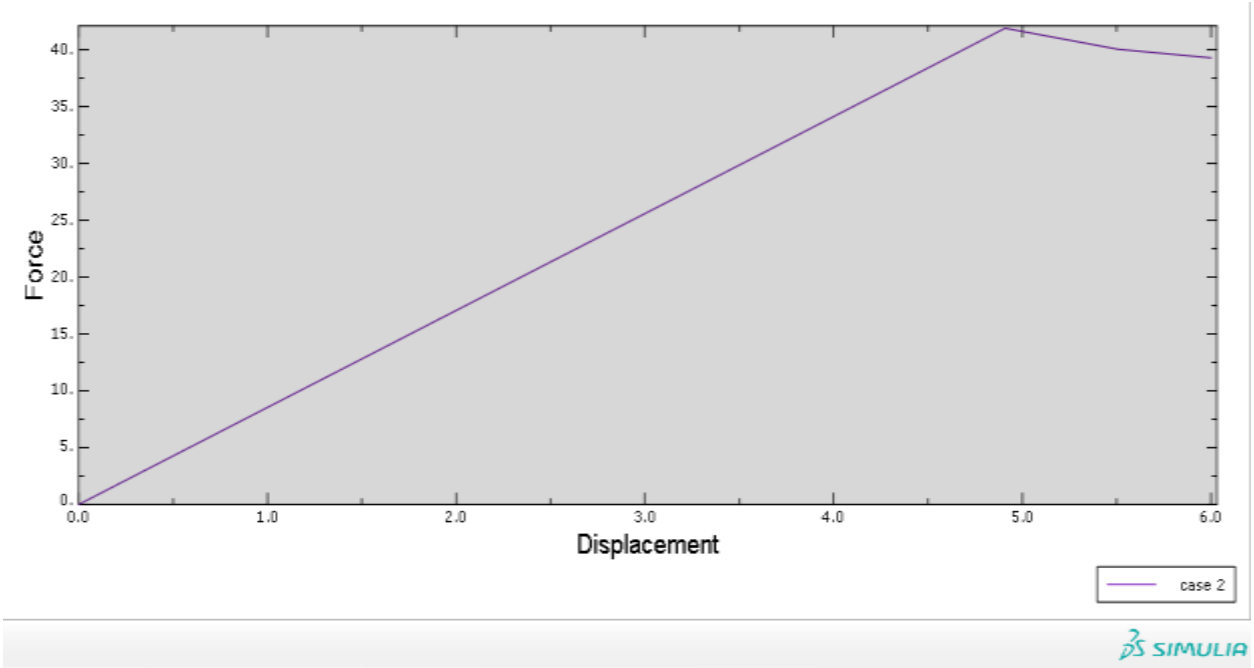

Fig 4. 21. CZM load-displacement output for case 2 of mesh density

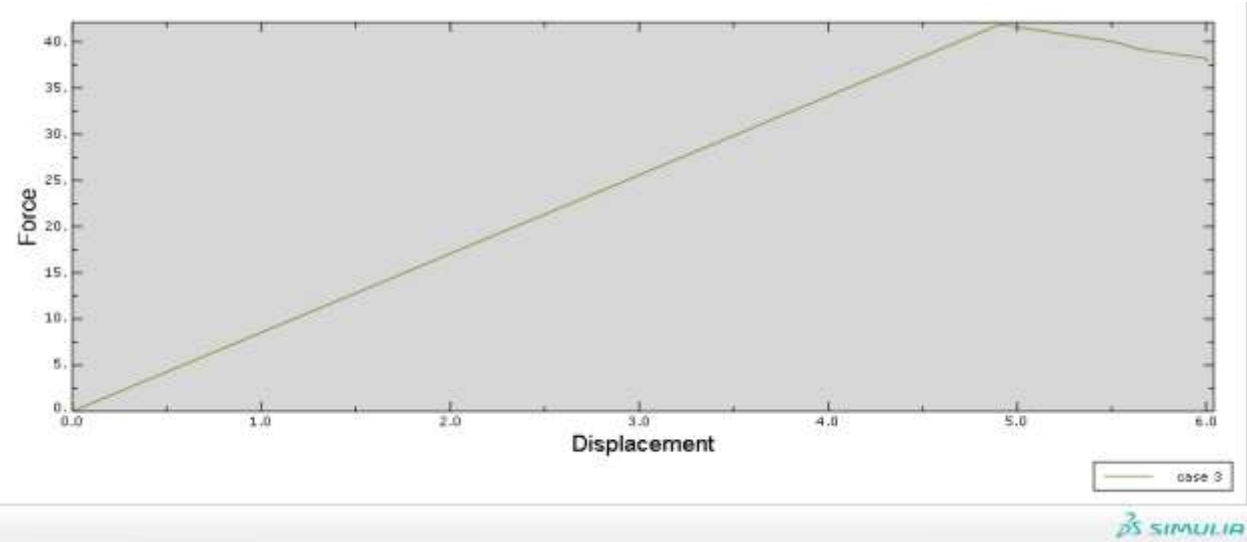

Fig 4. 22. CZM load-displacement output for case 3 of mesh density

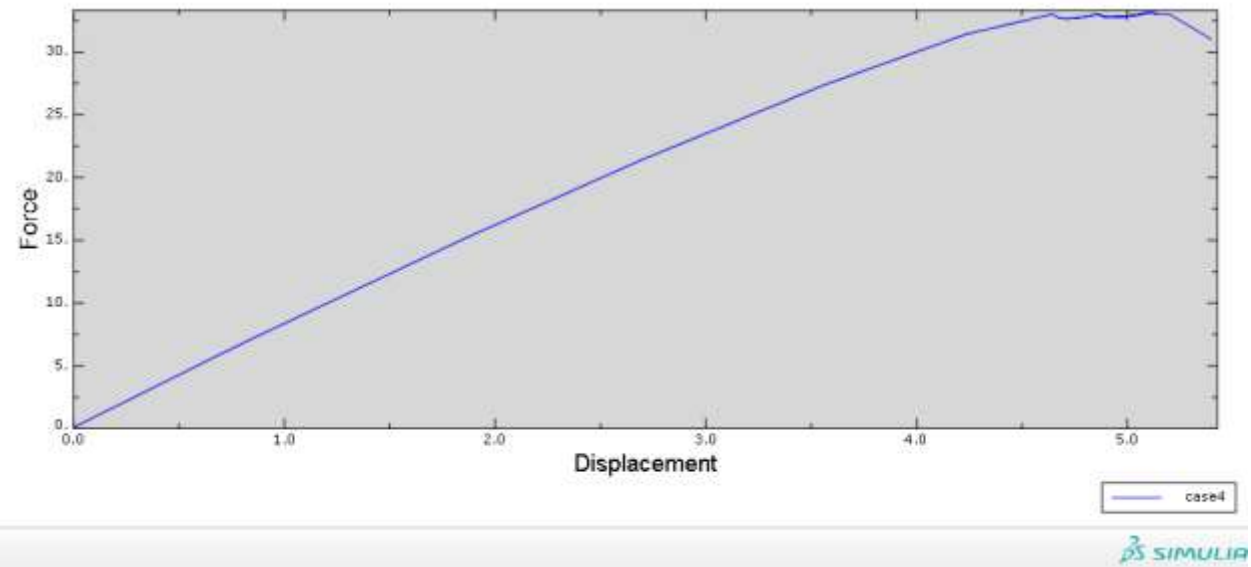

Fig 4. 23. CZM load-displacement output for case 4 of mesh density

Identification of control parameters for cohesive element simulations

For the cohesive element approach, selection of simulation parameters such as viscous regularization and automatic stabilization must be done by trial and error. Comparison of the stabilization energy and viscous dissipation energy to the overall strain energy of the model for validation of these parameters is also necessary. During the present study, a number of finite element simulations have been conducted to identify the appropriate element size and necessary minimal damping to avoid convergence issues while accelerating the solution process. Element sizes and viscous damping values used in these simulations are listed in Table 4.6. Fig 4.24, Fig 4.25 and Fig 4.26 below shows the load-displacement due to viscous effects and automatic stabilization for a selected set of simulations with an element size of 0.133. With an element size of 0.133mm, the crack propagation was unable to initiate without the use of viscous damping coefficient due to numerical convergence difficulties, as shown by Case 7 on the Table 4.6. But the same simulation with a smaller mesh size of 0.133mm was completed without viscosity, but took a longer time to complete the simulation Simulations with a higher viscosity value tends to over predict the response while producing a smooth load-displacement (time) curve avoiding oscillations, and the solution process is faster. Even though the response reflects small oscillations, a mesh size of 0.133 elements is sufficient enough to reach the mesh convergence, as verified by the simulations with finer mesh sizes of 0.133.

Table 4. 6. CZM load output for four different case Viscosity with constant mesh density.

CASE	Element Size of Composite	Element Size of Cohesive	Viscosity	Displacement	Critical Load (N)
case 5	0.133x0.133	0.0266x0.0266	1e^-5	5.58	30.82
case 6	0.133x0.133	0.0266x0.0266	5e^-4	4.2	30.12
case 7	0.133x0.133	0.0266x0.0266	0	..	no result
case 8	0.133x0.133	0.0266x0.0266	1e^-6	4.3	30

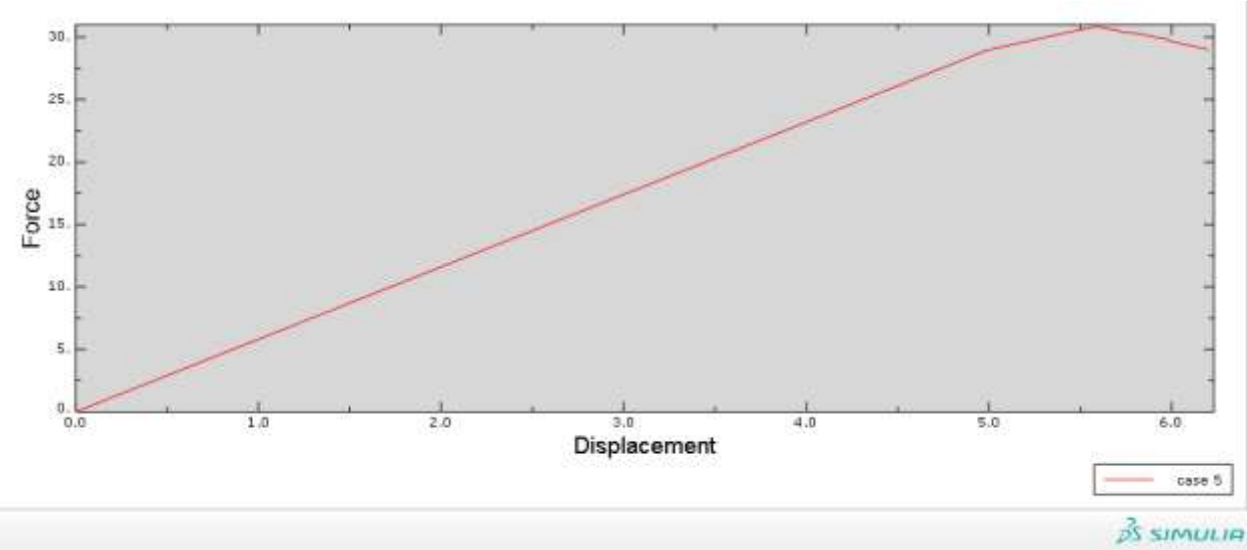

Fig 4. 24. CZM load-displacement output for case 5 of Viscosity

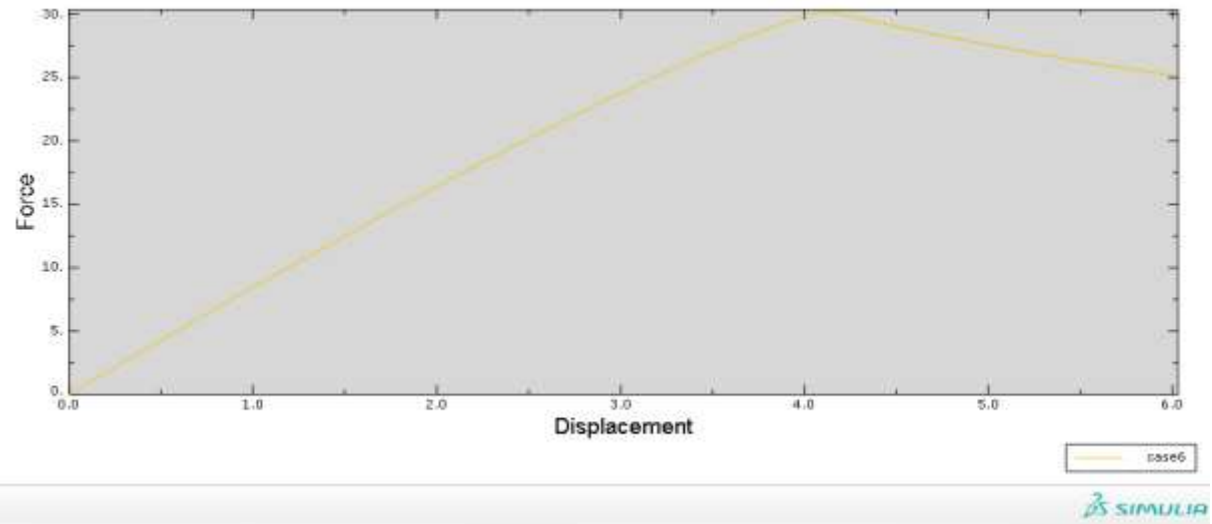

Fig 4. 25. CZM load-displacement output for case 6 of Viscosity

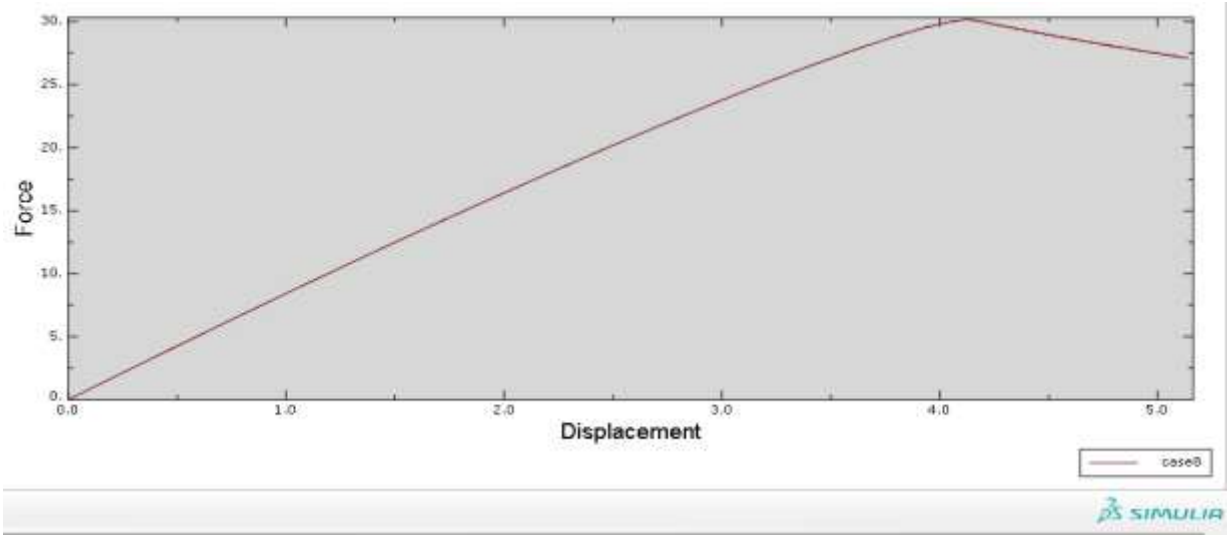

Fig 4. 26. CZM load-displacement output for case 8 of Viscosity

All the other material parameters have been kept the same as used in previous cases. Comparison of reaction forces predicted by VCCT and cohesive elements are shown in Figures. With the same material data used in both models, cohesive model displays a significantly lower reaction force compared to VCCT predictions. Even though the mesh size, lowest possible viscosity, element size, and interface strengths have been chosen based on previous simulation results to represent cohesive zone accurately, the cohesive model predictions are considerably lower to VCCT values.

Chapter Five

5. Conclusion and Future Work

5.1. Conclusion

Quasi-isotropic E-glass/Epoxy with stacking sequence $[(+45,-45.0_2,90_2)_S]$, balanced as well symmetrical lamina are developed using Autodesk Simulation Composite Design software. E-glass/Epoxy with young's modulus of 30.9GPa in both X and Y direction, shear modulus of 10GPa in both X and Y direction and possion's ratio of 0.293. Further, usually provide these properties at substantially less weight than metals: their "specific" strength and modulus per unit weight is higher than that of steel or aluminum. This means the overall structure is lighter, and in weight-critical devices such as automotive this weight savings might be a compelling advantage.
An approach to finite element simulation of composite delamination based on VCCT and cohesive element approach available in ABAQUS$^{@}$ 10.14 finite element software for simple plan strain Double Cantilever Beam (DCB) mode I delamination simulation was used. Yet it still required a great deal of excessive time to obtain reasonable results in the VCCT and cohesive elements.

For this paper I have used 2D- DCB using VCCT delamination implementing on commercial FE software ABAQUS $^{@}$10.14. Comparing different mesh density 32.3N, 4.9mm critical load and displacement of delamination propagation respectively are found using 0.01x 0.01 element size, 0.1 damping factor and 0.2 viscosity. VCCT does not require extra post-processing to extract fracture parameter nor does it place any special burden on definition of the body mesh. It presents no convergences issues is introduced as used for cohesive zone analysis.

Using 2D-DCB simulation for implementing on commercial FE software ABAQUS $^{@}$10.14, cohesive zone Method (CZM) is widely investigated, and the study is mainly focused on finite elements application of the method. In fact the motivation is to achieve a CZM interface element having high accuracy, high convergence characteristics, and consequently, high overall performance.

The investigation about CZM and VCCT is started with a discussion about theory in comparative way with each other in order of delamination propagation. A decrease interface strength in CZM gives better convergences rates and yet still accurate result cannot be guaranteed if the decrease

in interface strength are ‘’under control ‘’ Otherwise after a certain value, it is observed that the model starts to give inaccurate results. For the instance of DCB test It Seems like 40Mpa gives good results since the critical load is comparative with theoretically found, than those of 60Mpa, 45Mpa and 10Mpa interfacial strength. It should be noted that the weakening of the interfacial strength may give over-estimated allowable for delamination.

Likely observed for the weakening of the interfacial strength, decrease in the penalty stiffness has a similar effect. For the penalty stiffness 10^7 N/mm^3 the result is overshot critical load whereas the other 2.6 x 10^4 N/mm3 is lowered critical load. An excessively soft penalty stiffness is 2.6x10^4 behaves like the interfacial strength of 10Mpa with inaccurate and excessively softened results in my model perhaps it would be convenient to use a penalty stiffness 2.896x10^6.

Using interfacial strength 40Mpa and penalty stiffness of 2.896x106 it will get rid of the fine mesh requirement, comparing five different mesh density, I have come up with advantageous of using 0.133mm x 0.133mm element size in composite material and 0.0266mm x 0.0266mm size in cohesive interface element. For the type of mesh density, I have used four different viscosity value in order to target convergence difficulty and it shows smaller difference in critical load, but it has high processing time to complete simulation, so it is better to use viscosity of 5e^{-4}. Using those values, I am able to find more accurate load and displacement of delamination propagation.

5.2. Future work

The study definitely requires solving the erroneous response after the critical load is achieved. The same formulations are going to be implemented into ABAQUS which is widely used by researchers. If the problem still exists, than by comparing the inherent interface elements already implemented into ABAQUS, it would yield a chance to understand any error output of the developed interface element.

By using the same material as well the same procedure it is important to:

- Working on pure mode II delamination propagation and
- Mixed mode delamination propagation

References

[1] TENCATE, "Thermoplastic and thermoset composite for automotive application".

[2] E. Manino, "The future use of structural composite material in the automotive industry," 2004.

[3] B. Gozluklu, "Delamination analysis by using cohesive element," 2009.

[4] M.L.Williams, "The stresses around a faut or crack in dissimilar media. Bulletin of the seismological," 2009.

[5] A. Griffith, "The phenomena of rupture and flow in solids. Philiosophcal Transaction of the royal society of London," 1921.

[6] G. R. Irwin, "Analysis of stresses and strains near the end of a crack traversing a plate. J. Applied Mechanics," 1957.

[7] H. L. Groth, "Stress singularities and fracture at interface corners in bonded joints. Int. J. Adhesion and Adhesives," 1988.

[8] Y. L. X. J. Q. Xu, "Numerical methods for the determination of multiple stress singularities and related stress intensity coefficients," 1999.

[9] Wells, "Application of fracture mechanics at and beyond general yielding. British Welding," 1963.

[10] D. S. Dugdala, "Yielding of steel sheets containing slits. J. the Mechanics and Physics of Solids," 1960.

[11] G. F.Rosengren, "Plane strain deformation near a crack tip in a power law hardening material. J. the Mechanics and Physics of Solids," 1968.

[12] T. Jacobsen, "Determination of cohesive laws by the j integral approach," 2003.

[13] R. D. A. L. D. S. Z. Chen, "The use of the j-integral to analyses adhesive bonds with and without a crack," 2011.

[14] R. Krueger, "Virtual crack closure technique: History, approach, and applications," 2005.

[15] B. G, "The mathematical theory of equilibrium cracks in brittle fracture," 1962.

[16] M. M. Thouless, "The effect of damage nucleation on the toughness of an adhesive joint," 2001.

[17] A. G, "On the influence of the shape of the interface law on the application of cohesive-zone models," 2006.

[18] P. H. Jensen, "Cohesive zone modelling of interface fracture near flaws in adhesive joints," 2006.

[19] S. C. Jim ZH, "Cohesive fracture model based on necking," 2005.

[20] L. S. Thouless MD, "Mixed-mode cohesive-zone models for fracture of an adhesively bonded polymer–matrix composite," 2006.

[21] S. K. Ha, "Micro-Mechanics of Failure (MMF) for Continuous Fiber Reinforced Composites," 2008.

[22] P. K. Mallick, "Fiber reinforced composites: materials, manufacturing, and design," 2006.

[23] j. P. P. A. M. Dieffenbach, "Making the super car a reality with carbon fiber," *Automotive Engineers*, 1996.

[24] ASTM, "Standard Specification for Glass fiber," 2001.

[25] E. Ghassenieh, "Material in Automotive Application, state of the art and prospets," 2011.

[26] TENCATE, "Thermoplastic and thermoset composite for automotive application," 2012.

[27] H. T. h. loges, "Epoxy material resin," 2003.

[28] H. T. H. Logose, "Epoxy material resin," 2005.

[29] D. C. company, "Epoxy curing agent," 2007.

[30] H. B. K. W. G. Chai, "One dimensional modelling of failure in laminated plates by delamination buckling," 1981.

[31] B. S. B. Xie D, "Strain energy release rate calculation for a moving delamination front of arbitrary shape based on the virtual crack closure technique part 1," 2006.

[32] B. Xie D, "Strain energy release rate calculation for a moving delamination front of arbitrary shape based on the virtual crack closure technique. Part II:," 2006.

[33] P. Elisa, "Virtual Crack Closure Technique and Finite Element Method for Predicting the Delamination Growth Initiation in Composite Structures," 2008.

[34] D. Xiea, " Progressive crack growth analysis using interface element based on the virtual crack closure technique," 2006.

[35] M. M. Shokrieh, "Simulation of mode I delamination propagation in multidirectional composites with R-curve effects using VCCT method," 2012.

[36] M. Tadaoshi Yamanaka, "A new finite element method for modeling delamination propagation without additional degrees of freedom," 2016.

[37] A. Leski, "Implementation of the virtual crack closure technique in engineering FE calculations," 2007.

[38] C. J. H. M. Wua, "Interfacial delamination investigation between copper bumps in 3D chip stacking package by using the modified virtual crack closure technique," 2011.

[39] A. O. L. P. Daudevillle L, " Delamination analysis by damage mechanics," 1995.

[40] R. S. L. S. S. P. Zou Z, "Modelling interlaminar and intralaminar damage in filament wound pipes under quasi-static," 2002.

[41] D. v. Camanh P, "Numerical simulation of mixed-mode progressive delamination in composite materials," 2003.

[42] P. C. J. C. A. Turon C.G. Da´vila, "An engineering solution for mesh size effects in the simulation," 2006.

[43] I. GR, "Plastic zone near a crack and fracture toughness. Proceedings of the seventh Sagamore Ordnance materials conference," 1960.

[44] R. JR., "The mechanics of earthquake rupture," 1980.

[45] R. Borg, "Simulation of low velocity impact on fiber laminates using a cohesive zone based delamination model," 2006.

[46] A. M. De Xie, " Discrete cohesive zone model for mixed-mode fracture using finite element analysis," 2006.

[47] A. B. Morais, "Mode I cohesive model for delamination in composite beam," 2008.

[48] M. Heridari-Rarani, "Finite element modeling of mode I delamination growth in laminated DCB specimens with R-curve effects," 2012.

[49] W. L. B.C. Do, "Improved cohesive stress integration schemes for cohesive zone element," 2013.

[50] R. Borg, "Simulating DCB, ENF and MMB experiments using shell elements and a cohesive zone model," 2003.

[51] R. Borg, "simulation of delamination in fiber composite with a discrete cohesive failure mode," 2000.

[52] R. Borg, "Modeling of delamination using a discretized cohesive zone and damage formulation," 2002.

[53] S. R. R. Z. Zou, "A continuum damage model for delaminations in laminated composites," 2002.

[54] M. Shokieh, " A modified model for simulation of mode I delamination growth in laminated composite material," 2016.

[55] J. B. V. Mollon, "Finite element modeling of mode I delamination specimens by mean of implicit and explicit solvers," 2012.

[56] J. W. Simon, "Numerical analysis of layered fiber composites accounting for the onset of delamination," 2015.

[57] L. Yao, "Bridging effect on mode I fatigue delamination behavior in composite Laminates," 2014.

[58] M. S. M. Rehana, " Effects of fiber orientation of adjacent plies on the mode I crack propagation in a carbon-epoxy laminates," 2011.

[59] K. H. L. F.Shen, "Modeling delamination growth in laminated composites," p. 2001.

[60] N. B. ,. J. C. T.A. Sebaey, "Characterization of crack propagation in mode I delamination of multidirectional CFRP laminates," 2014.

[61] Y. G. J. Z. Libin Zhao, "Simulation of delamination growth in multidirection laminates under mode I and mixed mode I/II loadings using cohesive elements," 2014.

[62] M. N. Y. T. Wen-Xue Wang, "Experemental investigation on test methods for mode II interlaminar fracture testing of carbon fiber reinforced composites," 2006.

[63] V. K. Amir Arablouei, "Cohesive zone model properties for evaluating delamination of spray-applied fire-resistive materials from steel structures," 2015.

[64] G. L. J. F. Amir Shojaei, "Dynamic delamination in laminated fiber reinforced composites: A continuum damage mechanics approach," 2015.

[65] T. Diehl, "Modeling surface bonded structures with ABAQUS cohesive element," 2005.

[66] DESIDOC, Compsite Materials, 1990.

Appendix

Appendix. 1

```
First Ply Failure Stresses

+X-Direction
Matrix Failure in Ply: 9
8.81466E+01 (MPa)

-X-Direction
Matrix Failure in Ply: 1
-2.44152E+02 (MPa)

+Y-Direction
Matrix Failure in Ply: 5
8.81466E+01 (MPa)

-Y-Direction
Matrix Failure in Ply: 1
-2.44152E+02 (MPa)

XY-Direction
Matrix Failure in Ply: 3
7.41551E+01 (MPa)
```

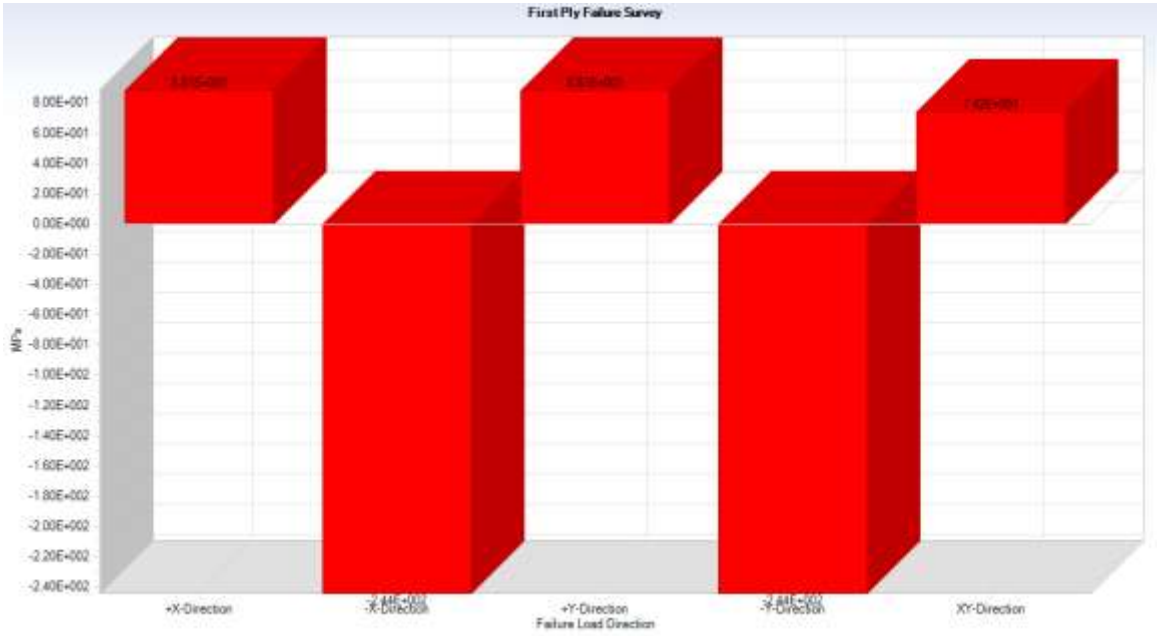

Appendix. 2

Global stress table for 24 play

Ply#	X (MPa)	Y (MPa)	XY (MPa)
1.00E+00	7.34E+01	7.34E+01	5.99E+01
2.00E+00	7.34E+01	7.34E+01	5.99E+01
3.00E+00	3.66E+01	3.66E+01	2.57E+01
4.00E+00	3.66E+01	3.66E+01	2.57E+01
5.00E+00	7.21E+01	3.79E+01	2.36E+01
6.00E+00	7.21E+01	3.79E+01	2.36E+01
7.00E+00	7.21E+01	3.79E+01	2.36E+01
8.00E+00	7.21E+01	3.79E+01	2.36E+01
9.00E+00	3.79E+01	7.21E+01	2.36E+01
1.00E+01	3.79E+01	7.21E+01	2.36E+01
1.10E+01	3.79E+01	7.21E+01	2.36E+01
1.20E+01	3.79E+01	7.21E+01	2.36E+01
1.30E+01	3.79E+01	7.21E+01	2.36E+01
1.40E+01	3.79E+01	7.21E+01	2.36E+01
1.50E+01	3.79E+01	7.21E+01	2.36E+01
1.60E+01	3.79E+01	7.21E+01	2.36E+01
1.70E+01	7.21E+01	3.79E+01	2.36E+01
1.80E+01	7.21E+01	3.79E+01	2.36E+01
1.90E+01	7.21E+01	3.79E+01	2.36E+01
2.00E+01	7.21E+01	3.79E+01	2.36E+01
2.10E+01	3.66E+01	3.66E+01	2.57E+01
2.20E+01	3.66E+01	3.66E+01	2.57E+01
2.30E+01	7.34E+01	7.34E+01	5.99E+01
2.40E+01	7.34E+01	7.34E+01	5.99E+01

Appendix. 3

Stiffness matrix Q, ABD matrix and invers ABD matrix in global coordinate system

Q-Bar for Ply: 1 Angle: 45
Material: quasi-iso

2.84E+04	1.22E+04	6.31E+03
1.22E+04	2.84E+04	6.31E+03
6.31E+03	6.31E+03	1.47E+04

Q-Bar for Ply: 2 Angle: 45
Material: quasi-iso
2.84E+04 1.22E+04 6.31E+03
1.22E+04 2.84E+04 6.31E+03
6.31E+03 6.31E+03 1.47E+04

Q-Bar for Ply: 3 Angle: -45
Material: quasi-iso
2.84E+04 1.22E+04 -6.31E+03
1.22E+04 2.84E+04 -6.31E+03
- -
6.31E+03 6.31E+03 1.47E+04

Q-Bar for Ply: 4 Angle: -45
Material: quasi-iso
2.84E+04 1.22E+04 -6.31E+03
1.22E+04 2.84E+04 -6.31E+03
- -
6.31E+03 6.31E+03 1.47E+04

Q-Bar for Ply: 5 Angle: 0
Material: quasi-iso
4.76E+04 5.66E+03 0.00E+00
5.66E+03 2.24E+04 0.00E+00
0.00E+00 0.00E+00 8.10E+03

Q-Bar for Ply: 6 Angle: 0
Material: quasi-iso
4.76E+04 5.66E+03 0.00E+00
5.66E+03 2.24E+04 0.00E+00
0.00E+00 0.00E+00 8.10E+03

Q-Bar for Ply: 7 Angle: 0

Material: quasi-iso
4.76E+04 5.66E+03 0.00E+00
5.66E+03 2.24E+04 0.00E+00
0.00E+00 0.00E+00 8.10E+03

Q-Bar for Ply: 8 Angle: 0
Material: quasi-iso
4.76E+04 5.66E+03 0.00E+00
5.66E+03 2.24E+04 0.00E+00
0.00E+00 0.00E+00 8.10E+03

Q-Bar for Ply: 9 Angle: 90
Material: quasi-iso
2.24E+04 5.66E+03 -3.21E-14
5.66E+03 4.76E+04 1.58E-12
-3.21E-14 1.58E-12 8.10E+03

Q-Bar for Ply: 10 Angle: 90
Material: quasi-iso
2.24E+04 5.66E+03 -3.21E-14
5.66E+03 4.76E+04 1.58E-12
-3.21E-14 1.58E-12 8.10E+03

Q-Bar for Ply: 11 Angle: 90
Material: quasi-iso
2.24E+04 5.66E+03 -3.21E-14
5.66E+03 4.76E+04 1.58E-12
-3.21E-14 1.58E-12 8.10E+03

Q-Bar for Ply: 12 Angle: 90
Material: quasi-iso
2.24E+04 5.66E+03 -3.21E-14
5.66E+03 4.76E+04 1.58E-12
-3.21E-14 1.58E-12 8.10E+03

Q-Bar for
Ply: 13 Angle: 90
Material: quasi-iso
2.24E+04 5.66E+03 -3.21E-14
5.66E+03 4.76E+04 1.58E-12
-3.21E-14 1.58E-12 8.10E+03

Q-Bar for
Ply: 14 Angle: 90
Material: quasi-iso
2.24E+04 5.66E+03 -3.21E-14
5.66E+03 4.76E+04 1.58E-12
-3.21E-14 1.58E-12 8.10E+03

Q-Bar for
Ply: 15 Angle: 90
Material: quasi-iso
2.24E+04 5.66E+03 -3.21E-14
5.66E+03 4.76E+04 1.58E-12
-3.21E-14 1.58E-12 8.10E+03

Q-Bar for
Ply: 16 Angle: 90
Material: quasi-iso
2.24E+04 5.66E+03 -3.21E-14
5.66E+03 4.76E+04 1.58E-12
-3.21E-14 1.58E-12 8.10E+03

Q-Bar for
Ply: 17 Angle: 0
Material: quasi-iso
4.76E+04 5.66E+03 0.00E+00
5.66E+03 2.24E+04 0.00E+00
0.00E+00 0.00E+00 8.10E+03

Q-Bar for
Ply: 18 Angle: 0
Material: quasi-iso

4.76E+04 5.66E+03 0.00E+00
5.66E+03 2.24E+04 0.00E+00
0.00E+00 0.00E+00 8.10E+03

Q-Bar for Ply: 19 Angle: 0
Material: quasi-iso
4.76E+04 5.66E+03 0.00E+00
5.66E+03 2.24E+04 0.00E+00
0.00E+00 0.00E+00 8.10E+03

Q-Bar for Ply: 20 Angle: 0
Material: quasi-iso
4.76E+04 5.66E+03 0.00E+00
5.66E+03 2.24E+04 0.00E+00
0.00E+00 0.00E+00 8.10E+03

Q-Bar for Ply: 21 Angle: -45
Material: quasi-iso
2.84E+04 1.22E+04 -6.31E+03
1.22E+04 2.84E+04 -6.31E+03
-6.31E+03 -6.31E+03 1.47E+04

Q-Bar for Ply: 22 Angle: -45
Material: quasi-iso
2.84E+04 1.22E+04 -6.31E+03
1.22E+04 2.84E+04 -6.31E+03
-6.31E+03 -6.31E+03 1.47E+04

Q-Bar for Ply: 23 Angle: 45
Material: quasi-iso
2.84E+04 1.22E+04 6.31E+03
1.22E+04 2.84E+04 6.31E+03

6.31E+03 6.31E+03 1.47E+04

Q-Bar for Ply: 24 Angle: 45
Material: quasi-iso
2.84E+04 1.22E+04 6.31E+03
1.22E+04 2.84E+04 6.31E+03
6.31E+03 6.31E+03 1.47E+04

[A]Matrix
9.84E+04 2.35E+04 0.00E+00
2.35E+04 9.84E+04 1.59E-12
0.00E+00 1.59E-12 3.09E+04

[B]Matrix
-9.09E-13 0.00E+00 0.00E+00
0.00E+00 -9.09E-13 0.00E+00
0.00E+00 0.00E+00 -1.36E-12

[D]Matrix
7.46E+04 2.31E+04 1.97E+03
2.31E+04 6.20E+04 1.97E+03
1.97E+03 1.97E+03 2.86E+04

[A]Inverse
1.08E-05 -2.58E-06 1.33E-22
-2.58E-06 1.08E-05 -5.56E-22
1.33E-22 -5.56E-22 3.24E-05

[B]Inverse
1.62E-22 -9.08E-23 -2.90E-23
-9.80E-23 1.92E-22 -3.84E-23
-4.40E-24 -6.99E-24 1.55E-21

[D]Inverse

1.52E-05	-5.63E-06	-6.56E-07
-5.63E-06	1.83E-05	-8.70E-07
-6.56E-07	-8.70E-07	3.50E-05

Appendix. 4

Hashin criterion

The Hashin criterion identifies four different modes of failure for the composite material: tensile fiber failure, compressive fiber failure, tensile matrix failure, compressive matrix failure.
S+11 ≡ Value of σ11 at longitudinal tensile failure
S−11 ≡ Value of σ11 at longitudinal compressive failure
S+22 ≡ Value of σ22 at transverse tensile failure
S−22 ≡ Value of σ22 at transverse compressive failure
S12 ≡ Absolute value of σ12 at longitudinal shear failure
S23 ≡ Absolute value of σ23 at transverse shear failure
If σ11 ≥ 0, then the Tensile **Fiber** Failure Criterion is:

$$F_f^+ \equiv \left(\frac{\sigma_{11}}{S_{11}^+}\right)^2 + \alpha\left(\frac{\sigma_{12}}{S_{12}}\right)^2 \geq 1.0$$

If σ11 < 0, then the Compressive **Fiber** Failure Criterion is

$$F_f^- \equiv \left(\frac{\sigma_{11}}{S_{11}^-}\right)^2 \geq 1.0$$

If σ22 ≥ 0, then the Tensile **Matrix** Failure Criterion is:

$$F_m^+ \equiv \left(\frac{\sigma_{22}}{S_{22}^+}\right)^2 + \left(\frac{\sigma_{12}}{S_{12}}\right)^2 \geq 1.0$$

If σ22 < 0, then the Compressive **Matrix** Failure Criterion is:

Note that the Hashin equations include two user-specified parameters: α and S23.
• α: User-specified coefficient that determines the contribution of the longitudinal shear stress to fiber tensile failure. Allowable range is $0.0 \leq \alpha \leq 1.0$, and the default value is α=0.

• S23: Transverse shear strength of the composite material in the 23 plane

Appendix. 5

Hashin criterion tensile fiber failure, compressive fiber failure, tensile matrix failure and compressive matrix failure